Exploration of the inter-areal cortico-cortical network of the macaque monkey

Nikola Markov

Thèse n° d'ordre : 79-2010 Année 2010

THESE

Présentée
devant l'Université Lyon I – Claude Bernard

Pour l'obtention

du DIPLOME DE DOCTORAT

NEUROSCIENCES

Exploration of the inter-areal cortico-cortical network of the macaque monkey

Présentée et soutenue publiquement le Jeudi 3 juin 2010

Nikola Markov

Directeur de Thèse : Henry Kennedy

Composition du Jury

Pr François Mauguiere (Université de Lyon, FR)	**Président**
Pr Wim Vanduffel (Harvard Medical School, US)	**Rapporteur**
Pr Peter Roelfsema (University of Amsterdam, NL)	**Rapporteur**
Pr Jon Kaas (Vanderbild University, US)	**Examinateur**
Pr David Van Essen (Washington University, US)	**Examinateur**
Dr Hendry Kennedy (Inserm U846, FR)	**Examinateur, Directeur de Thèse**
Dr Kenneth Knoblauch (Inserm U846, FR)	**Examinateur**

Aknowledgements

I am heartily thankful to my supervisors, Dr Henry Kennedy and Dr Kenneth Knoblauch, whose encouragement, guidance and support enabled me to develop my understanding of the anatomical organization of the macaque cortex and the ways of its analysis.

I am indebted to my colleagues Marie-Alice Gariel , Pascale Giroud, Pierre Misery, Camille Lamy, Julien Vezoli, Rene Quilodran for their great collaboration within the projects reported in this thesis.

I am grateful to Zoltan Toroczkai and Maria-Magdolna Ercsey-Ravasaz for their insightful regards on the network analysis and the discovery of the ability of the distance rule to constrain artificial networks to brain like architectures.

I am keeping a warm emotion and hopes of interesting discoveries in the collaboration with Nenad Sestan, Zeljka Krsnik and the other members of Sestan's lab.

I am honored by the members of the jury Pr Jon Kaas, Pr. François Mauguiere, Pr Peter Roelfsema, Pr. Wim Vanduffel, Pr. David Van Essen, who accepted to read this work and led the questions session in to a very enriching and pleasant discussion about the concepts and results presented in the thesis. Pr Van Essen has been crucially involved in the work on the connectivity profile by transposing our atlas in to the F99 atlas and the flattening of the cortical maps. His contribution in writing the paper was essential for its improvement.

Lastly, I offer my regards and blessings to all of those who supported me in any respect during the completion of my doctoral training.

The work reported here is the result of a collective effort detailed in the following tables:

Weight Consistency Specifies Regularities of Cortical Networks

	Markov	Misery	Falchier	Lamy	Vezoli	Quilodran	Giroud	Gariel	Ercsey-Ravasz	Pilaz	Huissoud	Barone	Dehay	Toroczkai	Van Essen	Kennedy	Knoblauch
Surgery		✓		✓			✓					✓	✓			✓	
data acquisition	✓	✓	✓	✓	✓	✓					✓	✓				✓	
data analysis	✓	✓	✓	✓	✓	✓		✓	✓	✓	✓	✓		✓	✓	✓	✓
experimental design	✓															✓	✓
writing the paper	✓													✓	✓	✓	✓

Heterogeneity of connection strengths and a distance rule specify cortical networks

	Markov	Ercsey-Ravasz	Gariel	Vezoli	Quilodran	Falchier	Huissoud	Clavagnier	Sallet	Giroud	Lamy	Misery	Sappey-Marinier	Barone	Dehay	Knoblauch	Kennedy	Toroczkai
Surgery										✓		✓		✓	✓		✓	
data acquisition	✓			✓	✓	✓	✓	✓	✓		✓	✓	✓	✓			✓	
data analysis	✓	✓	✓	✓	✓	✓	✓	✓	✓		✓	✓		✓		✓	✓	✓
experimental design	✓															✓	✓	✓
writing the paper	✓	✓	✓												✓	✓	✓	✓

The Anatomy of Hierarchy: Feedforward and Feedback Pathways in Visual Cortex

	Markov	Chameau	Falchier	Vezoli	Quilodran	Huissoud	Gariel	Autran	Lamy	Misery	Giroud	Barone	Dehay	Ullman	Knoblauch	Kennedy
Surgery											✓	✓	✓			✓
data acquisition	✓	✓	✓	✓	✓	✓		✓	✓	✓		✓				✓
data analysis	✓	✓	✓	✓	✓	✓	✓	✓	✓	✓	✓	✓			✓	✓
experimental design	✓															✓
writing the paper	✓											✓	✓	✓		✓
in vitro cell filling and anatomy	✓	✓						✓								✓

Summary

Abstract

The cortex can be viewed as a network of functional areas. A cortical area, composed of neurons forming local connections, interacts with other areas via long distance connections. Each neuron receives multiple inputs and has to integrate the incoming signals. This integrative capacity is the basis of the computational power of the brain. Our work concentrates on understanding the principles that govern the structure of the cortical network i.e. the allocation of neural resources as well as the anatomical segregation between processing steams. Using retrograde tracer injections we extract two quantitative parameters: (i) the proportion of Supragranular Labelled Neurons (SLN) identifies the feedforward (FF) or feedback (FB) operation between the source and target area; (ii) the Fraction of Labelled Neurons (FLN) identifies the magnitude of a connection pathway.

We have made repeat injections in V1, V2, V4 to investigate the consistency of cortical pathways. This showed that (i) connection weights are consistent between animals; (ii) the list of areas projecting to each injection site is highly reproducible. We find that there are fixed FLN values for each pair of interconnected areas. The FLN values of all the afferent pathways to a given target span over a factor of 6 levels of log and although there is some overdispersion their variability is not larger than one single level of log meaning that there is a specific connectivity profile for each area. Futermore the FLN follow a lognormal distribution. In lognormals the mode is lower than the median and the mean i.e. the majority of pathways have FLN weaker than the average FLN, meaning that strong projections are rare. If instead the distribution of FLN was to follow a power law, then high FLN values would have been even rarer. We found, a regularity in that the strongest input is invariably from within the injected area, second strongest are the inputs from areas sharing common borders with the target area. Sub-cortical inputs have a weak FLN, even when they are associated with an important functional role such as the LGN → V1 pathway. We found that projection distance is inversely related to the FLN value and an exponential distance rule operates that constrains short distance projections to high FLN and long distance projections to low FLN.

We injected a total of 26 cortical areas homogenously distributed across the cortex. This revealed 1232 projection pathways. Roughly 30% of pathways that we reveal have not previously been reported in the literature. Our ability to find new connections is due to the improved tracing and brain segmentation techniques. We scan the whole brain at up to 80μm intervals to detect projection neurons, and this, as discussed in the text, is a major advantage to existing studies. The weak long distance connections were shown to contract the characteristic path-length of the graph (number of hops needed to go between any two areas).

Our analysis of the graph showed that contrary to current belief the cortical inter-areal network is dense (i.e. 58% of the connection that could exist do exist). At such a density, models based on binary features such as small world cannot capture the specificity of the graph. Hence the cortex does not correspond small–world network, with sparse clustered graph possessing empowered by few critical projecitons that ensure short characteristic path-lengths. Further analysis of pathway efficiency showed that the short distance connections of high magnitude provide large bandwidth for local connectivity and form a backbone of clustered functionally related areas. This backbone is embedded in a sea of weak connections providing direct links between cortical areas. We refer to this architecture as a *tribal–network*. We speculate that the small scale and high density that characterize the cortico-cortical network is facilitating the emergence of synchrony between cortical areas.

Much of our understanding of cortical organization stems from theories of hierarchy in the visual cortex. SLN captures the FF or FB nature of a projection path and importantly provides a hierarchical distance measure. The SLN offers the possibility of determining the hierarchical interactions between cortical areas. We have shown that within a given area the cells of origin of the FF and FB paths are located in different layers. Bifurcation (ie neurons with axon collaterals to distinct targets) was frequent when both target areas are at lower or higher hierarchical levels than the source area, while there is virtually no bifurcation when one target is lower and the other is higher in the hierarchy. Furthermore, in the supragranular layers the FF projecting neurons are concentrated in layer 3b while the FB projecting neurons are concentrated in layer 3a. In the infragranular layers the FB projecting cells are slightly denser in layer 6 while the FF projecting cells are in both layer 5 and 6. Grossly the FF operations involve neurons and interactions in the center of the cortical sheet while FB processes involve neurons from the margins of the cortical sheet. Morphology analysis showed that all supragranular neurons extended an apical dendrite up to layer 1 where it forms a tufted terminal arbour. In the infragranular layers all the FB cells had slender apical dendrites but surprisingly half of the FF projecting cells from infragranular layers had apical tufts extending in to layer 1. This means that the infragranular neurons of FF type are sampling the FB recurrences terminating in layer 1 and can be modulated by these inputs.

In conclusion our work showed that the magnitude of projection pathways is an important descriptor of cortical connections, and is determined by the operation of an exponential distance rule. The network formed by inter-areal connections is dense and not a small world. Efficient information transfer is ensured by a backbone of strong connections, while weak connections provide direct access between almost all brain areas. FF and FB pathways are segregated within cortical layers. An important perspective will be to combine the hierarchical and graph theoretic analysis of the cortical network.

Chapter I:

Connectivity profiles

Introduction to connectivity profiles

Information flow through the cortex is via a complex network of cortico-cortical connections that are thought to have a crucial role in shaping functional specialization **(Rockland and Pandya, 1981, Boussaoud et al., 1990, Felleman and Van Essen, 1991, Kaas and Collins, 2001)**. Working on a database of 32 visual areas, Felleman and Van Essen reported a connection density of 30-45% (i.e. of the total possible connections, there was evidence that 30-45% exist) **(Felleman and Van Essen, 1991)**. A graph theoretic approach on an updated version of this database estimated a density of 59% **(Jouve et al., 1998)**. Given this high connectivity density, analyses based only on binary categorization (connected/not connected) provide limited insight into the specificity of cortical networks. An important aspect of network specificity may reside in the strength of connections.

The basic problem in evaluating this issue is that relatively few studies of cortico-cortical connectivity have reported quantitative neuroanatomical data. Further, a review of studies that do provide quantitative data suggests a high degree of individual variability (>100-fold range) in the strength of some specific pathways. This could mean that there is not a well-defined connectivity profile **(Musil and Olson, 1988a, b, Olson and Musil, 1992, MacNeil et al., 1997, Scannell et al., 2000)**. However, attempts to evaluate the consistency of connection strengths have mainly relied on data compilations across labs, often using different tracing techniques and definitions of areas, thereby contributing to the observed variability **(Scannell et al., 2000)**.

Using well characterized, highly sensitive retrograde tracers **(Kennedy and Bullier, 1985)**, we have applied quantitative techniques **(Batardiere et al., 1998, Vezoli et al., 2004)** to characterize the fraction of labeled neurons (FLN) **(Falchier et al., 2002),** in cortical and subcortical structures following tracer injections in target areas. Our results indicate three important findings. Firstly, cortical connectivity is largely local, and information exchange

between hierarchical levels depends on sparse connections. Secondly, brain-wide analyses reveal about 30% more pathways than previously reported. Thirdly, each cortical area exhibits a well defined connectivity profile.

Quantitative information derived from these tracer injections provides invaluable reference data for comparisons with connectivity patterns inferred using MR-based structural and functional imaging methods. These include tractography analyses based on diffusion imaging **(Johansen-Berg and Behrens, 2009)** and resting-stage functional connectivity (R-fMRI) that can be carried out in monkeys **(Vincent et al., 2007a)** as well as humans **(Fox and Raichle, 2007, Van Dijk et al., 2010).** To facilitate objective comparisons using these different methods, it is important to bring the data into a common spatial framework. Here, we bring the tracer-based connectivity data into register with the macaque F99 atlas, which has previously been used for analyzing functional connectivity **(Vincent et al., 2007a)** and as a substrate for interspecies comparisons with humans **(Orban et al., 2004, Vincent et al., 2009).**

Relative magnitude of gross projection paths in the brain

If one want to perceive the number of neurons involved in a given pathway as a resource allocated under the pressure of evolutionary cost it appears obvious that the distribution of this resource will be indicative of the construction constraints (cost vs benefit). At first we explored the investment preferences for neuronal resources in the brain. The total of labeled neurons was determined in a select number of injected areas (V1, V2, V4, 45B, 8A, 9/46d, F5, TEO, 7A**) (Fig 1.1)**. This made it possible to explore the relative magnitudes of the gross types of connectivity patterns i.e. local intra-areal projections, sub-cortical sources, projections from areas sharing a border with the target area (nearest neighbors) and all the long distance projections from cortical areas without a common border shared with the target area. The relative projection magnitude is evaluated by the measure of FLNt. FLNt is derived as the number of labeled neurons in a given source structure (cortical area or sub-cortical nuclei) relative to the total number of labeled neurons (for that injection) in the brain (including the injection area) $FLNt = \frac{Nb\ neurons\ counted\ in\ X}{Total\ of\ counts\ including\ the\ injected\ area}$ **(Fig S1) (Falchier et al., 2002)**.

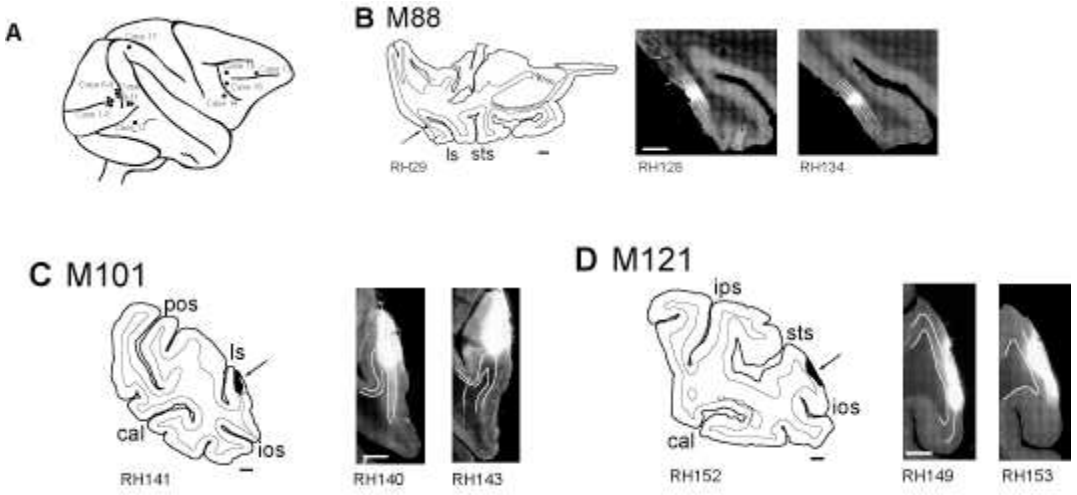

Figure 1.1 : Injection sites. A: Injection sites indicated on a lateral view of a cerebral hemisphere. Case numbers correspond to table 1. **B – D** illustrate a plot map of each injection site and two low power fluorescence photomicrographs objectif X10 filter D. **B:** Injection in area V1; horizontal section plane**. C:** Injection in area V2; coronal section plane. **D:** Injection in area V4; coronal section plane. White lines on the photographs indicate the limit gray white matter and layer 4. Scale bar = 2mm

The mean FLNt value for the intrinsic, within-area connectivity is 79% (68-89%) (**Fig 1.2A**). This intrinsic connectivity is highly local, with an exponential decrease in the density of labeled neurons along increasing distance from injection site (**Fig 1.2B**). Cumulative distance counts of intrinsic projections show that 80% of neurons arise within a radius of 1.2 mm from the injection site and 95% within 1.9 mm (**Fig 1.2C**). The next largest contribution is from the nearest neighbors, with FLNt values on the order of 14% (2.5-39%). The later actually corresponds to more than 80% of the extrinsic projecting neurons. The remaining connectivity is shared between long-range cortico-cortical connections (i.e. *all* the remaining cortical areas beyond the nearest neighbors) with a cumulative FLNt value of 3.3% (0.44-13%), and subcortical connections with a cumulative FLNt value of 1.3% (0.5-2.8%) (**Fig. 1.2E).**

Exploration of the distribution of subcortical inputs shows that the major subcortical input for all three visual areas is from the claustrum (0.3% FLNt); projections from the LGN never exceed 0.2% of FLNt **(Fig. 1.2F)**. The relatively high FLN value of the LGN projection to V2 includes many neurons (30-70%) in interlaminar portions of the LGN compared to only 10% of the LGN cells projecting to V1 as found in previous studies **(Bullier and Kennedy, 1983)**. Also it is to note that the total number of neurons counted in the LGN after V2 injections is on the order of few hundreds while, V1 injections generate more than thousand labeled neurons in the LGN and these majorly in the principal layers. Another argument comes from an injection that we do not report here but for which, the uptake zone is on the bank and deep within the lunate sulcus. This injection generated less than 100 labeled cells, showing that there is a topological specificity of LGN inputs to the region of V2 near the V1 border. The injections in parietal, temporal and frontal lobes showed that this pattern of high local connectivity coupled with a very small sub-cortical input and weak long distance connectivity is a consistent feature across the cortex **(Fig 1.2E)**.

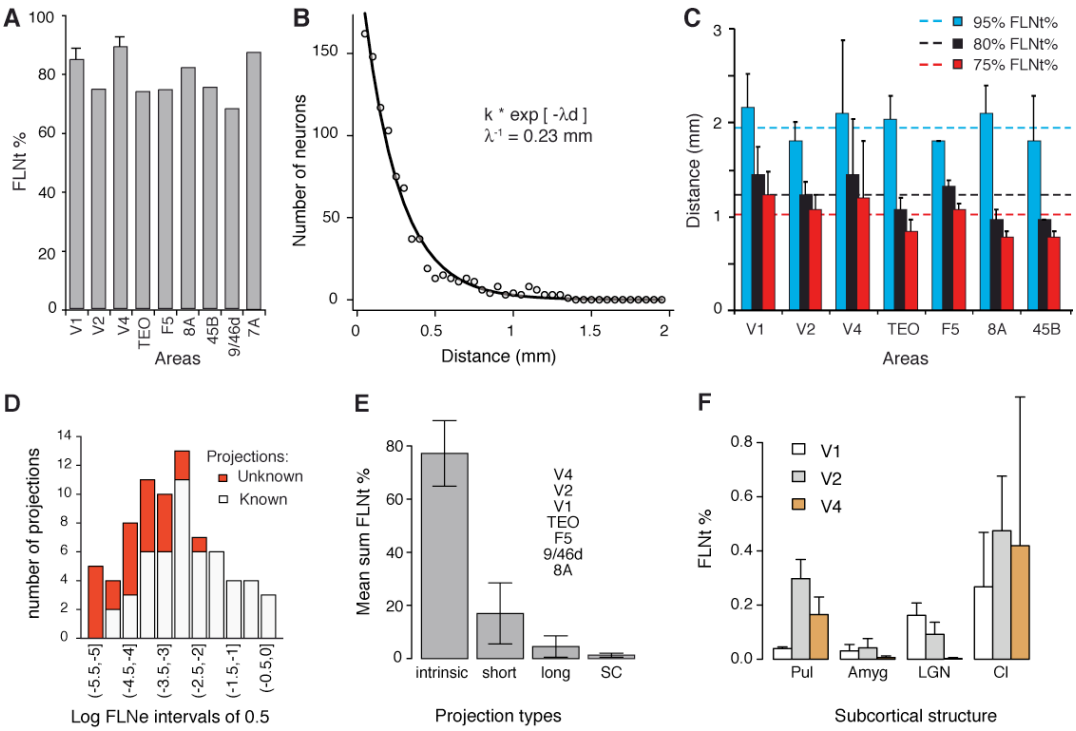

Figure 1.2. Intrinsic and extrinsic connectivity. **A**: Intrinsic FLNt values of 9 areas. V1 and V4 are averages for repeat injections. **B**: Exponential decay of density of intrinsic neurons with distance following injection in area V1. **C**: Distances within which the 3 thresholds (75%, 80%, 95%) of intrinsic FLNt are attained in 7 injected areas. Dashed lines indicate mean distance at which each threshold is

reached. Error bars are SD. **D:** Distribution of documented and undocumented projections as a function of projection magnitude (FLNe) at intervals of 0.5 log, generated after the injection of areas V1, V2 and V4. Areas and their FLN values are listed in table S1. **E:** Mean cumulated FLNt of 4 projection classes. Intrinsic: intrinsic; short: Projection from immediate neighbour(s); long: all the remaining cortico–cortical projections to the target area; SC: subcortical projections. Error bars indicate the SD. **F:** Mean FLNt of the subcortical structures projecting on V1, V2 V4. Error bars are SD.
LGN: lateral geniculate nucleus, Pul: pulvinar nucleus, Cl: Claustrum, Amyg: Amygdala complex Area, definitions and terminology see **Annex 1-abbreviations list and Annex 2-Atlas.**

Connections previously undocumented in the literature

The primary stages of the visual hierarchy have been frequently explored. Injections in areas V1, V2 and V4 have been reported to generate labeling in extensive regions of the occipital, temporal and parietal cortex **(Zeki, 1978b, Maunsell and van Essen, 1983, Kennedy and Bullier, 1985, Yukie and Iwai, 1985, Perkel et al., 1986, Boussaoud et al., 1990, Neal et al., 1990, Tanaka et al., 1990, Baizer et al., 1991, Boussaoud et al., 1991, Felleman and Van Essen, 1991, Seltzer and Pandya, 1991, Krubitzer and Kaas, 1993, Rockland et al., 1994, Rockland and Van Hoesen, 1994, Shipp and Zeki, 1995, Stepniewska and Kaas, 1996, Felleman et al., 1997, Barone et al., 2000, Falchier et al., 2002, Clavagnier et al., 2004, Gattass et al., 2005, Ungerleider et al., 2008)**. Label to all three targets has been reported consistently in a number of known visual areas: V1, V2, V3, V3A, V4, V4t, MT, FST, TE, TEO, LIP, STP, PIP. In addition areas TH/TF, the PERIRHINAL cortex, the CORE, MB, LB and PBc as well as FEF are known to project onto area V1. Areas DP, PGa and MST have been reported to project on V2. Finally 7A, DP, TH/TF and FEF are known to project on area V4. For a list of known source areas and references see **Table T1.1.** In this study we have employed tracers that have high sensitivities and when their conditions of use are optimized (post injection survival, histological processing) have revealed connections that have been missed using other techniques **(Bullier and Kennedy, 1983, Kennedy and Bullier, 1985, Perkel et al., 1986, Barone et al., 2000, Falchier et al., 2002).**

Our approach relies on two experimental advances. First, we quantitatively modeled the variability of cortico-cortical connections. To reduce between-individual variability, injections in areas V1, V2 and V4 were made in a stereotypic fashion. Criteria for inclusion were for injections to be large, parallel to the cortical surface and spanning all layers **(Fig 1.1)**. Dense spatial sampling was used to quantify connection strengths as described elsewhere **(Vezoli et al., 2004).** Second, so as to identify all areas projecting to the target area we used brain-wide scanning with improved mapping (Exploranova Mercator®) and detection tools (high gain CCD camera). The retrograde tracing techniques and the brain-wide search for projections revealed some previously unknown connections **(Fig 1.2D).** Injections in areas V1, V2 and V4 revealed a total of 75 pathways, of which 24 have not been previously reported (for the description of the projections to these areas and the relevant bibliography see **Table T1.1 and T1.2**).

We were able to identify tracer in the known source areas and some areas unexplored in previous studies. Label to all three targets was consistently present in a number of known visual areas: V1, V2, V3, V3A, V4, V4t, MT, FST, TE, TEO, LIP, TH/TF, Perirhinal, MST, STP, PIP, DP, PGa, IPa, 7A, LB as well as the FEF (**Fig 1.3, 1.5 A-L)**. The medial belt (MB) and caudal parabelt (PBc) of auditory cortex were found to project to V1 and V2 but not V4, and the core auditory region only to V1. Projections from VIP and PO were detected only for V2 injections while areas 9/46v, 9/46d, Insula and Entorhinal cortex were found to project only onto V4. A neuron was found in 8B after one of our V1 injections. To focus on the cortico-cortical connections we restricted our FLN measurements uniquely to the population of neurons located outside of the injected area. As shown in **Fig. 1.2D**, 80% of the additional connections had FLNe values that overlapped with those of known connections. The FLNe values of these projections (**Table T1.2**) confirm the extensive projection of extrastriate cortex to V1 (including projections from DP, 8A, IPa, PGa and 8B). The projections to area V2 revealed in this study increase the similarity of its inputs with those of V1. Like area V1, V2 receives newly found

projections from 7A, VIP, PO, IPa, PERIRHINAL, TH/TF, MB, LB, PBc and FEF. Injections in V4 show that this area, like both V1 and V2 receives inputs from PGa, IPa, PERIRHINAL, MST, ENTORHINAL, INSULA and LB. In addition to the input from FEF, this area also has projections from two other prefrontal areas 9/46d and 9/46v. Repeat injections made it possible to evaluate the consistency of the novel, connections **(Table T1.2, column 3).** Of the 5 newly reported connections in V1 having cumulative FLNe values of 0.01%, three (DP, Pga and IPa) were found in all 5 injections examined. For V2, of ten connections not referenced in the literature and having a cumulative FLNe = 0.27%, seven (TH/TF, Perirhinal, FEF, VIP and IPa) were present in all brains. For V4, of 9 novel connections having a cumulative FLNe of 1.2%, five (Perirhinal, IPa, PGa and MST) were present in all three brains). These results demonstrate that weak connections are not random but instead are part of a consistent connectivity pattern of cortical areas. Clearly, as FLN values get weaker the possibility not detecting a projection where only few neurons are labeled gets more likely.

The issue of what constitutes a new connection is open to debate. In a study such as this, some sections have to be held back for staining and are not available for examination of neuronal label. Hence, at very low FLN values where there are few labeled neurons, it is to be expected that some of these weak connections will not be found across all injections. One possibility is that increasing the injection size could increase numbers of neurons and lead to these weak connections being considered to be reliable projections to these target areas. In the meantime we suggest that those projections, which were found after all injections in a given area be considered as constituting new pathways (**Table T1.2**). We decided to declare as new source areas only source areas where label is present after all repeat injections and the FLN value is higher than 10^{-5}. Table T1.2 shows a list of all new source areas and identifies these, which fail to satisfy our inclusion condition.

Table T1.1. : Unknown and known cortico-cortical projections, with bibliographic references of the known projections to central representations of areas V1, V2 and V4.

	Col B			**Col D**	
Target AREA	Documented source areas	Total of col B	References	Undocumented source areas	Total of col D
V1	V2, V3, V3A, V4, V4t, LIP, PIP, STP, FST, MST, MT, TEO, PERIRHINAL, TE, TH/TF, CORE, MB, LB, PBc, FEF	20	1, 2, 3, 4, 5, 6, 7, 8, 9	DP, 7A, 8B, PGa, IPa	5
V2	V1, V3, V3A, V4, V4t, LIP, PIP, DP, STP, PGa, FST, MST, MT, TEO, TE, TH/TF	16	1, 10, 11	7A, VIP, PO, IPa, PERIRHINAL, MB, LB, PBc, FEF	9
V4	V1, V2, V3, V3A, V4t, 7A, LIP, PIP, DP, STP, FST, MT, TEO, TE, TH/TF, FEF	16	1, 3, 12, 13, 14	PGa, IPa, PERIRHINAL, MST, ENTORHINAL, INSULA, 9/46d, 9/46v, LB	9

References: 1- (Felleman and Van Essen, 1991); **2-** (Boussaoud et al., 1990); **3-** (Barone et al., 2000); **4-** (Boussaoud et al., 1991); **5-** (Falchier et al., 2002); **6-** (Felleman et al., 1997); **7-** (Rockland et al., 1994); **8-** (Rockland and Van Hoesen, 1994); **9-** (Clavagnier et al., 2004); **10-** (Gattass et al., 2005); **11-** (Stepniewska and Kaas, 1996); **12-** (Neal et al., 1990); **13-** (Seltzer and Pandya, 1991); **14-** (Ungerleider et al., 2008)

Table T1.2. : Undocumented Source areas and their average FLNe values to central representations of areas V1, V2 and V4. (yellow paint indicates the projections that we support as confirmed)

Source	*Target*	*Number of injections*	*Geo mean nb neurons*	*FLNe*
DP	V1	5 of 5	**41[18, 110]**	399E-06
Pga	V1	5 of 5	**56[26, 204]**	546E-06
7A	V1	2 of 5	**19[12,31]**	185E-06
IPa	V1	5 of 5	**21[8, 68]**	205E-06
8B	V1	1 of 5	**1[1,1]**	974E-08
PERIRHINAL	V2	3 of 3	**139[78,200]**	543E-06
FEF	V2	3 of 3	**35[28, 42]**	137E-06
VIP	V2	3 of 3	**28[11,88]**	109E-06
IPa	V2	3 of 3	**8[1, 27]**	313E-07
PO	V2	3 of 3	**8[5, 14]**	313E-07
7A	V2	2 of 3	**2[1,3]**	781E-08
MB	V2	3 of 3	**2[1,3]**	781E-08
LB	V2	2 of 3	**2[1,3]**	781E-08
PBc	V2	1 of 3	**1[1, 1]**	391E-08
PERIRHINAL	V4	3 of 3	**870[654,1159]**	920E-05
IPa	V4	3 of 3	**119[85, 192]**	126E-05
PGa	V4	3 of 3	**21[2, 75]**	222E-06
MST	V4	3 of 3	**12[8,24]**	127E-06
ENTORHINAL	V4	3 of 3	**12[6,40]**	127E-06
INSULA	V4	2 of 3	**7[5, 9]**	740E-07
9/46v	V4	2 of 3	**4[3, 5]**	423E-07
LB	V4	1 of 3	**2[2, 2]**	212E-07
9/46d	V4	1 of 3	**2[1,1]**	106E-07

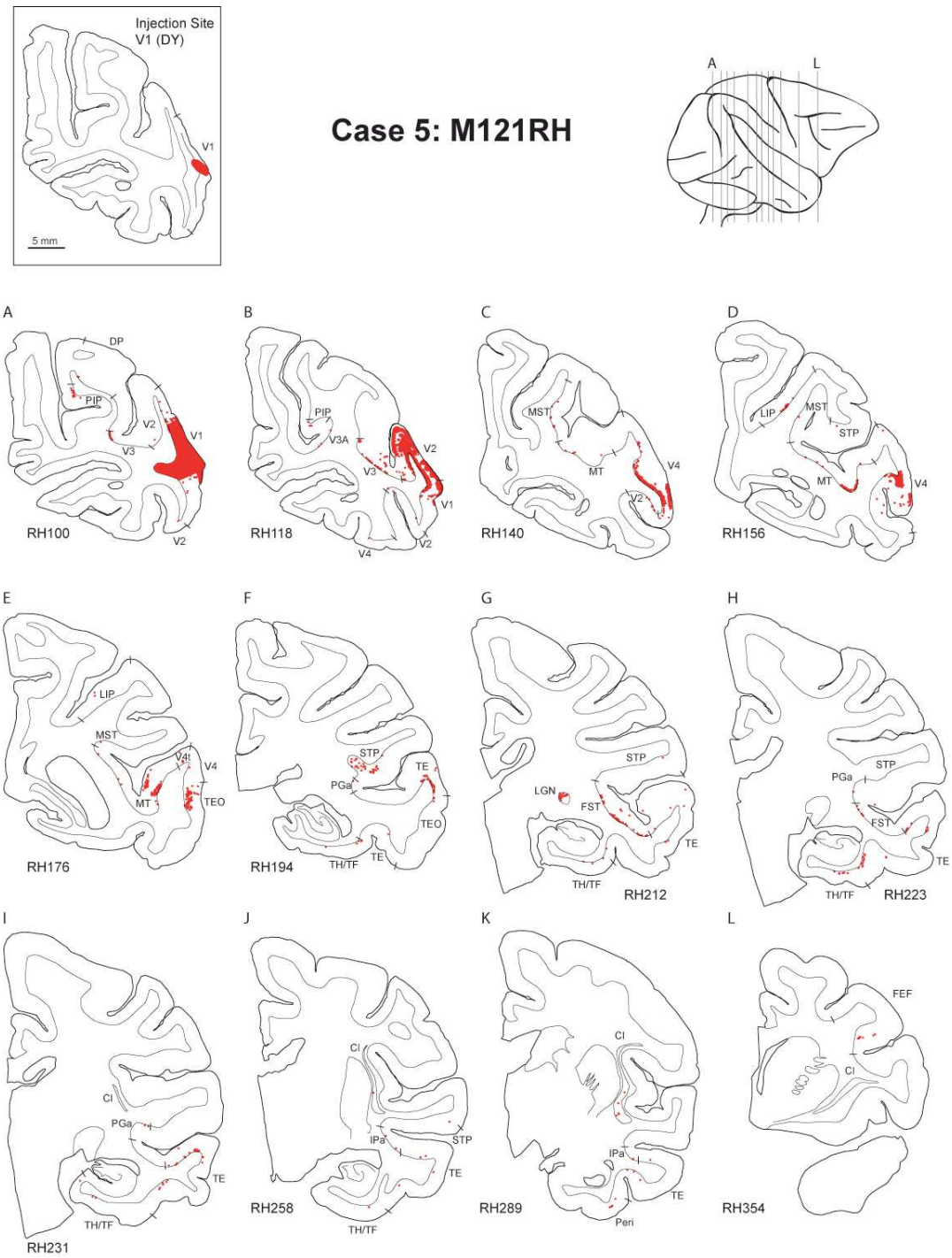

Figure 1.3. : Injection in central V1. **A-L**: Coronal plot maps of retrograde label generated after injection of DY inV1. Upper left side inset visualises the injection site. Section position is indicated on a lateral view of cerebral hemisphere.

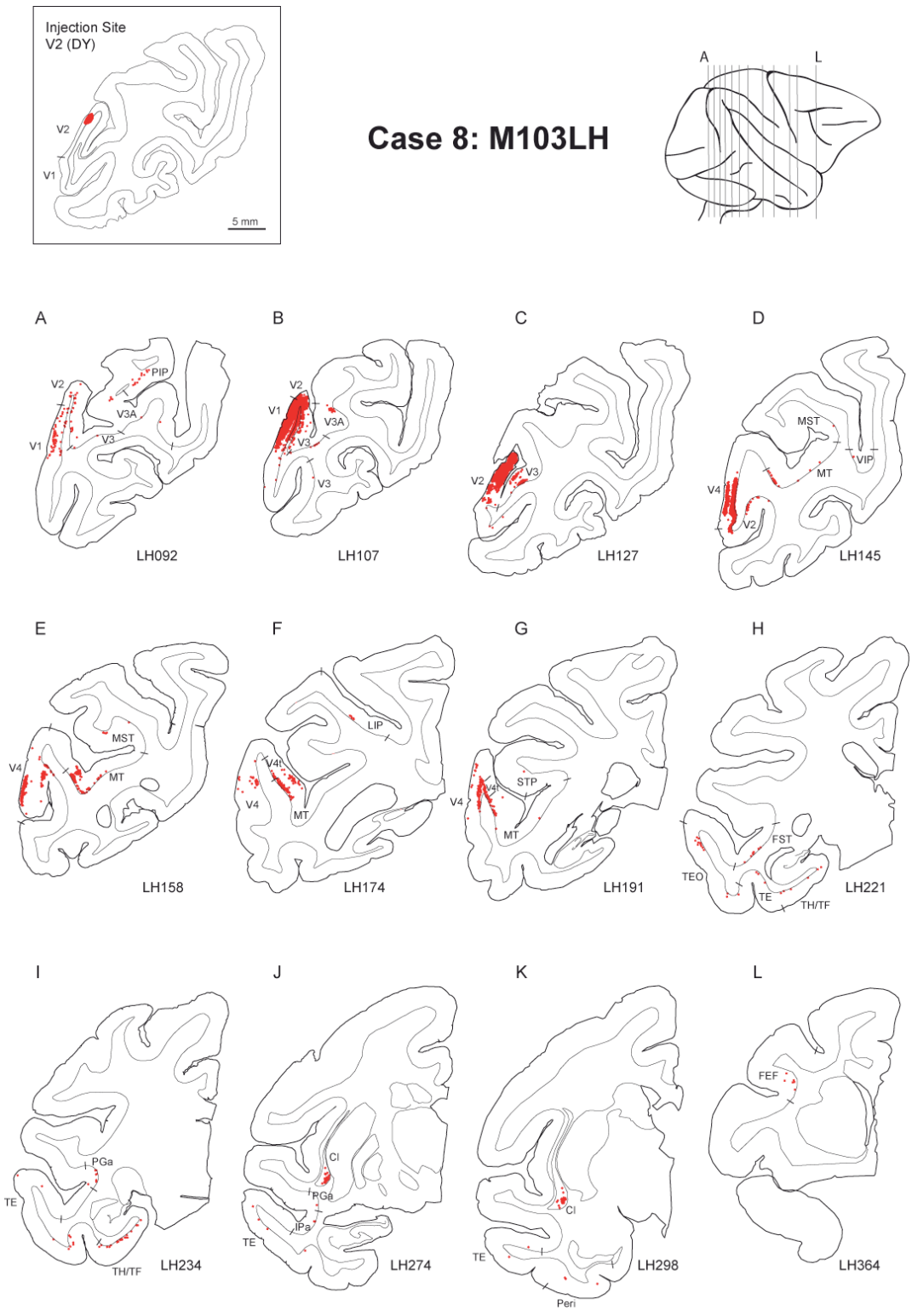

Figure 1.4. : Injection in central V2. **A-L**: Coronal plot maps of retrograde label generated after injection of DY inV1. Upper left side inset visualises the injection site. Section position is indicated on a lateral view of cerebral hemisphere.

Figure 1.5. : Injection in central V4. **A-L**: Coronal plot maps of retrograde label generated after injection of DY inV1. Upper left side inset visualises the injection site. Section position is indicated on a lateral view of cerebral hemisphere.

Are the new found weak connections consistently present in the cortex?

In areas V1, V2 and V4 our repeat injections made it possible to evaluate the consistency of the novel, connections (Table 2, column 3). Of the 5 newly reported connections in V1 having cumulative FLNe values of 0.01%, 3 were found in all 5 injections examined. For V2, of 10 connections not referenced in the literature and having a cumulative FLNe = 0.27%, seven were present in all brains. For V4, of 9 novel connections having a cumulative FLNe of 1.2%, five were present in at least three brains). These results demonstrate that weak connections are not random but instead are part of a consistent connectivity pattern of cortical areas.

The spatial distribution and strength of connections for each area can be visualized and compared using atlas surface maps **(Fig 1.6)**. The cortical areas initially charted on atlas section drawings **(Annex 2-Atlas)** were mapped onto a full-hemisphere surface reconstruction **(Fig 1.6A)** and registered to the macaque F99 atlas **(Fig 1.6B)**.

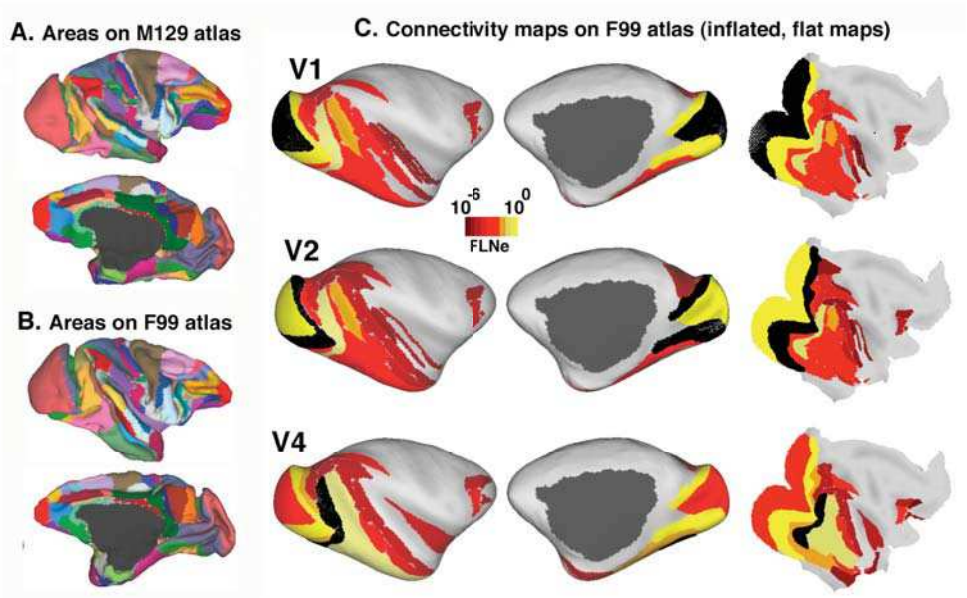

Figure 1.6: Connectivity profiles mapped to a surface-based macaque atlas. A: A set of 82 cortical areas represented on the M129 right hemisphere reconstructed from section drawings (**Annex 2 Atlas**) and displayed on lateral and medial views of the 3D anatomical surface. B: The same set of areas mapped to the F99 macaque atlas **(Van Essen, 2002b)** and displayed on lateral and medial views of the 3D anatomical surface. C: Average connectivity maps for V1 (top), V2 (middle), and V4 (bottom) displayed on inflated atlas surfaces and a cortical flat map, using a logarithmic scale to represent the range of connection strengths.

A connectivity matrix (average connection strengths for all source areas for V1, V2, and V4) was linked to these areal maps and visualized using Caret software **(Fig 1.6C)**, using a logarithmic scale to display the full range of connection strengths. Visual inspection confirms the preceding assertion that differences in areal connectivity patterns are mainly in the strength of pathways common to all areas rather than in the presence vs absence of connections. This raises importantly the question: Does connectivity profile expressed in the relative connection magnitudes exist?

FLN expresses density distribution

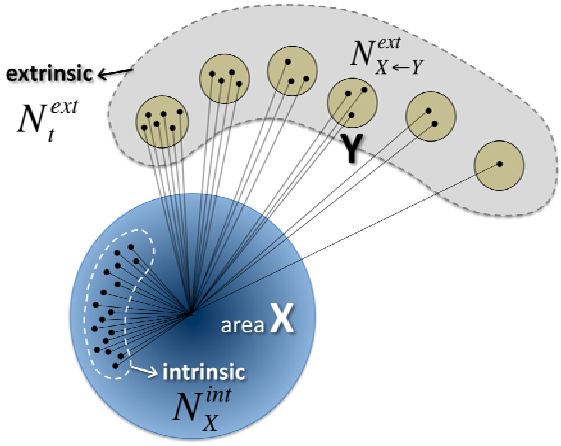

Fig. 1.7. Definition of neural counts. Blue circle represents the target area and the counts there are identified as "intrinsic". The gray zone groups the extrinsic source areas depicted as yellow circles. For definition of indices see text.

Our injection procedures are largely stereotypical and lead to a total number of labelled neurons that is fluctuating grossly within one order of magnitude.

Consider an injection in area X. As a result, a number of neurons become labeled in X (intrinsic) and other neurons become labeled in areas extrinsic to X. Let us denote the number of intrinsic labeled neurons by N_X^{int}, the number of total extrinsic labeled neurons by N_t^{ext} and by $N_{X\leftarrow Y}^{ext}$ the number of labeled neurons found in some area Y, external to X, see **Fig. 1.7**. Then, the FLNt(X←Y) of a projection (link) from area Y to injected area X is simply the fraction of labeled neurons found in Y:

$$\mathrm{FLNt}(X \leftarrow Y) = \frac{N_{X\leftarrow Y}^{ext}}{N_t}. \quad \text{(a.1)}$$

Here $N_t = N_X^{int} + N_t^{ext}$ is the total labeled neuron count for an injection in X. Therefore, the FLNt(X←Y) can be interpreted as the probability that a labeled neuron is projecting from area Y. The extrinsic FLNe(X←Y) on the other hand is defined as:

$$\mathrm{FLNe}(X \leftarrow Y) = \frac{N_{X\leftarrow Y}^{ext}}{N_t^{ext}}, \quad \text{(a.2)}$$

which can be interpreted as the probability of an extrinsic labeled neuron to project from area Y. Based on (a.1) and (a.2), FLNt(X←Y) and FLNe(X←Y) can simply be related:

$$\mathrm{FLNt}(X \leftarrow Y) = q\,\mathrm{FLNe}(X \leftarrow Y), \quad \text{(a.3)}$$

where $q = N_t^{ext}/N_t$ is the fraction of (total) external labeled neurons. **Fig 1.2A** shows the FLNt(X←X), that is the intrinsic fraction of labeled neurons, which is:

$$\mathrm{FLNt}(X \leftarrow X) = \frac{N_X^{int}}{N_t}, \quad \text{(a.4)}$$

hence

$$q = \frac{N_t^{ext}}{N_t} = \frac{N_t - N_t^{int}}{N_t} = 1 - \mathrm{FLNt}(X \leftarrow X). \quad \text{(a.5)}$$

Since the FLNt(X←X) =70-89% has small variability , it means that q in (a.3) is a fairly constant (10-30%) proportionality factor *compared* to the 6 orders of magnitude variability in the FLNe. Therefore, the FLNe can be substituted for FLNt, allowing us to compare FLNe values generated by injections in different areas. Additionally, when link weights are considered as –ln(FLNe), the proportionality factor q becomes an irrelevant overall shift in the weight distribution of the links.

Does connectivity profile of FLN exist?

We analyzed the connectivity profile to establish whether it is a reliable characteristic of each cortical area. To do this, we characterized the statistical distribution that best describes the data, including the average connection magnitudes and their variability. The variability impacts on the sensitivity for distinguishing significant differences between connection values, from random variation. Count data are intrinsically heterosedastic, i.e., the standard deviation (SD) depends on the mean (**Hilbe, 2007**). The simplest model of count data is the Poisson distribution, a distribution determined by a single parameter, its mean, and for which the SD is the square root of the mean. In our case, we normalize the neural counts in a projection by the sum of neurons from all areas projecting to the target site to obtain the FLNe. Poisson counts conditioned on a fixed total sum, N, follow a binomial law, in which the $SD = \sqrt{\frac{p*(1-p)}{N}}$, where p is the FLNe value.

Figure 1.8A displays the SD plotted against the mean of the FLNe values for multiple injections in areas V1 (5 injections, 4 animals), V2 (3 injections, 2 animals) and V4 (3 injections, 3 animals) (FLNe for all V1, V2, and V4 injections are provided in **Table S1**). Axes are scaled logarithmically here (and elsewhere) because the FLNe values span many orders of magnitude. The SD of the FLNe exceeds the prediction for a Poisson distributed variable (red curve). This phenomenon of overdispersion is not uncommon in count data. Modeling these data using a Poisson law would systematically underestimate variability and increase Type 1 or false positive errors.

The geometric distribution is an alternative model that predicts greater variation than the Poisson model (blue curve). Under this model, the SD increases as the square root of the mean plus the mean squared $SD = \sqrt{\mu + \mu^2}$. Most data points, fall below this curve, suggesting that it predicts too much variability in the data. Using this law would tend to generate Type 2 errors, failing to reject the null hypothesis when it is false. Both the Poisson and the geometric distributions are extreme examples from the negative binomial distribution family that has proven valuable in the analysis of over-dispersed count data **(Lindsey, 1999, Venables and Ripley, 2002, Hilbe, 2007)**. The negative binomial can be derived as a Poisson distribution modified to have a gamma distribution of the mean. A second parameter, θ, controls the dispersion of the distribution, with $SD = \sqrt{\mu + \frac{\mu^2}{\theta}}$. The green curve in Figure 4a indicates the prediction of a negative binomial distribution with the dispersion value for the curve that best fits the data and 95% confidence interval indicated in the figure. Similar relations were found when areas are considered separately **(Fig 1.9B, E, H)**. The observed over-dispersion cannot be accounted for by uncertainty in segmenting cortical areas because regrouping the areas into seven large regions having clear-cut boundaries did not eliminate over-dispersion **(Fig 1.9C, F, I)**. The over-dispersion can also in part be attributed to inter-individual differences, because comparing the SD's and means for the two cases of multiple injections within an animal indicates a small decrease in dispersion with respect to the between individuals comparison **(Fig 1.8E,F)**. A negative binomial is also supported by examination of the symmetry of the distribution of the data. The 95% confidence interval of the average of the median/mean of the FLNe **(Fig 1.8B**, open circle with error bars) differs from the geometric prediction (ln(2) = 0.69,

red line) and includes the value indicated by the SD/mean relation of **Fig 1.8A** (green dashed line in **Fig 1.8B**) .

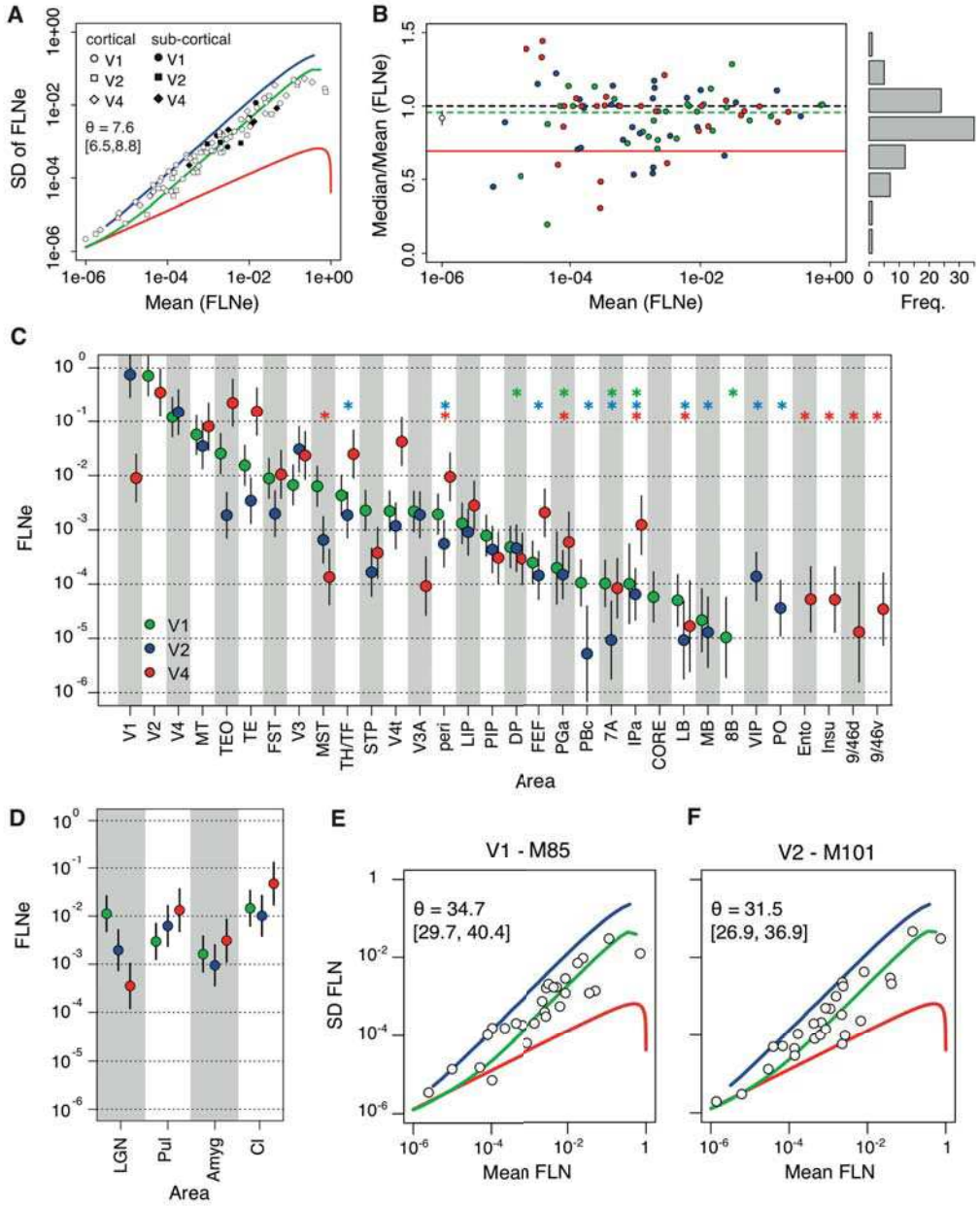

Figure 1.8. Variance and connectivity profiles of areas V1, V2 and V4. A: FLNe standard deviation as a function of the mean; green curve: negative binomial; θ overdispersion of cortical projections; brackets 95% confidence interval; blue; geometric distribution; red: Poisson distribution. **B**: Distribution symmetry as measured by the median/mean as a function of FLNe for area V1; green circle and error bars, mean and 95% confidence interval [0.87, 0.97]; red line: (log(2), limiting value for geometric distribution; black dashed line, a symmetric distribution; green dashed line (0.96) negative binomial distribution. **C**: Extrinsic FLNe values of cortical projections and 95% confidence intervals for V1 (green), V2 (blue) and V4 (red) as estimated with a negative binomial model. **D**: Mean log FLNe of subcortical projections with standard deviations. For other conventions see **Fig 1.2.** (here we set N to 6 * 10^5, the approximate average of the total number of extrinsic neurons observed across injections). When counts are normalized by a total, as here, the variability is constrained at extreme values, e.g., shown here by the downturn of the curve near FLNe = 1. **E-F:** Within individual analysis of variance (SD as a function of the mean of the FLNe).

Armed with a description of the distribution of the data, we can now evaluate the profiles for each target area. For each injection site, models of the number of cells from each source area as a function of various explanatory variables were fitted with a generalized linear model **(McCullagh and Nelder, 1989)** initially with a Poisson and subsequently with a negative binomial family. In both cases, the link function was chosen to be logarithmic. The log of the total number of cells counted from each injection was used as an offset or constant component added to the model so that in fact the connection density was modeled. Four explanatory variables were evaluated: AREA (a factor with a level for each source area), BRAIN (the individual from which the counts were obtained), DYE (a two level factor indicating the tracer used), HEMISPHERE (the hemisphere of the injection). For example, if AREA is considered as an explanatory variable then it is treated as a factor with as many levels as source areas that contained marked cells from the injections in the target areas. A model fit to the data containing only this factor provides estimates of the average FLNe and its variability for each level of AREA.

The selection of the factors and interactions that best described the data was initially based on the Akaike Information Criterion **(Akaike, 1993, Venables and Ripley, 2002)** (AIC) which is defined as: -2×log(likelihood) + 2×(number of parameters used to fit the data). Including more factors and interactions will improve the fit to the data. The AIC introduces a penalty for additional parameters, so that the model with the lowest AIC corresponds to one in which likelihood and numbers of parameters are optimized. The best model, selected in this way, was subsequently verified by evaluating the statistical significance of adding and/or dropping additional terms. The principle hypothesis tested was whether the neural counts across areas were independent of the factor BRAIN. The absence of a main effect and interaction with BRAIN is consistent with a common profile of connectivity to a given cortical area.

For all three areas with repeated injections (V1, V2 and V4) the model with the lowest AIC included no main effect of the factor BRAIN, subsequently confirmed by likelihood ratio tests (V1: $F(3, 30)=2.1$, $p=0.1$; V2: $F(1, 29)=0.07$, $p=0.78$; V4: $F(2, 32)=0.91$, $p=0.41$). Thus, the simpler models without the BRAIN term were retained. That there is no effect of the term BRAIN means that the profiles of connectivity do not differ significantly between BRAINS, and therefore a signature exists. **Figure 1.8C** shows the predicted profiles from the model fits with the 95% confidence intervals for each area (V1 green, V2 blue, V4 red). **Figure 1.8D** shows the profiles of subcortical inputs.

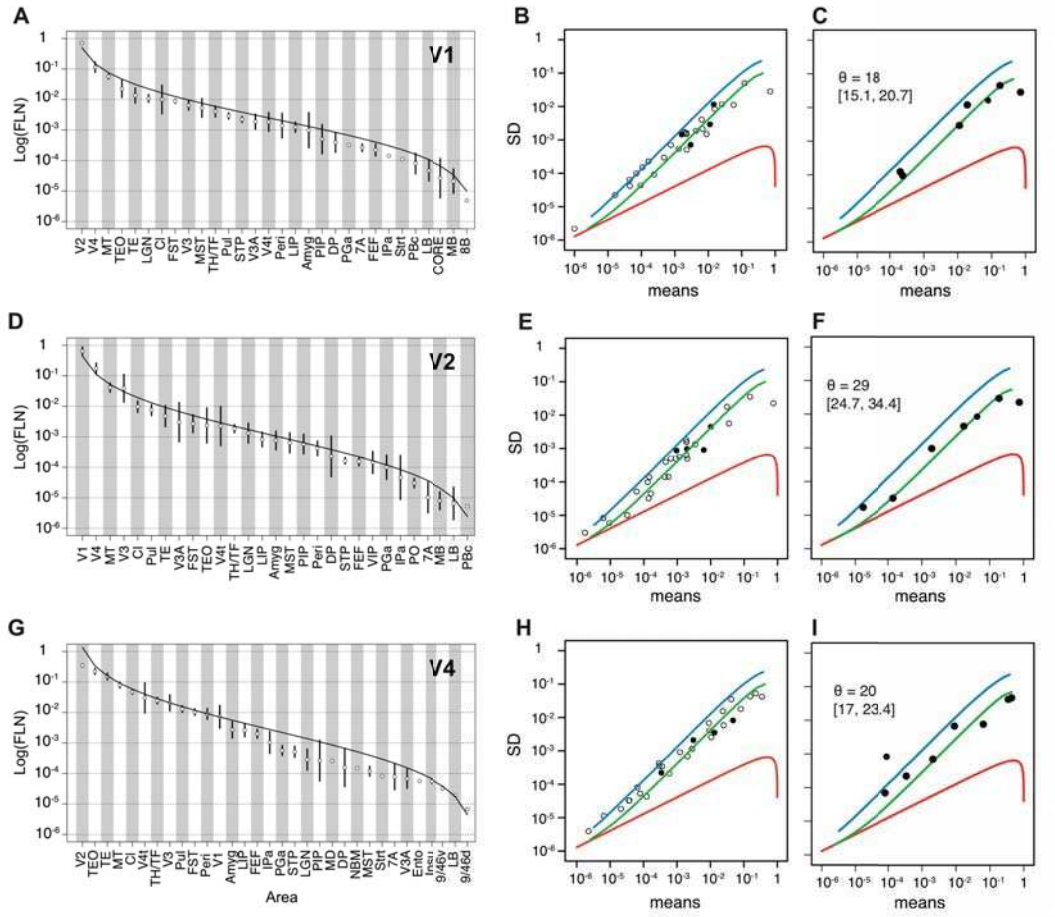

Figure 1.9. Log normal distribution of FLN values and effect of segmentation on variance. The observed means (points) and standard deviations (error bars) of the logarithm of the FLNe for the cortical areas projecting on injection sites **A** : V1 (n = 5), **D** : V2 (n = 3) and **G** : V4 (n = 3). The relative variability increases as the size of the projection decreases. Over most of the range, the variability is less than an order of magnitude. The estimated SD will tend to be biased for the largest FLNe values as the upper limit of 1 is approached. This accounts for the downturn in the curves of SD vs mean FLNe at large FLNe values **(Fig 1.8A).** The curves are the best fit log normal distribution. **B, E and H:** The standard deviation as a function of the mean of the FLNe for the individual projections to V1, V2 and V4 respectively. The estimated over-dispersion is similar across each injection site. **C, F and I** The mean/SD relation for the FLNt values pooled into 7 large regions where areas with disputable limits are fused. V1, V2, ventral pathway, dorsal pathway, frontal, sub-cortical excluding the thalamus. Such pooling that would minimize variability that might occur from areas in segmenting cortical regions produces only minor improvements in the over-dispersion of the data. Color codes and symbols as in **Fig 1.8,** other conventions see Fig **1.2**

FLN span 6 orders of magnitude and is best described by lognormal distribution

The previous paragraph confirmed that a connectivity profile of relative projection magnitudes exists and the systematic variability is related to the mean as $SD = \sqrt{\mu + \frac{\mu^2}{7.6}}$. We then injected 26 cortical areas distributed across the occipital, temporal, parietal, frontal, and prefrontal lobes, and explored the FLNe distribution of all source areas. Remarkably, the full range of cortical FLN values spans 6 orders of magnitude even when the intrinsic connections

are excluded. **Figure 1.10A, B** illustrates the scaling of the FLNe distribution where the drop off with FLNe increase looks like exponential or at least very steep. Actually lot of distributions can seem to have such a steep decrease. From the shape of **Fig 1.2D** where injections are made in only two areas one could suppose that the probability density distribution of the FLNe after injections in only V1, V2, V4 may be approximated by a bell curve. In probability theory if the logarithm of a random variable has a normal density distribution, the variable is said to have a lognormal distribution ($If\ \log(Y) \mapsto normal\ distributed \Rightarrow Y \mapsto \log normal\, distributed$). We visualized the distribution of log(FLNe) in **fig 1.10C** together with a normal fit (red curve) with a μ=2.9 and SD=1.2. The Q-Q (quantile- quantile) plot **fig 1.10D** provides an assessment of "goodness of fit" that is graphical, rather than reducing to a numerical summary. Here the plot of the predicted vs. empirical quantiles follows pretty well a unit slope indicating that the normal model is a good descriptor of the data. We also applied a Shapiro-Wilk normality test. The test statistic is:

$W = \dfrac{\left(\sum_{i=1}^{n} a_i x_{(i)}\right)^2}{\sum_{i=1}^{n}\left(x_i - \bar{x}\right)^2}$ where $x_{(i)}$ is the i^{th} smallest number in the sample and $\bar{x}$ is the sample mean.

The weights (a_i) are available in a statistical table. This test probes normality by matching two alternative variance estimates: a non-parametric estimator got by a linear combination of ordered sample values and the usual parametric estimator. The nul hypothesis H_o is that the data is normally distributed. We have a $p<<<0.05$ so we are forced to reject H_o and so consider that the log(FLN) frequency distribution is not normal. This leads to the conclusion that the data is not strictu sensu normal but the normal fit is the best approximation as opposed to any **t** function. A normal fit means fewer values in the tails as the **t** function has fatter tail.

In fact, the distribution of FLN values most closely resembles a log normal distribution. In (**Fig 1.9A, D, G**) we have fitted to the ordered log(FLNe) values a curve of predicted ordered values from a lognormal distribution. These curves satisfy the confidence intervals of the majority of data points in each of the three injections.

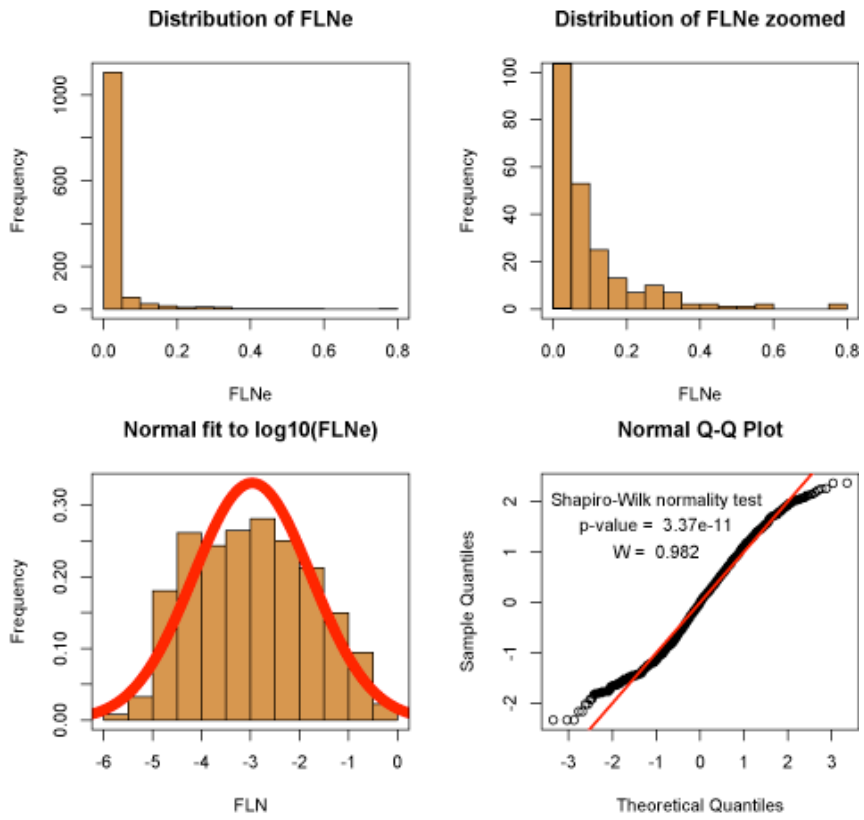

Fig 1.10 Distribution of FLNe. A: Histogram of FLNe values with unaltered scales. **B:** Same plot as in A but the y scale has been stretched so as to zoom-in to the low frequency values. **C:** Histogram of log(FLN) frequency distribution fitted by a normal distribution with the same mean and SD. **D:** Q-Q plot so as to graphically analyze the goodness of fit of a normal model.

An exponential distance rule (EDR) explains the lognormal FLN

Next we describe in detail a simple argument for the source of lognormals for FLNe distributions. The FLNe (denoted here by f_{ij}) of the projections from an area *j* to an area *i* is by definition the fraction of neurons projecting from the source (*j*) to the target (*i*), and as shown in (title 1.X) it can be used as the probability that an external projection (along single axon) into *i* is coming from *j*. Clearly, the distribution of the FLNe values is a *distribution of connection probabilities*.

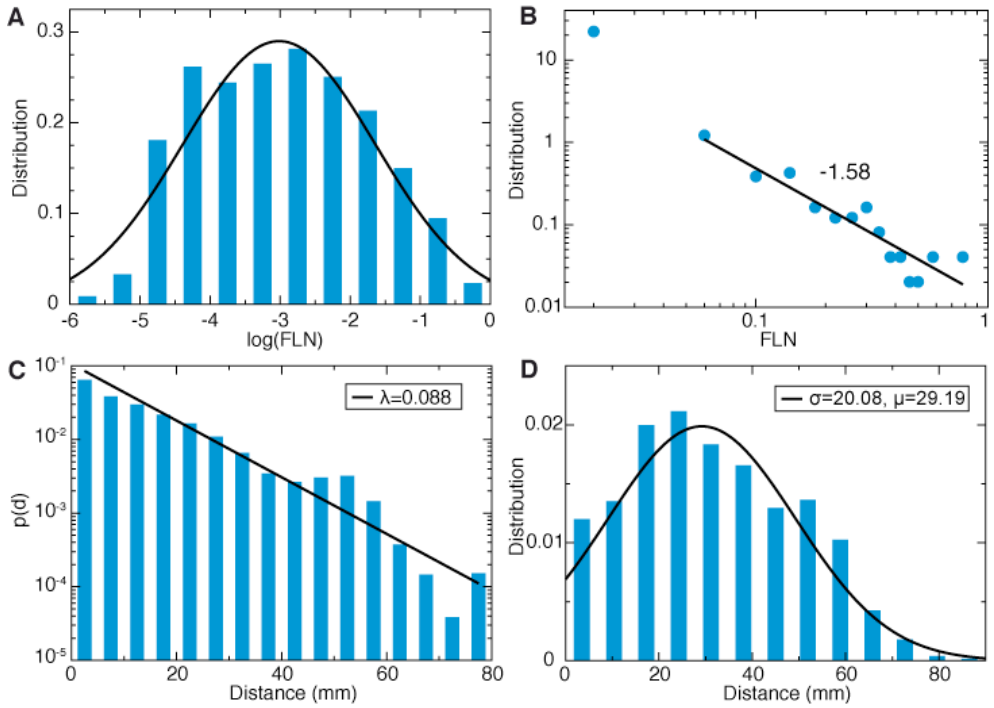

Fig. 1.11 Cortical distance rule. (**A**) The FLNe distribution is approximated by a lognormal: $\left(\beta\sqrt{2\pi}f\right)^{-1}\exp\left[\left(\ln f-\alpha\right)^2/\left(2\beta^2\right)\right]$, where *f=FLNe, α = 3.36, β = 3.21*. Here we show the plot in terms of log(*f*) (base 10) values, to better reveal the range of variability in decades (6 orders of magnitude variability, bin size 0.5). The continuous line is a normal distribution fit. (**B**) The FLNe distribution plotted on a log-log scale. The tail can be fitted by a power-law with scaling exponent -1.58. (**C**) Collecting all injections and all connections of $\boldsymbol{G}_{26x83}$, the fraction of labeled neurons projecting to a given distance (bin size 5*mm*) through the white matter decays exponentially with distance: $p(d)=\lambda exp(-\lambda d)$, $\lambda=0.088mm^{-1}$ (continuous line). (**D**) Distances were measured for each connection (ordered area-pair) in $\boldsymbol{G}_{26x83}$. The fraction of connected area-pairs separated by a given distance through the white matter (bin size 7*mm*) is approximated by a Gaussian (continuous line), $\mu = 29.19$ (mean), and $\sigma = 20.08$ (sd).

The pooled FLNe distribution for the 26 injections is heavy-tailed **(Fig 1.11B)** and resembles a lognormal (**Fig 1.11A**). The lognormal distribution of the FLNe is found to be the expression of a *distance rule* described as follows. The axonal lengths from the target areas to the source areas were estimated through the white matter as shown on (**Fig. 1.11.C)**, the fraction of labeled inter-areal neurons extending to length *d*, reveals an exponential drop with distance described as:

$$p(d) = \lambda\exp(-\lambda d), \qquad \text{(b.1)}$$

where $\lambda \cong 0.088mm^{-1}$. This can be interpreted as the *probability* of a single neuronal projection having a length *d* and will be coined hereafter as the Exponential Distance Rule (EDR). Next, we assume that this is an *average* physical property of neuronal projection lengths across the whole cortex, independent of the areal division (we will return to this later).

Accordingly, if the distance measured through the white matter from area *j* to area *i* is d_{ij}, then the probability of a projection into area *i* coming *from* area *j*, namely, the FLNe from *j* to *i*, is just simply $p(d_{ij})$, that is:

$$f_{ij} = p(d_{ij}) = \lambda\exp(-\lambda d_{ij}) \qquad \text{(b.2)}$$

or, alternatively

$$\ln f_{ij} = -\lambda d_{ij} + \ln \lambda \qquad \text{(b.3)}$$

Eq (b.3) shows that distances are in a linear relationship with the corresponding ln(FLNe) values, *on average:*

$$d_{ij} = -\frac{1}{\lambda}\ln\left(\frac{f_{ij}}{\lambda}\right) = -\lambda^{-1}\ln\left(f_{ij}\right) + \lambda^{-1}\ln\lambda \qquad \text{(b.4)}$$

As shown on (**Fig. 1.11.D)** the distribution of *inter-areal* distances (i.e., the fraction of *area pairs i,j* separated by a given distance *d*) can be closely approximated by a Gaussian:

$$\rho(d) = \frac{1}{\sigma\sqrt{2\pi}}\ \exp\left[-\frac{1}{2\sigma^2}(d-\mu)^2\right] \qquad \text{(b.5)}$$

where $\mu = 29.19$, $\sigma = 20.08$ **(Fig 1.11.D)**. Substituting for the distance values their expression as function of ln(FLNe)s from Eq. (b.4), we obtain the fraction of (ordered) area pairs that have a given FLNe value (connection probability) f:

$$\rho(d) = \frac{1}{\sigma\sqrt{2\pi}}\exp\left[-\frac{1}{2\sigma^2}\left(-\lambda^{-1}\ln f + \lambda^{-1}\ln\lambda - \mu\right)^2\right] = \frac{\lambda}{\gamma\sqrt{2\pi}}\exp\left[-\frac{1}{2\gamma^2}\left(\ln f - \nu\right)^2\right] \qquad \text{(b.6)}$$

where $\gamma = \lambda\sigma$ and $\nu = \ln\lambda - \mu\lambda$. Eq (b.6) shows that indeed, the FLNe distribution follows a lognormal and thus it is a heavy-tailed distribution. The fitted values of λ and σ yield $\gamma = 1.76$, which, however, is smaller than the one fitted from the experimental data, which is $\beta \cong 3.2$ (using natural logarithms). This discrepancy is an important aspect, and we discuss it next.

The exponential distance rule (b.1) is a property *averaged over a very large area* of the cortex (all labeled neurons for all injected areas), and therefore the averaging removed *all the biologically specific information* from this distribution. It is a *physical* property of a *typical* inter-areal neuron, and biological specificity will be organized around this property. Indeed, analysis of the axonal length distribution per every injection site reveals variability from site to site, however, these variations are all around the same average decay function described in (b.1). Accordingly, Eqs (b.2) and (b.3) also hold only *on average*, that is, *only part* of the FLNe between two areas is explained by the distance rule, the rest being determined by the biological and information theoretical specificity of the connections. **Fig. 1.12** displays all the ln(FLNe) values as function of their distances, indicating the variability around the average plotted with red symbols. The blue straight line is Eq. (b.3) with $\lambda \cong 0.088$ mm^{-1}.

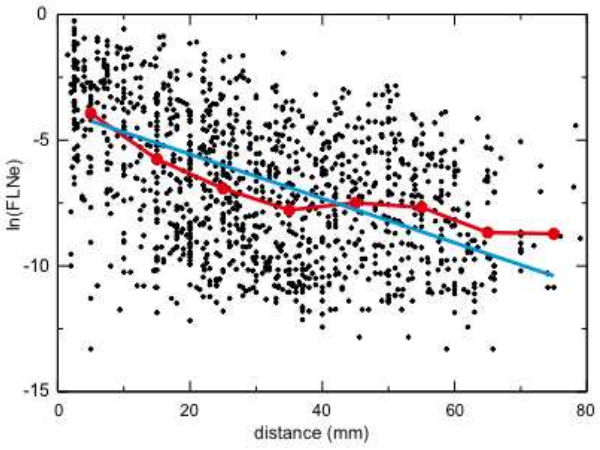

Fig 1.12 Scatterplot of log(FLNe) vs distance. Red curve indicates the average FLNe calculated at 10 mm intervals. Blue line corresponds to the prediction from equation b.3.

The distance rule is biologically non-specific, however it expresses the strong economy around connection lengths, which is large costs are associated with long wiring. This strongly shapes the cortical network structure, and since network topology heavily influences function, one expects this to be a selector for the types of information theoretic algorithms that the brain uses. Biological specificity is organized around this physical property of axonal lengths.

If instead of the distribution of the experimental ln(FLNe) values (approximated by a Gaussian) we consider the distribution of the *deviations from the average* of the ln(FLNe) for every injection site, that is $q_{ij} = \ln f_{ij} - \nu_i$, we remove some of the non-distance specific variability, associated with an injection. **Fig. 1.13** shows the distribution of q_{ij} where for each injection i, the ν_i was calculated from the experimental data as the average of the ln(FLNe) values ($\nu_i = \langle \ln f_{ij} \rangle_i$). Fitting the data yields a standard deviation of *2.08* (black curve), indeed, much closer to the theoretically predicted value of $\gamma \cong 1.76$ (blue curve in **Fig 1.13)**.

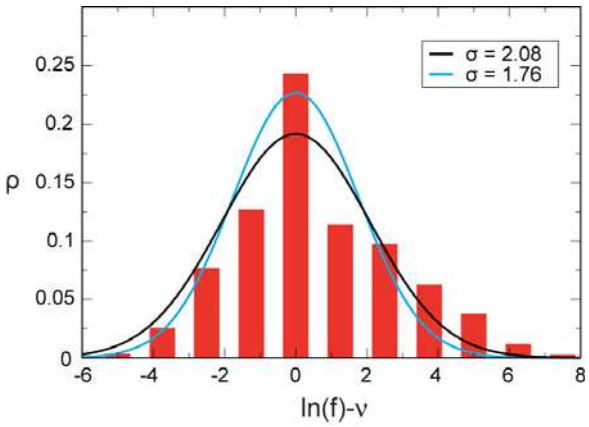

Fig 1.13 Histogram of the deviation from the average Log(FLNe). Light blue is a normal fit with sigma parameter corresponding to the value estimated by the distance rule. Black curve is a normal fit with sigma parameter derived from the experimental data.

Discussion on the connectivity profiles

A major finding of the present study is that our optimization allows us to obtain evidence of a large number projections previously unreported. One concern could be that the way we use these tracers could allow transynaptic transport. We have firm evidence that this is not the case. Area V1 is devoid of callosal connectivity **(Dehay et al., 1988)**. In the present study even the massive injections of area V1 failed to show labeled neurons in the contralateral hemisphere, which would be the case if label were to be trasported transynaptically via extrastriate cortex.

Scannell et al **(Scannell et al., 2000)** suggested that connection strengths are as variable as a geometric distribution and might require the analysis of 10 - 20 injections to adequately characterize the profile for a given area. We demonstrate here that while connectivity strengths do display significant overdispersion, we can exclude the hypothesis that they are geometrically distributed; their variability can be bracketed and their distribution characterized. This characterization has permitted us to obtain reliable estimates of connectivity profiles and their variability using data from 3 - 5 injections.

The small FLNt of the thalamic input to the cortex **(Fig 1.8D and Fig 1.2F)** coupled with the high FLNt values of intrinsic connectivity **(Fig 1.2A)** fits with the evidence that local recurrent excitatory networks amplify a numerically sparse feedforward signal **(Douglas et al., 1995)**. For instance, we find that the FLNt of the lateral geniculate nucleus projection onto area V1 is 0.16% **(Fig 1.2E)**. This result is consistent with the fact that fewer than 6% of all synapses found in area V1 arise from the lateral geniculate nucleus **(da Costa and Martin, 2009)**. The

intrinsic FLNt of area V1 that we observe is 85%, consistent with the vast majority of synapses in area V1 originating from local neurons **(Binzegger et al., 2004)**. The present results showing low subcortical FLN values indicates that this pattern is repeated across the cortex and reveals the high investment of the cortex in local processing. The massive allocation of the neuronal resources of the cortex to local processing and its ongoing patterned activity likewise accounts for much of the brain's energy consumption **(Tsodyks et al., 1999, Kenet et al., 2003, Raichle and Mintun, 2006)**. This view of the cortex emphasizes the importance of intrinsic operations, so that the input to a given level of the cortical hierarchy interacts with ongoing activity.

Short-distance interareal connections from neighboring areas may provide inputs that interact with recurrent local connectivity very much in the same way as the feed-forward inputs from the thalamus to cortex as described above. However, long-range interareal pathways have FLNe values up to 4 orders of magnitude weaker than the FLNe of the lateral geniculate (see **Fig 1.8.CD**). Plausibly, these surprisingly weak cortico-cortical connections are employed for long-range coordination of neuronal assemblies, possibly required for high level representations **(Buzsaki and Draguhn, 2004).** Interaction of ascending activity with ongoing activity of dense local networks may contribute to multiple brain rhythms, which are in some way controlled by the long-range very sparse connections **(Kopell et al., 2000, von Stein et al., 2000, Buzsaki, 2007, Lakatos et al., 2008, Uhlhaas et al., 2009).** Importantly, these long-range connections are not randomly organized but instead, as shown here, link specific sets of areas (**Table 1.2**) and have strengths that are consistent within a range of 5-8 although some of the weakest projections have a variability exceeding 10-fold **(Fig 1.8C)**. The function of the long-range cortical connections could complement non-specific cortico-thalamic loops **(Llinas et al., 1998)**. In this respect cortical-claustrum loops could also be important **(Crick and Koch, 2005)**, as an intriguing finding in the present study is that the claustrum input to the cortex is the strongest subcortical input (**Fig 1.2F, Fig 1.8D**).

We find that the FLNe values for injection in a given target area follow a log normal distribution. This is a heavy-tailed and heterogeneous distribution but is different from a power law. While log normal distributions have been reported for a number of biological phenomena, importantly they are found for the non-zero synaptic strengths on single cortical neurons **(Song et al., 2005).** An interesting parallel can be drawn between inter-areal (long-range) and intrinsic (local) properties: (i) As we have shown here, local, intrinsic connectivity, shows an exponential decay in density, echoing the decrease in the likelihood of synaptic contact with distance **(Braitenberg and Schüz, 1998);** (ii) Intrinsic source distributions, just like the extrinsic inter-areal source distributions, have a "patchy" character **(Yoshioka et al., 1992)**; (iii) lognormal distributions like that described here for interareal weights, have been found for the distribution of synaptic strengths of single neurons **(Song et al., 2005)**. These parallels, at both the cellular and areal levels, suggest that similar logical principles might be functioning over multiple scales.

The present findings increase by nearly 30% the number of projections on to the well-studied visual areas, confirming that an analysis based purely on binary connectivity reveals little specificity. Areas V1, V2 and V4 each receive input from 26 areas (including the intrinsic connectivity). V1 and V2 are distinguished by input from only 4 different areas, meaning that they have a 15% difference in their input profiles. The differences between V1 and V4, and between V2 and V4 are both double that of V1 and V2, indicating a difference of 31% in both cases. If we consider inputs from areas that have no overlapping error bars in Fig 4C as being distinct, then the input differences double and become 31% for V1 vs V2, and 69% for V1 vs V4, and 73%for V2 and V4. Hence these results show that the strength of connection makes an important contribution to defining the connectivity profiles of these areas, despite the high variability of the strengths of the weakest projections. The observed projection strength variability is sufficient to endow specificity to the circuit given the nearly 6 orders of magnitude of the connectivity profile span. In this respect it is worth noting that increase in the size of the injection showed an important increase in the strength of the weak projections, suggesting that connectivity profile span could be greater than 6 orders of magnitude (**Fig 1.14**).

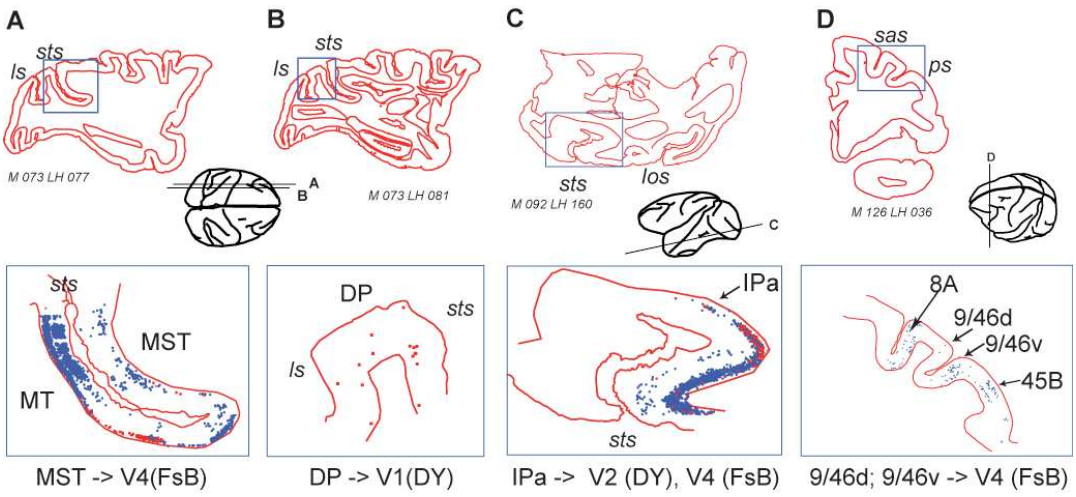

Fig 1.14 Effect of increased injection size on the number of neurons in weakly labeled new projections. **A:** Massive injection of diamidino yellow on the lateral part of the dorsal operculum of the striate cortex and the fast blue on prelunate gyrus generate increased label in area MST. **B:** Same injections on the operculum as in **A** leads to increase of label in area DP on medial levels of the prelunate gyrus. **C:** Horizontal section and pattern of labeling in areas TE and IPa after massive injections in V2 (red) and V4 (blue). **D:** Increased labeling in the region of the arcuate sulcus and the principal sulcus of prefrontal cortex (8A, 9/46d, 9/46v, 45B) after massive injections on the prelunate gyrus. Abbreviations: FsB: fast blue; DY: diamidino yellow

The availability of quantitative macaque connectivity maps plus associated visualization software (**Fig 1.8E**) provides a valuable resource for the nascent field of connectomics, which ultimately aims for a comprehensive understanding of local and long-distance brain circuitry **(Sporns et al., 2005)**. MR-based neuroimaging methods now enable inferences about long-distance cortical connectivity patterns in humans and nonhuman primates. However, technical limitations to these imaging methods are fraught with technical limitations can lead to many false-positives as well as false-negatives when estimating the likelihood of connections **(Honey et al., 2009, Johansen-Berg and Behrens, 2009)**. Thus, there is an acute need for independently derived high-fidelity connectivity maps that can serve as references for evaluation and quantitative comparisons. The maps reported here, plus additional data on connectivity for many other areas **(Markov et al., 2011)** will be invaluable in this regard. The most direct use will be for comparison with other studies of connectivity in the macaque (e.g., **(Vincent et al., 2007a)**). Comparisons with human cortex will be facilitated by methods for landmark-constrained interspecies registration between the macaque F99 map used here and the human PALS-B12 atlas **(Van Essen, 2005)** on which R-fMRI connectivity maps **(Fox et al., 2005, Fox and Raichle, 2007)** and many other data have been mapped. Even though there assuredly are major differences in cortical connectivity between macaque and human, many pathways are likely to have been conserved over evolution. Hence, macaque connectivity maps registered to human cortex using known or strongly suspected homologies as constraints will provide an important basis for evaluating in vivo estimates of human connectivity.

In summary, the present results show two general features of the cortex. Firstly, cortical neurons are massively involved in local circuitry; relatively sparse connections form the main links between processing levels. Secondly, the strength of a given pathway is consistent across individuals, and the range of strength of connections within an individual extends over 6 orders of magnitude, resulting in a stereotyped connectivity profile for each area. Together these findings emphasize the role of strength of connectivity in specifying the connectivity of the cortex and are expected to be important in future and ongoing endeavors directed at elucidating

the connectome. FLN values are expected to provide further functional insight concerning individual projections. For instance, the newly discovered projections of PERI onto the early visual areas like the amygdala have FLN values that are surprisingly high for these extremely distant projections, and lend support to recent cortical theories of inference based on memory prediction **(Hawkins et al., 2009)**.

Chapter II

Network properties of the cortical Graph

Introduction to graph analysis

There is considerable interest in understanding how information flow through the cortex at the areal level is shaped by its organizational principles **(Felleman and Van Essen, 1991, Young, 1992, Goodhill et al., 1995, Jouve et al., 1998, Sporns et al., 2000, Kaas and Collins, 2001, Laughlin and Sejnowski, 2003, Vezoli et al., 2004)**, and the expectation that, an important grasp of the computational capabilities of the cortex will be obtained from a network description of its structure **(Watts and Strogatz, 1998, Barabasi and Albert, 1999, Watts, 1999, Newman, 2003, Boccaletti et al., 2006)**. Previous descriptions of cortical topology have been restricted to binary connectivity (areas being connected or not) **(Felleman and Van Essen, 1991, Young, 1992, Goodhill et al., 1995, Jouve et al., 1998, Scannell et al., 2000, Sporns et al., 2000, Kaas and Collins, 2001)**. One conclusion that came out of this work was that the interareal network shows high clustering and short path lengths and therefore, it qualifies as a small-world graph **(Hilgetag et al., 2000a, Sporns et al., 2000, Stephan et al., 2000, Sporns and Zwi, 2004)** as defined by Watts and Strogatz **(Watts and Strogatz, 1998)**. The small-world architecture is a provocative concept for understanding the brain, as it suggests an efficient means of optimizing the integration of local and global processing **(Bullmore and Sporns, 2009)**. However, the claims for a small-world interareal network were based on the analysis of collated anatomical databases in which the connectivity status of pathways was incomplete **(Hilgetag et al., 2000a, Sporns et al., 2000, Stephan et al., 2000, Sporns and Zwi, 2004)**. Our cortex-wide tract-tracing experiments reported here reveal that over 66% of all the possible interareal connections exist. At such high densities, binary graphs carry little structural specificity (short paths and high clustering being a direct consequence of high density), forcing us to go beyond binary representations.

Previous work showed that the link strength between areas has a strong signature as well as a range over *6* orders of magnitude. Together, these two features suggest that link strength may be important in determining cortical physiology and function **(Markov et al., submitted)**. Here we uncover the relationship between link strength (based on neuron counts) and projection distance (a physical property) that in turn predicts both binary and weighted properties of the empirical interareal network. These physical and geometrical parameters

(Feinerman et al., 2008) must be taken into account in order to understand the fundamental features of cortical organization **(Barthélemy et al., 2005, Boccaletti et al., 2006).**

Construction of the cortical graph

Graph analytical studies usually rely on the available databases, (ex. CoCoMac) in order to build networks representing cortico-cortical projections. The disadvantage of this method is the existence of contradictory and incomplete data in these collated information sources. In our large-scale anatomical investigation of the macaque cortex we employed retrograde tract-tracing with identical protocols so as to generate a consistent and extensive database where the prospection for pathways outstands in rigour the usual anatomical explorations restrained to subsystems within the cortical network. Moreover we have quantified the weight and length of interareal connections, (data fully available in **Table S1**). In the previous chapter we have shown that retrograde tract-tracing with high sensitivity fluorescent tracers (fast blue and diamidino yellow) reliably labels the somas of neurons in the (source) area projecting to the injected (target) area **(Barone et al., 2000).** We segment the brain in to 83 areas covering the whole cortical sheet, these represent the maximum set of possible source areas to a given cortical target. By brain-wide scanning of 40μm histological sections we determine the full set of source areas for each injection from the maximum set of 83 areas **(Annex 2-Atlas)**. When a projection is present from area Y on the injected area X we record the physical distance of the projection as well as the projection magnitude expressed in the FLN value of Y that is calculated as $FLNe = \frac{Nb\,neurons\,counted\,in\,X}{Total\ of\ extrinsic\ counts}$ (**Table S1**). The FLNe is comparable across injection sites and can be used to characterize the strength of the pathways for network analysis. Previously we have shown that for any given target, both the source list and its FLNe profile is highly reproducible and therefore, even the weakest pathway provides a reliable participation to the connectivity pattern **(Markov et al., submitted)**. Injections were made in 26 target areas (V1, V2, V4, TEO, TE, DP; PBr; STPr, STPi, STPc; 7A, 7B, 2, 5, F1, F2, F5, F7; 24c, ProM, 46d, 9/46d, 9/46v, 8A, 8B, 45B), evenly distributed across the cortical lobes **(Table 2.1)**.

Table 2.1: Distribution of injection sites and labeling in cortical lobes.

						Column G		
Lobe	**Nr of areas injected**	**list of injected areas**	**Nr of areas in the lobe**	**% in the lobe being injected**	**% of labelled areas not being injected**	**Average total degree in each lobe**	**Total brain areas**	**Brain density if all areas with degree as in column G**
Occipital	4	V1, V2, V4, DP;	8	50	50	32,75	83	39
Parietal	4	2, 7A, 7B, 5	18	22	78	39	83	47
Temporal	6	TEO, STPr, STPi, STPc, PBr, TE;	21	29	71	52,16	83	63
Frontal	5	24c, F5, F1, F2, F7	13	38	62	46,6	83	56
Prefrontal	7	ProM, 8A, 45B, 9/46d, 9/46v, 46d, 8B;	23	30	70	57	83	69
Total brain	26		83	31		47,38	83	57

The N_F = 83 areas form the Full Inter-areal Network (FIN), which is a directed, weighted, spatially embedded graph $\boldsymbol{G}_{83x83}$ on 83 nodes. The projections among the N = 26 injections have uncovered a total of E = 1232 edges of $\boldsymbol{G}_{83x83}$, forming the currently known subgraph $\boldsymbol{G}_{26x83}$ of FIN. The link weight w_{ij} of a projection (ißj) is associated with its magnitude of neuronal resources of the projection (FLNe), f_{ij}. In the efficiency analyses we set w_{ij} = -log(f_{ij}), for information theoretic purposes.

The 26x26 directed graph $\boldsymbol{G}_{26x26}$ formed by projections *among the injected sites only*, has full connectivity information within this set. Accordingly, $\boldsymbol{G}_{26x26}$ is an *edge-complete* subgraph of the FIN. Given that injected areas are evenly distributed across the cortex, many statistical properties of $\boldsymbol{G}_{26x26}$ are representative of that of the FIN.

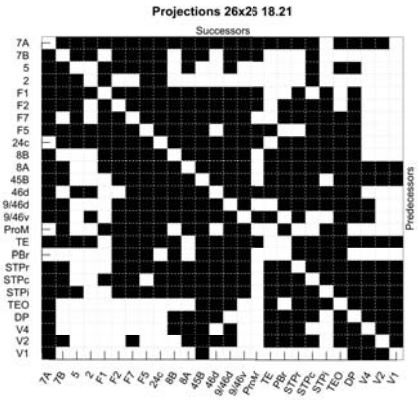

Figure 2.1. Adjacency matrix of the $\mathbf{G}_{26x26}$ cortical graph.

It is not a "small-world" it is a "tribal" network

The small world phenomenon

In the late 90's some papers describing the dynamics in oscillating systems expressing "small-world" architecture gained large popularity (Watts and Strogatz, 1998, Watts, 1999). The attractiveness of the "small-world" concept resides in the discrepancy between the perception of a highly ordered system where the characteristic path length should be long and the actual measures revealing $L \approx \frac{\ln n}{\ln k}$. Watts formalized 4 necessary conditions in order of assessing a network as having the small world property:

1. The network is numerically large i.e. the number of nodes is high $n >> 1$.
2. The network is sparse in the sense that $if\ n \approx 10\text{^}6\ then\ k \approx 10\text{^}3$.
3. The network is decentralised in that there is no dominant central vertex to which most other vertices are directly connected. This implies a stronger condition than sparseness: not only must the average degree k be much less than n, but the maximal degree k_{max} over all vertices must be much less than n.
4. The network is highly clustered.

Small world phenomenon was described to occur as the coincidence of high local clustering and short global separation, shown to be a general feature of sparse, decentralized networks that are neither completely ordered, nor completely random (**Watts, 1999**). These properties characterize a range of graph configurations where the two extremes are on one side a completely regular and a completely random graph on the other side **(Watts and Strogatz, 1998**). Starting with the regular graph one can rewire this sparse network with given probability ($0 \leq p \geq 1$) where the fully random graph corresponds to p=1. Rewiring with full spectrum of

the probability p generates an interval where the graphs satisfy the up-mentioned conditions and the characteristic path length is comparably low as in the random graph while the average clustering is as high as in an ordered graph. It is not clear how this property is affected by the density of the graph (cf. "small-world" condition 2). We have tested this and the results shown in **Figure 2.4** actually illustrate the dependence of the occurence of the small world permissive conditions on the graph density where densities above 45% do not permit the definition of the region with low *L* and unaltered *C*. The "small-world" property has been found in networks of : film actors collaborations, power grid and neuronal connections of *C. Elegans*. All these networks respond to the 4 conditions postulated by Watts, but what about the inter-areal cortical network? Before answering to this question we will draw a very rough sketch of the importance of the "small-world" concept about the understanding of the structure of the cortical network.

Is the "small-world" concept improving the understanding of the brain network?

Small world networks have been described as being optimal on one side for functional segregation (clustering) and global integration (short characteristic path length) (**Basset Bullmore 2006, Bocaletti 2006,Deco Friston 2008, Fair Petersen 2009,Sporns 2007,Sporns and Honey 2006 small worlds big brains,** Newman 2003). Another attractive characteristic is the fact that, if you consider the wiring minimisation, "small-world" show to be very economical by minimising total wiring length (**Chklovskii et al., 2002**).

While the small world property has various definitions and usages in the literature, it was originally defined within the context of social networks, expressing the surprising fact that everyone in the world is connected through a few handshakes (small diameter: "six degrees"). The small world effect happens in spite of the large size and *sparse character* (the number of our acquaintances is extremely small compared to the whole population of more than 6 billion) of the social network and the fact that our friends tend to also know each other (high clustering). It is a mathematical fact that it is easy to rewire any *sparse graph* (the number of edges is on the order of the number of nodes) to have large diameter and low clustering, and therefore if a sparse real-world network was observed to have small-world properties, then this is due to the special processes that have led to its formation, presenting new/independent information about the system. In contrast, dense networks (number of edges approaching to the order of the square of the number of nodes) will invariably have low diameter and high clustering, and the small world property in this case gives no independent/additional information about the system.

What is the density of the cortical network?

The cortical density in previous studies

The cortical network of the mammal brain has been extensively explored in the frame of the small world phenomenon **(Hilgetag et al., 2000a, Sporns et al., 2000, Stephan et al., 2000, Sporns and Zwi, 2004)**The exploration and description of brain connectivity is a hard task that can be undertaken at different levels of the cortical structure. Since Brodman, the exploration of the monkey brain has separated the cortex in to ~100 areas based on cytoarchitectural, functional and connectional characteristics. It is of broad interest to understand the architecture of the network formed by the interconnections amongst these areas. The original anatomical studies were describing the afferences of few areas and more frequently were restraining the interest of the exploration to the lobe being injected. Low tracer efficiency and not exhaustive prospection for projections, make the data in the vast majority of publications not complete for a network approach. Tempts to compile the knowledge about the cortical brain network have been done first by anatomist and later on by network scientists. The following table shows some of the milestone studies since an effort is made in exploring the brain network with graph theoretical methods.

Table T2.2. History of..

Authors	Density	Binary	Note

FVE91	*30 - 40% up to45%*	*No*	*Acknowledging lack of data and possible density up to 50% if all projections were reciprocal*
Jouve 98	*37% predicts 59%*	*Yes but he takes in to accont the undocumented projections*	*He updated FVE with later bibliography and has more stringent area definitions.*
Tononi Sporns 2000	*~25-35%*	*Yes; Unknown is put absent*	*Compares random n/k defined graphs to FVE91*
Sporns 2007	*23%*	*Yes, handmade extraction of cocomac*	
Young 1993	*15%whole cortex (73 areas 758 conexions); 37% Auditory system (16 areas/95 conn) 35% Somatomotor system (17 areas 100 conn)*	*Yes. Recognizes that further studies will uncover new projections.*	*Unexplored pathways are declared absent*

If we follow the timeline of this process we see that. The study of Felleman and Van Essen considers the known and unknown connections and acknowledges that the brain connectivity is only partially known (**Felleman and Van Essen, 1991)**. The authors of this paper that makes a compilation of around 300 existing studies show that they are conscious about the fact that the density of the cortical network is unknown. They try to estimate the density of the network based on their "partial data" and suggest that if you estimate the density of only the explored projections the brain density is of 45%, if on the other hand the observed tendency of reciprocallity of brain projections is taken in to account and the known projections are considered reciprocal the estimated density of the brain attains 50%. In his later publication Jouve tackles the question of the brain density in an elegant and objective manner. Jouve increments the network of FVE with several newly discovered projections. He obtains a density of 37%, only 7% more than FVE. He observes that cortical connections are characterized by a property that is the second order connectivity i.e. that the existence of many second order connections between two areas is very strong predictor for the existence of a direct connection between the two areas. Running an algoritm implementing this rule Jouve predicts a density of 59%. Young also will publish a brain network that he builds based on available data (**Young, 1993**). He tempts to build a network of the whole brain and obtains a sparse network of 73 areas and 758 connections with density = (15%) where different subsystems show higher density (35-37%). The author acknowledges that this tempt to build a network is subjected to the limited knowledge of the time.

The interesting results obtained by the exploration of the brain network led to the idea to deposit in to a database what is known about the brain pathways. Later studies of the brain will rely on this database for obtaining their networks. The graphs build of these databases are with density of (23-30%) (Honey et al., 2007, Sporns et al., 2007). The reason of this decrease in the estimated density of the brain network is that when the interest on the brain shifted from anatomical to network science descriptions there was a shift in the paradigm where all unknown projections suddenly become considered as absent. This was caused by the constraint of using binary adjacency matrices for graph-theoretic analysis. Although fortuitous this made the network sparser and let the door open to having, a "small-world" architecture of cortex. In parallel the sparse neuronal ganglion network system of a worm (*C. Elegans*) that does not present high level of cephalisation has become completely known. It has been qualified as a "small-world" (**Watts and Strogatz, 1998**).

Our exploration of the cortical network reveals a dense graph

We did an extensive effort to compile the reported cortico-cortical projections by a large exploration of the available literature (cf **Table S2**). When compared to our results this revealed that we have discovered 30% more pathways than previously reported. This has been made possible by the optimized labelling techniques combined with improved and extensive brain scanning **(Barone et al., 2000, Falchier et al., 2002)**. If we fill up $\mathbf{G}_{26x26}$ with only the connecitons published in the litterature we obtain a graph density of around 47% already higher than the maximum that will permit the occurrence of the small world phenomena. This means that we have a connectivity matrix density considerably higher than those used in earlier studies of cortical networks (**Table S2 anf figure 2.2**) **(Felleman and Van Essen, 1991, Young, 1993, Sporns et al., 2000, Honey et al., 2007)**, but importantly comparable to earlier anatomical studies (**Table 2.2**.) **(Jouve et al., 1998, Kaas and Collins, 2001)**. The novel projections are predominantly long distance and weak (small FLNe) and therefore have an important influence on the average shortest path length (**Fig 2.5A**). **Fig 2.5A** shows that the average shortest path length is most sensitive to the sequential removal of the weakest links, when compared to random link removal.

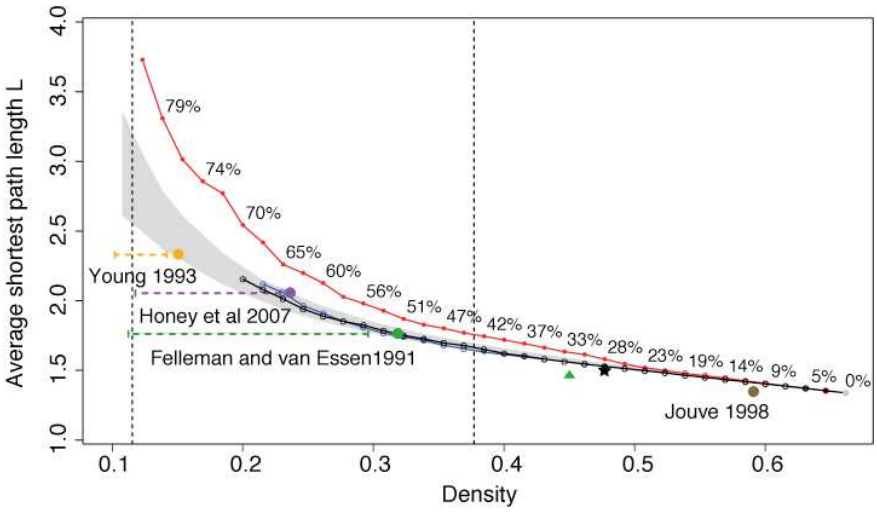

Figure 2.2 Average shortest path length *L* (directed, binary) for various link removal scenarios in $\boldsymbol{G}_{26x26}$, matched with known densities from literature. Grey dot: $\boldsymbol{G}_{26x26}$ (66% density, 26 nodes, 430 links). Removal of connections, red: weakest, blue: strongest, black: intermediate. Curves stop when removal of additional ten connections causes unreachability. Grey area: 95% confidence interval following random removal. Green: Felleman and Van Essen, 1991; orange: Honey et al., 2007 (47 nodes, 505 links); purple: Young 1993 (71 nodes, 746 links). Green triangle: value predicted by Felleman and Van Essen. Black star: removal of all new connections in present study. Brown: predicted value Jouve et al., 1998.

The $\boldsymbol{G}_{26x26}$ graph has M = 430 links from the maximum possible of $N(N-1)$=650, and therefore it is densely interconnected, with a graph density of $p=M/N(N-1)$=0.661 (66%). At such high density values, these graphs have necessarily a short average path length (average directed binary path length = 1.34 for $\boldsymbol{G}_{26x26}$), small diameter (= 2), and high clustering coefficient (= 0.87 for $\boldsymbol{G}_{26x26}$) **(Watts and Strogatz, 1998)**.

Given that $\boldsymbol{G}_{26x26}$ is dense, $\boldsymbol{G}_{83x83}$ is also dense, as shown next. The in-degrees in $\boldsymbol{G}_{26x83}$ range from 23 to 68 with a mean of 47.38 and a distribution that is fairly concentrated around the mean (**Fig. 2.3**). The injected areas represent 31% of the total of 83 areas so the average degree calculated for $\boldsymbol{G}_{26x83}$ is expected to be a good estimator of the average degree of FIN. The density of FIN can be easily predicted by $p_F = \langle k_F \rangle /(N_F-1)$ = 0.578 (57%). This infers that the total cortical network is also a dense graph.

Dominating sets

Additionally, a simple dominating set analysis on $\boldsymbol{G}_{26x83}$ provides further evidence that the FIN is dense. Injection into only 5 areas suffices to recover projections from all 83 areas, revealing a minimum dominating set (MDS) of 5. A low MDS indicates either a very dense graph, or a graph dominated by hubs (**Barabasi and Albert, 1999**). The latter property is, however, unsupported by the in-degree distribution **Fig. 2.3**, and by the fact that there are many (203) different sets of such 5 areas. Moreover, all combinations of 8 sites (out of 26, about ~1.5 million) will dominate at least 90% of all the areas (**Table 2.3**). As more injections add links but not nodes, they can only enhance these strong domination effects confirming that the FIN is indeed a dense graph.

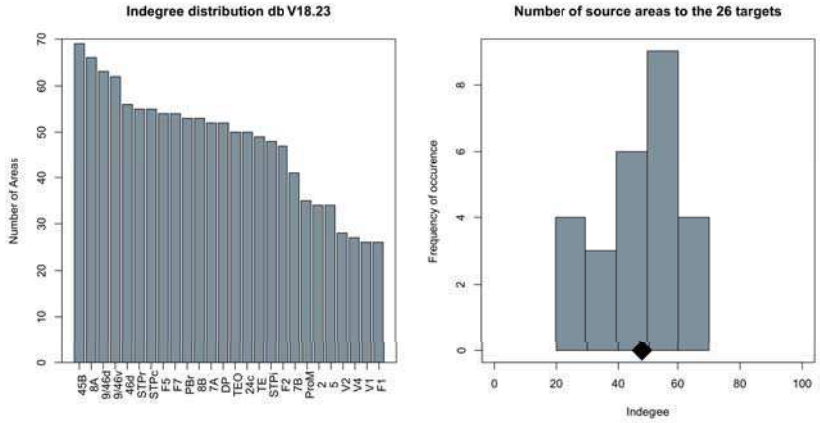

Fig. 2.3. In degree distribution in G_{26x26}

In graph theory, a subset D of nodes of a graph G with node set V is said to be dominating G, if all elements of V outside of D have a link to a node (or more) in D. Here we slightly modify this definition by saying that *D dominates x% of the nodes of G*, if an x% of *all* nodes in V have a link incident to a node (or more) in D. The x%=100% corresponds to "full" domination. Note that our definition includes also nodes from D. The minimum dominating set D_{min} fully dominates G and it has the smallest size (nr of elements). As one can see from **Table 2.3**, for example, considering all sets of 3 target area combinations from the 26 (a total of 2600 combinations), 51.8% of them dominate between 80% and 90% of the 83 areas. Specifically, over 2600×0.518≈1346 injected area triples will have between 66 and 74 areas projecting into them. There are 203 (= 0.003087×65780) combinations of 5 injected areas, the minimum dominating sets, which will have all the 83 areas projecting into them.

Table 2.3. Dominating sets for the cortex. 'Targets' is the dominating set *D* size (nr of injected sets).

Targets	1	2	3	4	5	6	7	8
Nr of sets	26	325	2600	14950	65780	230230	657800	1562275
Dominated size (%)	Percentage of sets							
0-10	0.0	0.0	0.0	0.0	0.0	0.0	0.0	0.0
10-20	0.0	0.0	0.0	0.0	0.0	0.0	0.0	0.0
20-30	3.8	0.0	0.0	0.0	0.0	0.0	0.0	0.0
30-40	15.4	0.9	0.0	0.0	0.0	0.0	0.0	0.0
40-50	11.5	0.3	0.0	0.0	0.0	0.0	0.0	0.0
50-60	7.7	2.8	0.1	0.0	0.0	0.0	0.0	0.0
60-70	46.2	12.0	1.6	0.1	0.0	0.0	0.0	0.0
70-80	11.5	35.1	8.8	1.4	0.1	0.0	0.0	0.0
80-90	3.8	44.9	51.8	21.2	5.6	1.1	0.2	0.0
90-100	0.0	4.0	37.7	77.4	94.0	97.4	95.9	92.4
100	0.0	0.0	0.0	0.0	0.3	1.5	3.9	7.6

Does the small world have sense in a dense network?

A lattice network has high clustering and long path-lengths. A random has low clustering and short path-lengths. The small world stands midway between the highly ordered lattice network architecture and the random network architecture. The architectural originality of the small world resides in the fact that it reveals the high clustering relevant for an ordered lattice network and an element of randomness that ensures short path-lengths as in the random graph. Rewiring a sparse lattice network shows an interval where the clustering remains high while path-lengths become low. Rewiring a dense network does not lead to a, interval where pathlength decreases while clustering remains high (**see fig 2.4**).

On the other hand the average path-lengths lower than 2 are obvious for a density above 50%. In a dense network it is highly likely that some nodes attain high degree of connectivity and so the requirement of decentralisation is hard or impossible to obtain. In conclusion short path-lengths and high clustering are not typical of sparse graphs, but if they do occur, they signal a very special property of the network, namely its "small-world" architecture. However, for dense graphs (such as $\boldsymbol{G}_{26x26}$) short paths and high clustering are a direct consequence of density, and they are uninformative about architectural specificity.

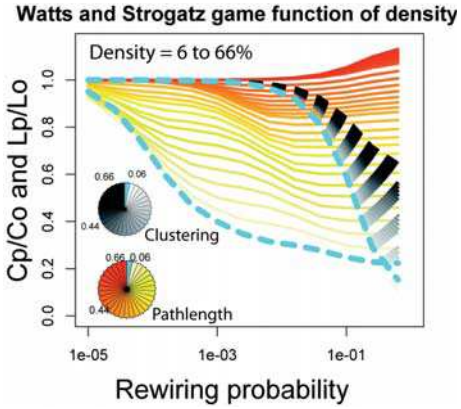

Fig 2.4 The effects of graph density on the extent of small world permissive interval. Starting with a lattice of 1000 nodes and 30 neighbors per node (density 6%) we explore the effect of increasing rewiring probability on the measures of characteristic path-length and average clustering. The game is repeated for graphs with increasing density (results are coded by a color gradient). At density 44% there is no more reduction in path-length going from the lattice to the random end of the chart. The color wheels show the code for the density of the network being rewired.

To confirm the no small world nature of the real cortical network we compared the removal of connections starting from the weakest with the effect of simple random removal of the same number of edges (**Fig 2.5**). This confirmed that the effect of removal of either weak links or random edges does not affect the clustering in a sensitive way. On the other hand the characteristic path length has been significantly more increased by the removal of weak links than by the random edge removal i.e. the weak links are collapsing the graph diameter.

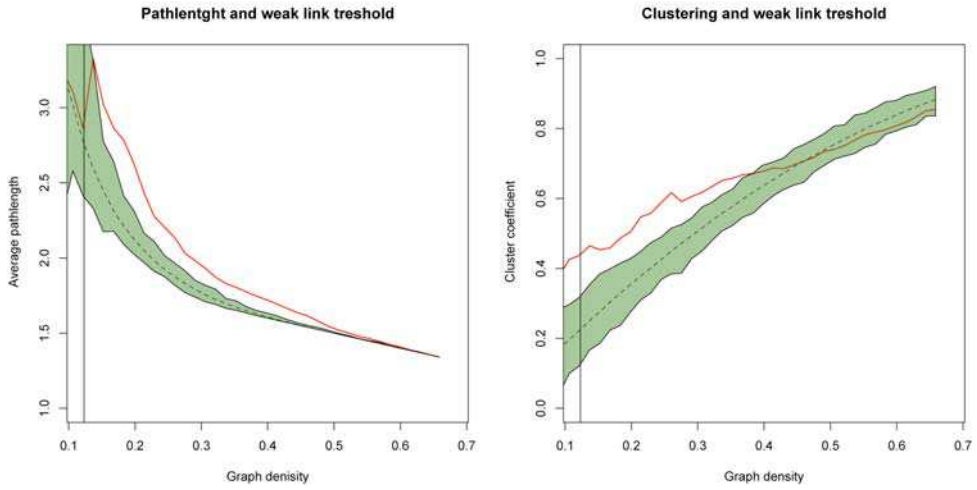

Figure 2.5 Effect on path-length and clustering on the removal of week links. The green zone corresponds to 1000 measures for random $G_{n,k}$ graphs with 26 nodes and density varying between 10 and 66%. A dashed line indicates the mean value. Red line corresponds to G_{26x26} after gradual treshold starting from the weakest connections. Vertical line indicates the density of the first moment when unreachability occurs within G_{26x26}. Note that this also corresponds to what we later identify as the "backbone" graph (cf. the paragraph on weighted network analysis).

The "tribal" network

The interareal network is actually a dense network, and it does not correspond to a "small-world". One of the fascinating aspects of network science is that basic properties of networks are found across many widely different physical systems. If the binary properties of inter-areal cortical connectivity do not constitute a small world, what type of social network does it resemble?

Analogy can be found in another class of social networks. Human societies are evolving systems and small world networks have been identified in modern urban society. An early societal structure is the tribe, which is composed of 100-200 individuals, unified by common language, and culture. The characteristic feature of the tribe is that the majority of individuals are directly related to each other (high density). In the evolving human society the increase in scale (size) first led to the imperial structure where the network of interactions is centralized around a principal node, "the emperor", and the density of the network is reduced compared to the tribal society. This intermediate structure has given rise to modern society, retaining the sparse structure of the imperial network but at the same time it has also been decentralized. The major difference between the tribal and modern world is in the density and scale of the connected network.

Up to the 1960's anthropology largely focused on the social structure of tribes in different parts of the globe, employing largely empirical methodology, without the use of graph theoretical methods. Later when studies focused on the modern society the graph theoretical methods became an increasingly attractive method of investigation. Milgram's famous chain-letter experiment (**Milgram, 1967**) emphasized the surprisingly small diameter of the large-scale modern society and introduced the concept of the "small-world".

Hence, the notion of "small-world" is very descriptive and useful in the framework of modern society, as it gives insight in to the role of social dynamics in shortening the diameter of an otherwise very large graph. But the small world graph is irrelevant to the tribal societal structure. The anthropologists who have explored the tribal network have rightly paid little attention to the "small-world concept". On the contrary, they claim that the high density and small scale of the tribal network are the major elements underlying its functionality. It is then interesting to uncover graph theoretic methods that will be able to analyse such, small scale, dense graphs as the tribe or the cortical network. Some of the suggestions of social sciences are that these networks are well adapted for rumor propagation and building of consensus. This may find echo in the ability of the cortical network to operate through synchronizing areas operating on the same task.

Conclusion. Our proposition of a tribal cortical network has profound implications for understanding cortical function. Coming back to Felleman and Van Essen's model, a small world network would envisage connections spanning multiple levels like so many information highways, providing numerous shortcuts across the graph. In such a network, one would envisage the long-distance connections of the cortex providing an integrated circuit, allowing messages to shuttle back and forth in the cortical loom across multiple levels. We would expect to find hubs, perhaps in the posterior parietal cortex or in the prefrontal cortex. One might expect to see some sort of essential feature attached to such a hub, perhaps a sense of self, crouching like a homunculus in the middle of the web of connections, directing all. Under the light of our findings this is highly unlikely as the long distance projections have low compliance to information transfer. Instead, what one has in the tribal networks are strong 'driving' connections mostly between neighboring areas on the same hierarchical level and adjacent levels. No centers, no hubs, no information highways. Instead, distributed processing dependant on myriad trickle down and trickle up effects from a sea of weak connections, acting upon and coordinating the neuronal assemblies of synchronized, reverberating activity.

We need to ponder the advantages of such, dense tribal networks, envisage the high density not as a constraint but as a necessary advantage. This type of network offers the synchronization properties that are thought to play a major role in cortical operations and relates the wide range of strength of projections (a newly documented fact) to spatial distance in the brain. The high density constrains the functional algorithms that can be implemented within such a network, bridging the gap between local and global processing. It hints that brain connectivity could be governed by such rules as the EDR both at the area and cell levels.

The notion that the cortex is a small world and scale free, thus echoing the planetary society and the world wide web (amongst many others) has an enormous appeal. The fact the principles of cortical organization may have far more in common with the, small-scale, high-density tribal networks may to some come as a disappointment. But let us remember, it is the dense social network that saw the emergence of man. It could be the large-scale, sparse network that sees civilization's demise.

Network analysis

We have shown in chapter one that the lognormal distribution of the FLN values of inter-areal connections can be explained by the exponential distance rule. The EDR does not only explain the observed lognormal distribution of the link weights, but as we show next, a weighted random graph model based on the EDR reproduces with high fidelity virtually all the statistical binary (local and global) properties of $\boldsymbol{G}_{26x26}$.

Artificial networks generated by EDR or CDR

We generated two, weighted random model graphs based on different distance rules (constant and exponential) with the same total number of *binary connections* (N = 430) as the cortical network $\mathbf{G}_{26x26}$. For the constant distance rule (CDR), we have $p(d)$ = constant, and for

the exponential distance rule (EDR), $p(d) = \lambda \exp(-\lambda d)$. We first choose a connection length *d* according to the distance rule *p(d),* then pick *uniformly at random* (to avoid introducing unmotivated biases according to Jaynes' Maximum Entropy Principle **(Jaynes, 1957)**) an area pair (*i,j*) from the set of those area pairs in the 26x26 matrix of measured distances, whose separation is *d,* and insert a connection in the graph directed from *j* to *i*. Multiple connections from *j* to *i* are allowed, thus generating its *weight*, and the process is stopped, once 430 *binary connections* are reached.

Binary analysis

The average number of unidirectional and bidirectional (reciprocated) connections measured on 1000 random graphs based on the EDR matches perfectly the data, while for CDR it differs considerably (**Table T2.4**).

Table 2.4

	Total nunber of links (N)	Total number of Unidirectional links	Total number of Bidirectional links
Cortical Data	430	88	171
CDR	430	136.95	146.525
EDR	430	88.16	170.92

When one compares the EDR and CDR model he will note that the CDR is actually a special case of the EDR in which the parameter $\lambda = 0$ and the value of λ for the EDR has been derived from the date. It is interesting to compare how the prediction power of the model will behave for different values of λ. **Figure 2.7** shows that actually starting from $\lambda = 0$ as lambda gradually increases the model approaches better the values measured in the data. The EDR model also describes the binary degree distributions better than the CDR (**Fig 2.8**).

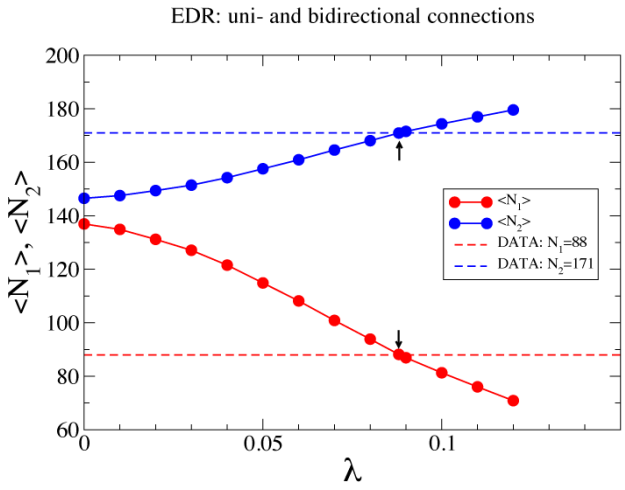

Fig 2.7 Predictive power of EDR according to the value of λ. The points at $\lambda = 0$ correspond to the ratio uni- to bidirectional projections under the CDR. Black arrows indicate the value of λ extracted from the FLN/Distance data and the horizontal dashed lines indicate the numbers of uni or bidirectional connections in the actual data.

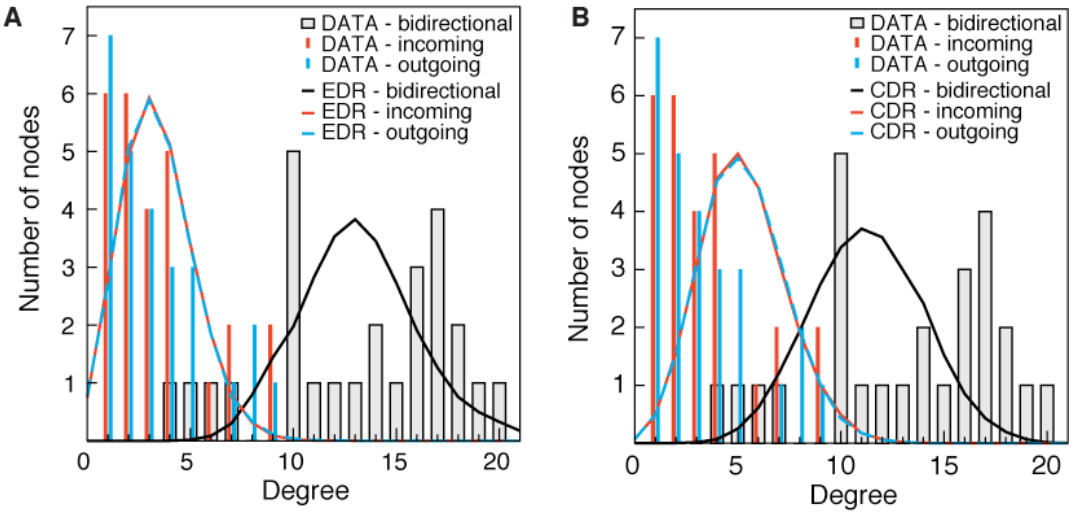

Fig 2.8 Degree distribution in the data is better predicted by EDR. A) Data and EDR fit of bidirectional and incoming ; outgoing links. B) CDR fit to the data.

Another basic binary characteristic of a directed network is its distribution of motifs or directed binary subgraphs, that are considered as network building blocks **(Milo et al., 2002)**.

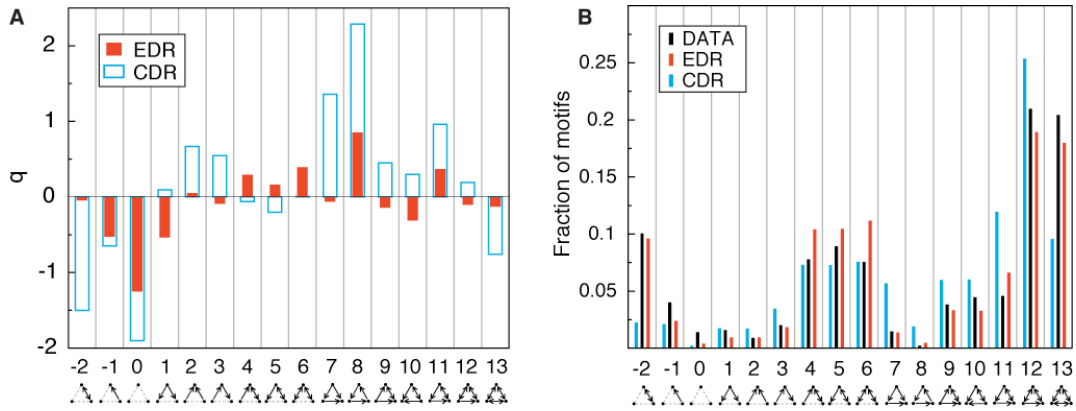

Fig 2.9 Network motifs are better reproduced by EDR than CDR based artificial graphs. A) Difference between data and artificial graphs build either using CDR or EDR. **B)** Histogram comparison of the motif distribution expressed as fraction from the total number of triadic motifs in the graph.

It is obvious from **Fig 2.8A** that the EDR tracks the data much better than CDR: the standard deviation between the experimental data and CDR is over 2.6 times larger (= 0.043) than the deviation of EDR (= 0.016).

The motifs distribution is an evaluation of the most frequent tripartite patterns that has been suggested to be indicative of the type of processing within the network (**Milo et al., 2002**). The distribution of motifs is a basic characteristic of a directed binary network. Since the 26x26 subgraph ($\boldsymbol{G}_{26x26}$) of the cortical inter-areal network has full connectivity information, we analyzed the distribution of 3-motifs and compared the results obtained from the experimental data and the two random models (CDR and EDR).

As expected from the strong connectivity of the network, the most frequent motifs in the experimental data (black bars in **Fig 2.9B**) are 12 (5 connections in a triangle) and 13 (all 6 connections). The EDR fairly well recovers these frequencies, the CDR on the other hand gives a deviation by a factor of 2 for motif 13. The situation is similar in the case of motif -2 (one single bidirectional edge), which has an unexpectedly high abundance. This is a consequence of

the exponential distance rule, assuring an unusually high number of bidirectional connections. This is confirmed by the fact that EDR almost perfectly recovers the frequency of motif -2, while CDR again produces a huge deviation (**Fig 2.9**).

Motifs 9, 10, 11 (4 connections in a triangle) show almost equal frequencies in the experimental data and are well recovered by EDR. In the experimental data between the motifs with 3 edges (4, 5, 7, 8), the completed triangles (7, 8) are much less frequent with the feedback loop (motif 8) being the least frequent. This is again a consequence of the high number of bidirectional connections. EDR shows slightly larger deviations for motifs 4, 5 and 6, but for motifs 7 and 8 the CDR produces huge deviations.

Motifs 1, 2 and 3 (two connections) show relatively small frequencies, as expected from the high connectivity of the network. Motifs 0 (no connections) and -1 (one connection) are underestimated by both models, although the deviations of EDR are smaller. Again compared to CDR, EDR is clearly superior in matching the data.

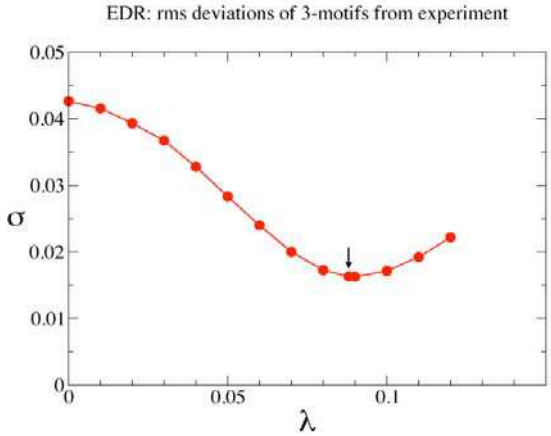

Fig 2.10 Statistical analysis of the dependence between lambda and goodness of fit to the data for the motif distribution comparisons in fig **2.9A.**

Finally, we analyzed a non-local property, namely the average shortest path length (directed, binary) as links were gradually removed in increasing order of their weights, starting from the weakest link. This was carried out for the two models, the data ($\boldsymbol{G}_{26x26}$) and a randomized version of the data (RND), (see **Fig2.11)**.

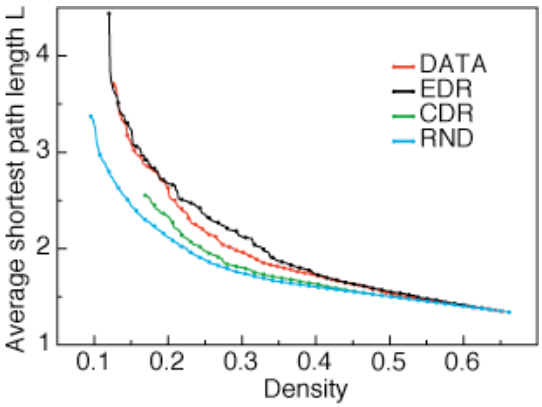

Fig 2.11 EDR architecture has, brain like path length to FLN dependence. Starting with a graph of 26 nodes and 430 links based on either CDR, EDR or random generation is compared to the real data of G_{26x26}. Links are sequentially removed by starting from the weakest. EDR based graph matches well to the dependence between connection magnitude and characteristic path length observed in G_{26x26}. CDR based graph follows effect more similar to a simple random network.

RND was generated by randomly shuffling around all the weighted links of $\boldsymbol{G}_{26x26}$. The removal of edges was stopped just before unreachability occurred (the first time when a node can no longer be reached from *all* other nodes along directed links).

Summarizing these observations, the binary properties of the $\boldsymbol{G}_{26x26}$ network are well captured by the EDR based random graph model. (For sensitivity analysis on λ see (**Figs 2.10 and 2.7**). Note, that although the binary properties are based on the connections existing or not, they are nevertheless generated from a *continuous spatial property* of the system (distance rule). While the EDR is an averaged, biologically non-specific rule, it however, expresses the strong economy around physical connection *lengths*, with higher costs associated with longer distances. This strongly shapes the cortical network structure, and accordingly, one expects this to be a selector for the types of information theoretic algorithms the brain uses.

Weighted network analysis

Next using communication efficiency we show that the EDR captures in part the functional organization of the interareal network. Since we have weighted data we can use efficiency instead of path length and clustering to characterize the graph. Efficiency presents the additional advantage of being a single feature that can be measured at both global and local scales **(Latora and Marchiori, 2003)**. Systems with high local and global efficiencies are highly fault tolerant **(Latora and Marchiori, 2003)**. The f_{ij} can be interpreted as a measure of the capacity of information transfer between the source j and the target i. The higher f_{ij}, (the stronger the projection), the higher the bandwidth of information transfer along the $j \to i$ link. For every pair of nodes (i,j) we define r_{ij} as the minimum sum of link weights (sum of w_{lk} weights taken along a path) amongst all paths directed from j to i. For constant weights, r_{ij} is proportional to the length (number of links) of the shortest directed path from j to i. To a first approximation, the probability for pulses along the $j \to i$ link to induce activity in node k along the $i \to k$ link is proportional to the product $f_{ki}f_{ij} = \exp\left[\ln(f_{ki}) + \ln(f_{ij})\right]$. For this reason, it is more convenient to work with $w_{ij} = -\ln(f_{ij}) \geq 0$ as link weights, being additive along directed paths. The w_{ij} is synonymous with link *resistance*, (larger w_{ij} means weaker link or larger resistance). We examined two communication efficiency measures, namely a global measure E_g **(Latora and Marchiori, 2003)**, and a local measure E_l **(Vragovic et al., 2005)**. E_g is a global conductance measure between two arbitrary nodes, calculated as the mean of the conductance $1/r_{ij}$ over all the $N(N-1)$ possible pairs. The global network communication efficiency measure E_g introduced by Latora and Marchiori is defined as:

$$E_g = \frac{1}{N(N-1)} \sum_{i \neq j} \frac{1}{r_{ij}} \quad , \qquad (7)$$

where the summation is over all the $N(N-1)$ possible pairs (i,j) of nodes.

The local efficiency E_l measures the average conductance between all pairs of neighbors of a node *after* that node's removal, then averaged over all nodes. The local network communication efficiency measure E_l introduced by Vragovic et. al. is defined as:

$$E_l = \frac{1}{N} \sum_i \frac{1}{k_i(k_i-1)} \sum_{j \neq k \in \{i\}} \frac{1}{r_{jk/i}}. \qquad (8)$$

Here a local efficiency is calculated for all pairs j,k of neighbours of node i *after* node i and its links are removed from the graph (obtaining $r_{jk/i}$ through the remaining graph), then this is averaged over all nodes i. The local efficiency is essentially the average conductance between all the areas connected to an area X, after removal of area X. It is similar to assessing how easily one can travel between the satellites of a town, without using routes passing through the town.

Again this is averaged across the entire graph.

In order to test the ability of EDR to model the cortical connectivity we first explored the effects of connection weights on communication efficiency in the real brain network. Progressive ordered removal of strongest connections had immediate and pronounced effect, as it reduced both E_g and E_l (black and red solid lines in **Fig 2.12A**). On the other hand the removal starting with the weakest links (green and blue solid lines in **Fig 2.12A**) shows an effect on global efficiency only when 81% of links (containing 7% of total neurons) have been removed. This clearly indicates that the largest band paths of the network are arranged in such a way that the graph can be efficiently navigated without using the low magnitude paths. Hence, efficiency is assured by the remaining 19% of links exhibiting the largest FLNe values and accounting for 93% of neurons.

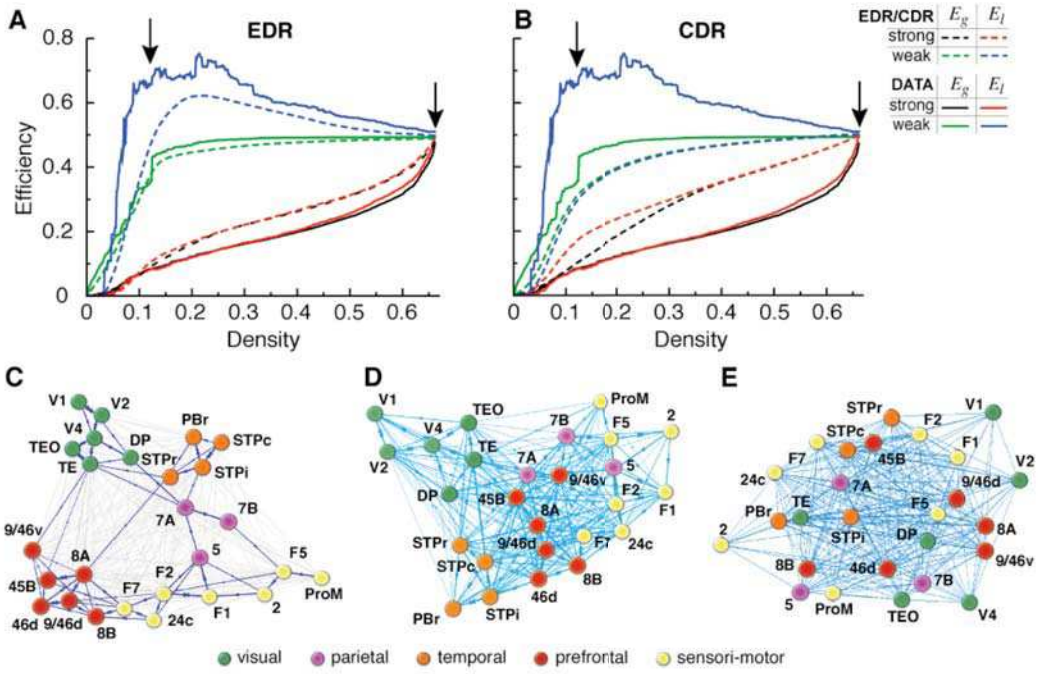

Fig 2.12. The weighted analysis A) The effects of edge removal on efficiency measure. Solid lines correspond to the $\mathbf{G_{26x26}}$ network and dotted lines correspond to the efficiency of EDR based artificial network. Black arrows indicate the density level before the removal of edges has been started and the density at wich there is an inflection point for the real network. B) Same as in A but for CDR based artificial network.(same conventions) C) The backbone network plotted using Kamada-Kawai algorithm to generate the network layout. Thick blue lines indicate the edges present in the backbone, while light gray are the edges that we can remove without affecting the efficiency of the network. D) The unattacked network ploted with the same algorithm, weight information available. E) The unattacked network ploted with the same algorithm, weight information NOT being provided (i.e. binary plot). Note that without weight information the algorithm is unable to cluster the areas in functionally meaningful clusters.

The effect on E_g of strong and weak link removal and the existence of inflection point make it possible to define the network that constitutes the *global efficiency (GE) backbone* of the graph, shown in **Fig 2.12C**. The Kamada-Kawai algorithm is able to automatically cluster the nodes of a network in accordance to the connections strength and connectivity pattern. Surprisingly when applied to the GE backbone it reveals a layout comprised of modules corresponding to functionally related areas connected into a circuit-like structure. This graphic analysis also reveals the role of weights in determining the clustered topography of the graph. In

the binary version of $\boldsymbol{G}_{26x26}$ (at 66% density, but no weights) there is no coherent clustering **(Fig 2.12E),** however, with weights included, it shows a clustered network **(Fig 2.12D)** that is more pronounced in the GE backbone **(Fig 2.12C).** The fact that these clusters correspond to well defined functional and spatially related areas shows that the connectivity weights are a strong determinant of this embedded network.

The links with the highest FLNe that constitute the GE backbone have a mean projection distance of 14*mm*, considerably shorter than the 38*mm* mean in the weak links component of the graph. The high FLNe/shorter projections component vs lower FLNe/longer projection components are echoing the distance to strength relation modeled by the EDR.

Evidence that the differential effect of link removal is due to the distance rule is shown in **Figs 2.12A,B**. Both efficiencies decay slowly for the CDR, while the EDR displays a qualitatively similar behavior as the data. The difference in the E_l curve for the EDR and data is due to the fact that although the EDR respects the distance rule, its strong connections still form a locally random network, while the cortical circuitry is functionally structured

The structure of the backbone

We have isolated in our 26*26 matrix the minimal network that has high efficiency. We call this network "The backbone". This backbone network has a large average directed binary path length (= 3.7) and diameter (= 9) and so although sparse it does not qualify for a small world.

In **figure 2.13** we illustrate different graph structures. Some of them ("Chain", "Tree", "Bipartite" and "Isolates") are by definition excluded of the possible solutions for our backbone because they have very low global efficiency. Meanwhile they could have corresponded to the structural arrangement of the strong inter-areal connections (our data proves that the brain has not retained any of these solutions). So for the possible solutions only the star, the circuit and their variants remain as plausible solutions given that these graphs can have high global efficiency. The star implies the existence of one or few hubs that will broadcast strong connections to all of the neighbours. This we know is not the case in the brain as we have for each area only few very strong connections and then a whole pleiade of weak connections. From the previous lines it seems like the circuit backbone is a natural solution but it is not an obvious solution. There is really a circuit of strong connections in the graph and by the "Efficiency" measure we have been able to visualize it. The Circuit backbone gives possibility to access any point in the graph by using only the strong connections; if there were interruptions in the available paths we could have had the structure of the "isolates". In such a situation there would have been drop in efficiency in after the removal of some crucial weak connections that would have had larger effect than the removal of some strong connections. **Figure 2.13 bis** shows the backbone structure and the effect of randomization on it. The backbone expresses characteristics that can describe the interrelation of strong connections. i)The backbone offers a path between any two nodes in the 26 graph. ii)The transitivity of the backbone is 0,43 while the randomized backbone has transitivity of 0,19. (the transitivity is the tendency of connections to form triangles If A<->B and A<->C, then B<->C) iii)The path-lenght in the backbone is larger than in random 3,72 vs 2,60. iv)The diameter of the backbone is larger than random 9 vs 7. v) The backbone shows very high reciprocity 62% vs 5-20% in random. These characteristics of the backbone are also characteristic for the typical arrangement of strong inter-areal connections in the brain.

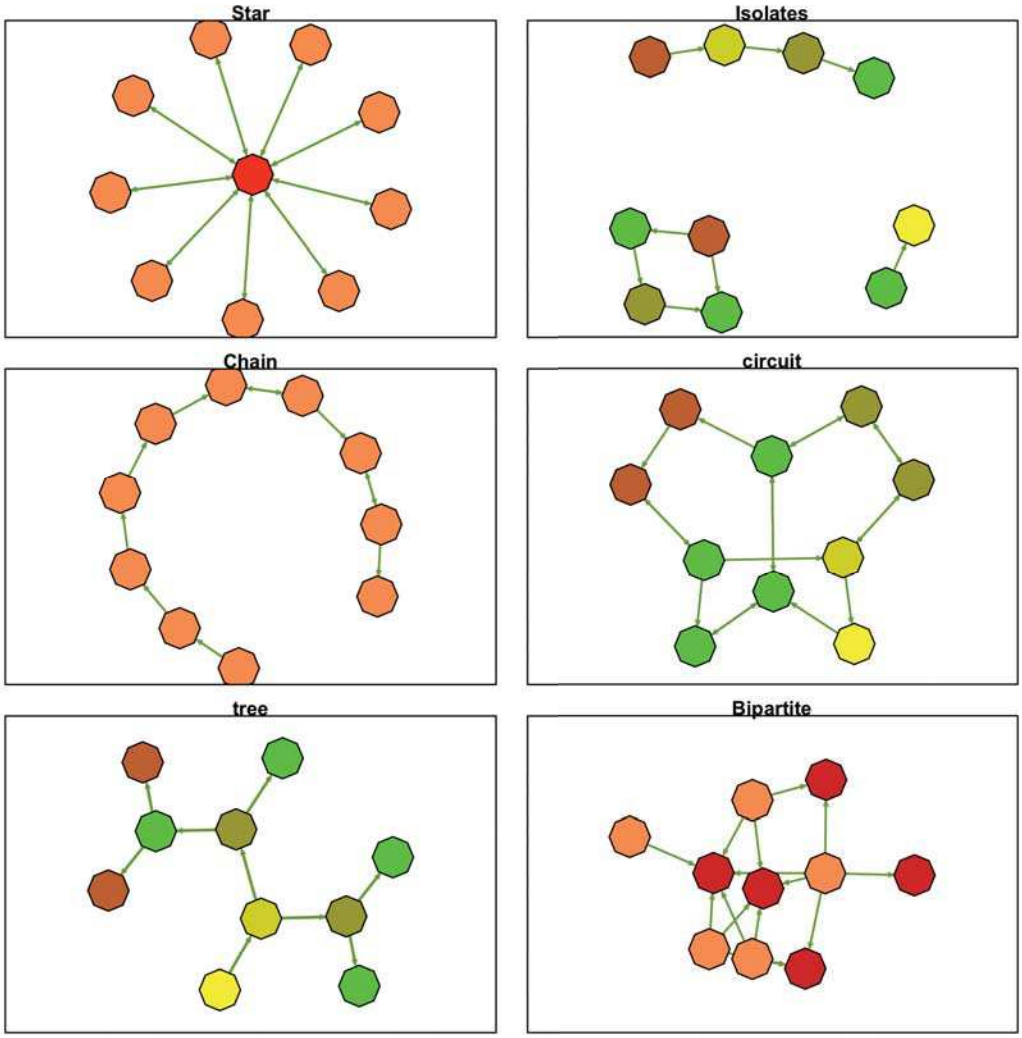

Figure 2.13 Six different types of possible arrangement of strong connections. A) One central node sends strong connections to all other nodes ; B) Groups of nodes are interconnected in isolated networks with variable structures (like the backbone of Song); C) Hierarchical chain where there is possible beginning and end of flow but there is lot of unreachable nodes ; D) A circuit where any node may serve as an entry of information and there is a path from any node to any other node. E) Tree structure where there is an entry and lot of parallel paths (here the entry is in yellow); F) Bipartite graph where a set of nodes has direct links to a set of other nodes .

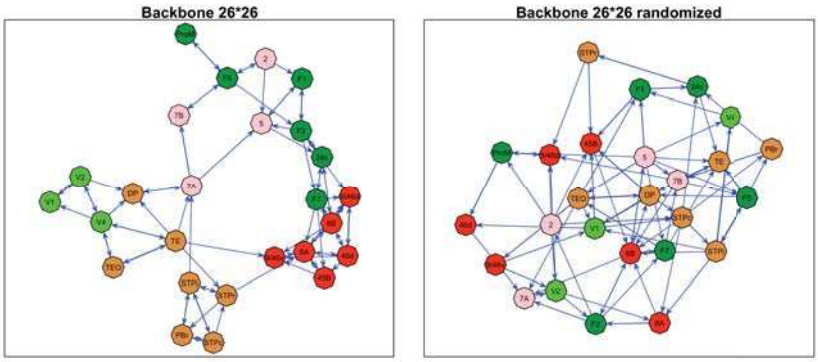

Figure 1.13 bis The backbone has some biological specificity ; A) the experimental backbone shows to be of circuit type with clustering of functionally related areas. B) The randomization of this backbone destroys the functional clusters and leads to loss of the high transitivity.

The FLN between areas is strongly optimised to minimize the wiring length

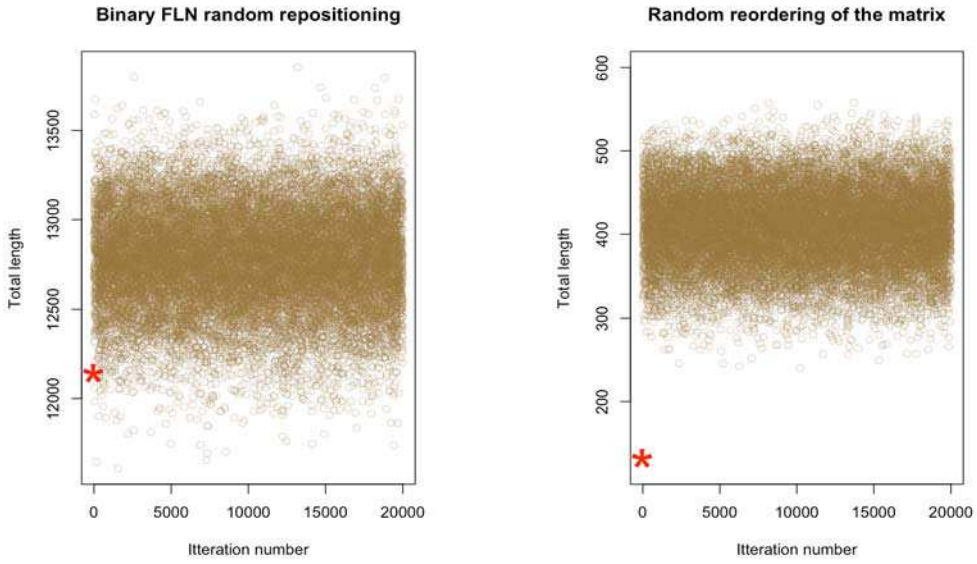

Here **Fig 2.14** FLN and distance of projection are maximally optimized to minimize the total wire length. A) The random replacement of area positions in the binary avatar of G26x26 B) The same procedure in the weighted version G26x26.

The cortical architecture has been claimed to express an evolutionary tendency to minimizing of total wire length in the brain **(Cherniak et al., 2004).** The binary architecture of the network that we have revealed is of high density. One may express the concern that this would lead to a very uneconomical network in terms of total wiring length. The FLN vs distance plots (**figure 1.12**) and the distance rule already show that there is a strong wiring economy but they do not give a clue if the 3D placement of the areas is maximally optimal or could it be other solutions. **Figure 2.14 A** illustrates the effect of random replacement in the positions of the areas in the binary G_{26x26}. **Figure 2.14B** illustrates the measure of total wiring length in the weighted graph after 20 000 random replacements of the cortical areas. To simulate area replacement we use two matrices i) the distance matrix and ii) the adjacency matrix. If we multiply every element of i by the corresponding element of ii and we sum we obtain the total wiring length. If now we replace one column and one row, with another column and row of the adjacency matrix we will end up in the sum/multiplication procedure with a result identical to interchanging the spatial positions of two areas without affecting their connectivity pattern. It is like answering the question what would it mean for the brain if area V2 was in the prefrontal cortex and the FEF had the occipital position of area V2. This procedure enabled us to question the minimization of the wiring length. Simply associating the

strongest FLN with the shortest available distances without taking in to account the bio specificity yields a huge reduction in total wiring but loses the bio specificity. If instead the replacement keeps unaffected the graph architecture (list of inter-area connections and their magnitude) then it becomes almost impossible to find a more optimal solution than the one of the brain. These plots indicate that the total wiring length in the 3D arrangement of cortical areas is optimally solved, by adapting the strength of FLN to the projection distance.

Discussion

The inter-areal cortical network presents a novel graph structure that merits further study for its implications in brain function and computation. Many real-world networks, are sparse and typically have small-world properties with a heterogeneous distribution of node degrees **(Watts and Strogatz, 1998, Barabasi and Albert, 1999, Watts, 1999, Newman, 2003, Boccaletti et al., 2006)**. In contrast, the network uncovered here is dense, non small-world and exhibits a homogeneous node degree distribution. A novel feature of the cortical network compared to previously described networks is that the heterogeneity required for complex function appears in the link weights and not the degree distribution. The constraints on connectivity are imposed by its spatial embedding and connection weights are described by an EDR. The EDR captures the increase of the average path length with weak link removal, the average degree distribution as well as the dyadic and triadic motifs and therefore accounts for all the binary properties of the network. In the interareal network the wide range of link strengths introduces a layering in the graph expressed in the backbone versus weak link component of the graph. The communication efficiency lies in the structure of the weight distribution rather than in the binary connectivity. Interestingly, the high-bandwidth communications backbone of this network shows functionally related clusters and no central dominating nodes.

There is increasing evidence that cell assemblies carry information in the cortex **(Braitenberg and Schüz, 1998, Tsodyks et al., 1999, Kenet et al., 2003, Buzsaki, 2007)**. The high network density and thus the small graph diameter that we report here, ensures direct access between almost all pairs of areas for reliable high-level integration. There is evidence that a rise in cortical activation could generate higher levels of inhibition leading to higher firing thresholds **(Braitenberg and Schüz, 1998, Destexhe and Pare, 1999, Azouz and Gray, 2003, Haider et al., 2010)** The effects of removal of connections on the global and local efficiencies (**Fig 4A**) suggests that activity-dependent modulation in response threshold would lead to small changes in global efficiency, off-set by potentially large changes in local efficiencies and cooperative interaction between functionally clustered areas, similar to what has been suggested at the single neuron level in the local microcircuit **(Binzegger et al., 2009)**.

There is evidence at the single neuron level that the distribution of synaptic strengths follows a log normal distribution similar to the distribution of link strength at the interareal level **(Song et al., 2005)**. Likewise, the connectivity matrix for local connections has a high density similar to that found at the interareal level **(Binzegger et al., 2009),** suggesting that a similar functional logic is operant across different scales. In this way the control of assembly dynamics in the cortex will have a spatial component in large part due to the geometry and weight characteristics of the cortical network. These design principles may serve to optimize global and local integration while minimizing the energy requirements for neuron communication **(Laughlin and Sejnowski, 2003).**

Chapter III :

Anatomy of hierarchy

Introduction

There are strong regularities in the cortical projections of early visual areas: rostral directed pathways originate mostly from supragranular layer neurons and terminate in their anterior target areas in layer 4 **(Cragg, 1969, Spatz et al., 1970, Lund et al., 1975, Martinez-Millan and Hollander, 1975, Van Essen and Zeki, 1978, Wong-Riley, 1978, Rockland and Pandya, 1979),** while caudal directed pathways mostly originate from infragranular layers and terminate outside of layer 4 in their more posterior target areas **(Kuypers et al., 1965, Tigges et al., 1973, Kaas and Lin, 1977, Wong-Riley, 1978, Kennedy and Bullier, 1985) (Fig 8a).** By analogy to the pathways linking thalamus and cortex, these findings have led to the suggestion that rostral directed connections are feedforward pathways channelling information from lower to higher order areas, while caudal directed pathways constitute feedback pathways **(Rockland and Pandya, 1979)**. Analysis of feedforward/feedback relations made it possible for Felleman and Van Essen to establish a hierarchical ordering of areas, which has provided important insight into cortical structure and function **(Felleman and Van Essen, 1991)**. However, the computerised analysis of the same database used by Felleman and Van Essen while confirming a strong hierarchical order, shows that due to the absence of a hierarchical distance measure, their model of the visual cortex is indeterminate with 150,000 equally plausible solutions **(Young, 1992, Hilgetag et al., 1996, 2000b)**. One possible method of obtaining a determinate model of the cortical hierarchy is to use quantitative data on connectivity that has been shown to provide a measure of hierarchical distance **(Barone et al., 2000)**.

The structural regularities that underlie the Felleman and Van Essen hierarchy are thought to have a physiological underpinning. Many workers in the field subscribe to the notion that feedforward signals generate receptive field properties and feedback streams have a modulatory role **(Hupé et al., 1998, Ekstrom et al., 2008).** A number of studies have demonstrated physiological activity in early visual cortices that were thought to be characteristic of higher areas **(Moran and Desimone, 1985, Motter, 1993, Ishai and Sagi, 1995, Miyashita, 1995, Watanabe and Iwai, 1996, Cornette et al., 1998, Lamme et al., 1998, Somers et al., 1999, Super et al., 2001, Lee et al., 2002, Roelfsema et al., 2004)**. These finding alone

suggests that we do not have an operationally simple definition of higher and lower areas, and current theories of visual perception emphasise the complex interactions between different levels of the hierarchy **(Cauller, 1995, Pascual-Leone and Walsh, 2001, Juan and Walsh, 2003, Tong, 2003)**. For instance it has been suggested that activation of the feedforward pathways gives rise to a rapid automatic characterisation with little perceptual detail, the latter being supplied by reiterative engagement of feedback pathways **(Pascual-Leone and Walsh, 2001, Hochstein and Ahissar, 2002, Juan and Walsh, 2003, Lamme, 2003, Tong, 2003, Jehee et al., 2007)**.

While the debate on the respective roles of the feedforward and feedback pathways is clearly still open we believe that the nature of the interaction between higher and lower areas maybe shaped by the structural features of the feedforward and feedback pathways. Feedforward and feedback pathways in the visual system are reported to show strong asymmetries in their structural features. Two general claims have been made. Firstly, that feedforward connections are topologically organized in contrast to a more diffusely ordered feedback connections both in terms of the spatial extent of parent neurons and terminals as well as the frequency of axonal bifurcation **(Rockland and Pandya, 1979, Maunsell and van Essen, 1983, Bullier et al., 1984b, Kennedy and Bullier, 1985, Ungerleider and Desimone, 1986, Bullier and Kennedy, 1987, Zeki and Shipp, 1988, Krubitzer and Kaas, 1989, Rockland and Virga, 1989, Shipp and Zeki, 1989b, Shipp and Zeki, 1989a, Zeki and Shipp, 1989, Krubitzer and Kaas, 1990, Henry et al., 1991, Shipp and Grant, 1991, Salin et al., 1992, Rockland and Van Hoesen, 1994)**. Secondly, that feedback pathways are more numerous and cross more hierarchical levels than do feedforward pathways **(Zeki, 1978b, Kennedy and Bullier, 1985, Yukie and Iwai, 1985, Perkel et al., 1986, Iwai and Yukie, 1988, Webster et al., 1991, Nakamura et al., 1993)**.

Because the nature of the feedback and feedforward pathways is at the heart of our understanding of cortical hierarchy their organizational principals will have important consequences for general theories of cortical function. One theory points to the above mentioned asymmetries of the feedforward and feedback projections in support of the cortex having an inference function **(Friston, 2003)**. An alternative, theory insists on the equivalence and segregation of the two-counter streams that converge to interact with the local processing of the cortex **(Ullman, 1995).**

Here we implement quantitative techniques to better characterise the structural features of these two types of pathways. Firstly we use SLN, a quantitative measure of the laminar distribution of parent neurons of cortical projections, to model the hierarchal organization of early visual areas. Secondly, we show that SLN reflects combinatorial distance rules of infra- and supragranular projecting neurons. Thirdly we determine the relative strength and number of feedforward and feedback pathways. Fourthly, we examine the topography of feedforward and feedback pathways. Fifthly, we estimate the segregation of the two pathways.

SLN determines the hierarchical organization of early visual areas.

SLN as Hierarchical distance measure

Following retrograde injections in the target area, the proportions of parent neurons of a pathway in the source areas that are located in the supragranular layers **(SLN)** defines it as feedforward or feedback, and the fraction of neurons in a given pathway **(FLN)** defines the strength of the pathway (**Fig S1**) **(Barone et al., 2000).** The SLN indicates the hierarchical distance of a pathway and therefore holds the promise of generating a determinate model of the cortical hierarchy **(Barone et al., 2000)**. The FLN allows us to weight the SLN values **(Fig S1).**

Injections in V1, V2, V4, 7a, TEO and 45B enabled us to identify a total of 93 pathways interconnecting the principle areas in the early visual cortex. Of these 93 pathways, 13 have previously not been reported. We estimated the SLN and FLN values of these afferent pathways and so as to construct model of their hierarchy **Fig 3.4** (**Table S3**).

The sets of SLN values for areas labeled from injections in areas on different hierarchical levels showed remarkable coherence **Fig 3.2E** (**Table T3.1 and T3.2**). The pairs plot **(Figure 3.1 and 3.2C)** compares the SLN values obtained from 6 injections of retrograde tracer. We consider the hypothesis that SLN provides a measure of hierarchical distance between areas in the cortex. The strong version of this hypothesis would state that the difference between the SLN values obtained between two areas would be the same independent of the injection site. Under this hypothesis, the SLN is considered as a rigid ruler that can be shifted to have a reference point at the injection site. Wherever it is shifted, the difference between SLN values is unchanged. The prediction of this hypothesis is that the points will fall along a line of unit slope, shown by the dashed lines in each plot. This hypothesis can be weakened by assuming instead that SLN measures rigid hierarchical distance from each injection site, that the ruler might be stretched or contracted with respect to different injection sites. This hypothesis predicts simply that the relation between SLN values obtained from different injection sites follows a straight line with arbitrary slope. Because there is error in the SLN estimates of both the abscissa and ordinate values in the plots, we estimate this line using major-axis regression that chooses the best fitting line that minimizes the shortest distance to the points rather than just the ordinate distance. The best fit major axis lines are indicated by the solid lines. If the strong SLN distance hypothesis were true, then the dashed lines would not be significantly different from the solid lines. This does not seem to hold in all of the plots.

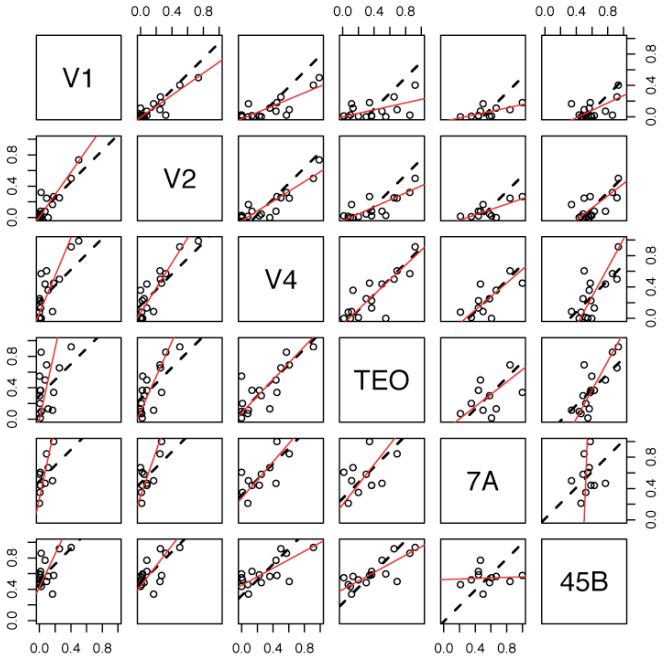

Figure 3.1 Plot of SLN correlations The pairs plot shows a scatterplot of the SLN values for projections from corresponding areas to the injection site for each pair of injected areas (plots below the principal diagonal are the same as those above with the axes reversed). If the SLN values provide a rigid ruler of hierarchical distance, then all scatterplots will be best described by a line of unit slope (dashed line in each graph). A weaker version of this hypothesis posits that a linear relation exists between the SLN values from different areas (the ruler undergoes a uniform contraction or expansion). This hypothesis predicts that the scatterplots will be best described by a straight line of arbitrary slope. Since there is error in the estimated SLN values on both the ordinate and the abscissa, this line must be estimated with major-axis (or principal component) regression which minimizes the perpendicular distance to the line rather than just the ordinate distance. The best fit line is shown by the solid line in each plot. If the rigid ruler hypothesis is correct the dashed and dotted lines will agree. For 5/15 pairs, the 95% confidence interval for the slope of the major-axis regression line includes the value of 1. The median slope is 0.70 with interquartile range (0.43, 0.90). Even if the rigid ruler hypothesis is not fully supported, the strong linear relation implies that SLN values provide a common view of the cortical hierarchy across the cortex.

The correlation coefficients for each plot indicate the goodness of fit for this weaker hypothesis.

The median value of the 15 pairs is 0.71 with inter-quartile range (0.58, 0.8) **(Table T3.1)**. It is reasonable to suppose that the SLN values based on strong connections (high FLN) values are the most reliable. So, we recalculated the correlations between SLN values for each pair of injections weighting each pair of points by the strongest FLN value for the pair **(Table T3.2)**.

Table T3.1. Corelation of the pairs plot

	V1	V2	V4	TEO	7A	45 B
V1	1.000	0.891	0.814	0.482	0.659	0.522
V2	0.891	1.000	0.892	0.786	0.729	0.635
V4	0.814	0.892	1.000	0.806	0.688	0.707
TEO	0.482	0.786	0.806	1.000	0.387	0.791
7A	0.659	0.729	0.688	0.387	1.000	0.055
45B	0.522	0.635	0.707	0.791	0.055	1.000

Table T3.2. Corelation of the pairs plot after FLN weighting

	V1	V2	V4	TEO	7A	45 B
V1	1.000	0.605	0.969	0.841	0.832	0.938
V2	0.605	1.000	0.978	0.891	0.862	0.850
V4	0.969	0.978	1.000	0.942	0.351	0.915
TEO	0.841	0.891	0.942	1.000	-0.051	0.888
7A	0.832	0.862	0.351	-0.051	1.000	0.320
45B	0.938	0.850	0.915	0.888	0.320	1.000

Twelve of the 15 correlations increased ($Chi2 = 4.27$, $df = 1$, $p = 0.039$). The median value increased to 0.86 with interquartile range (0.72, 0.93).

A more general SLN distance hypothesis would allow that the true distances are a function of the SLN values from a given injection. We might imagine, for example, that values near the injection site (SLN near 0.5) are more reliable and that some foreshortening of the estimates occurs at the extremes. This idea is not unlike Steinberg's New Yorker's View of the World, in which distances are compressed as they increase from the observer. Such a transformation would imply that the true distances are related to the SLN values through a sigmoidally shaped function. We test this idea by plotting the SLN values transformed by an inverse cumulative normal distribution function **(Figure 3.2.C)**. The dashed and solid lines again show respectively the best fitting unit slope and major axis lines. The two lines seem more similar now for areas that are more closely related. These analyses support the hypothesis that the SLN values contain similar information about the relation between areas independently of the injection site upon which they are based and thus can be used for construction of hierarchical model.

For injections in areas V1, V2 and V4, hierarchical distance of a projection was defined by the following procedure. First, the difference of SLN from that of V1 was computed. This set the level of V1 at 0 for the three injections. For the TEO, 7A injections, there were no projections from V1. To normalize these injections with respect to the other three, we considered the projections from areas from which all injections received projections. These were 7A, LIP, FST, MT, TE, TH/TF, 45B and TEO. The correlations of the SLNs for TEO, 7A and 45B for these areas were highest with V4. We normalized the SLNs by the average SLN of these mutual projections with respect to that of V4 for the same projections. We then

normalized these with respect to the average SLN difference from V1 for these areas for the V4 injection. To construct a hierarchy, we computed a weighted mean of the SLN differences with the FLN values serving as weights. We then normalized the resulting hierarchy so that V1 was at level 1 and the highest level, 36, was as level 10.

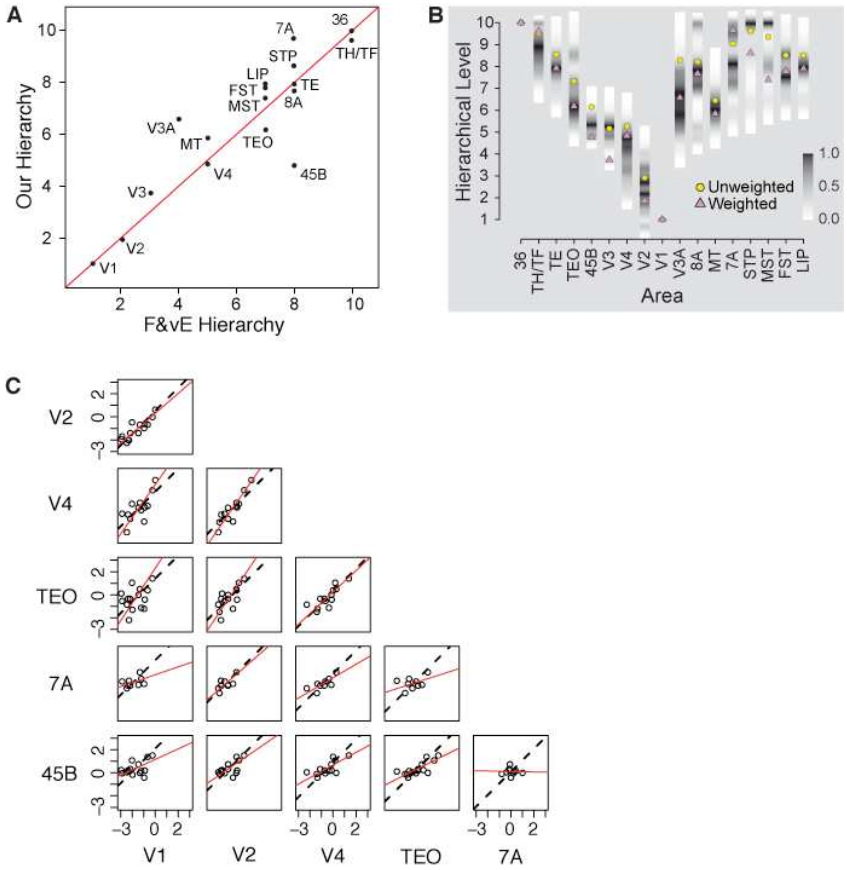

Fig 3.2 SLN as hiearchical measure A) Comparison of the hierarchy shown in Fig 3.3**B** with the Felleman and Van Essen model shown in Fig 3.3**A**; **B**) Effect of randomization of FLN values. For each source area, the FLN values from the 6 injections sites were permuted randomly and a weighted hierarchy was built as in 3.3.**B**. This was repeated 10000 times to evaluate how the choice of weights influence hierarchical position in the weighted hierarchy.; **C**: Corelation between SLN transformed by an inverse cumulative normal distribution function.

The role of the weights was evaluated by randomizing them for a given projection across the injection sites, independently for each of the 17 projections considered after which a new hierarchy was generated. This was repeated 10000 times and we examined the distribution of levels for each of the 17 projections **(Fig 3.2B)**. The FLN weights were found to have relatively little impact on determining the organization of the hierarchy, so that the hierarchy obtained with SLN alone was not very different from that obtained by SLN weighted by FLN (**Fig3.2B**). Importantly however, the actual weights are not arbitrary, as random assignment of the weights shifts areas by 2-8 levels (**Fig3.2B**).

These two sets of findings suggest that there is a relationship between FLN and SLN, which in fact is the case. The effect of FLN weighting on the hierarchical order was mild while the randomization of the FLN values shifted areal positions with 2-8 levels. This indicates that FLN and SLN are related. The relation between FLN and SLN was examined. A smooth function was estimated to describe log(FLN) as a function of SLN using both a loess (local regression) fit (**Cleveland et al., 1992**) and using a generalized additive model (Hastie and

Tibshirani, 1990, Wood, 2006). In both cases, a reversed U-shape curve was found to fit the data best **(figure 3.3)**.

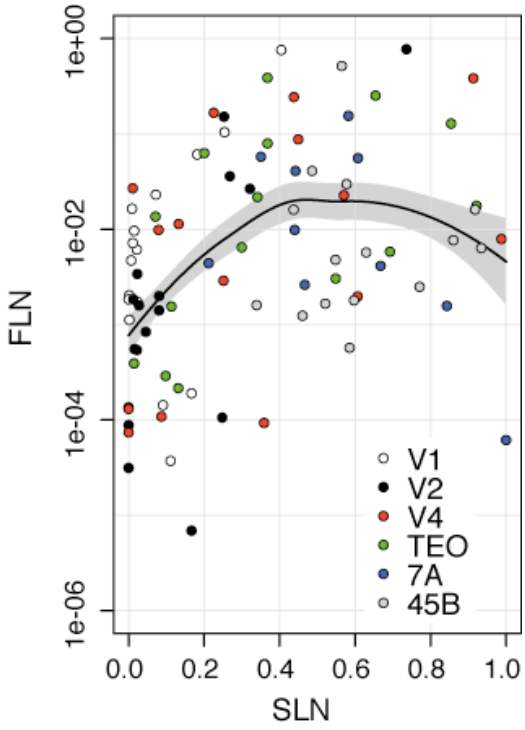

Fig 3.3 SLN vs FLN The fit corresponds to gam function with a significant U-shape.

Connections between areas on the same hierarchical level, termed lateral connections **(Felleman and Van Essen, 1991),** were found to have roughly equivalent supra/infra numbers of neurons (i.e. SLN nearly 50) and tended to have high FLN values. On the other hand long-distance feedforward and feedback projections have SLN close to 0 or 100 and low FLN values. Hence, although a scatter plot of FLN vs. SLN for the six injection sites considered here is quite noisy, a local regression curve fitted to these data indicates the expected relation (**Fig 3.3**).

We used FLN to weight the observed SLN values so as to obtain a unique hierarchy and compared it to the hierarchy of Felleman and Van Essen.

Figure **3.4,** allows the comparison between the Felleman and Van Essen qualitative hierarchy and that based on the SLN weighted by FLN. **Fig 3.2A** shows that there is a good correlation between the two hierarchies. Where as the Felleman and Van Essen's (FVE) model shows a regularly staggered progression going from V1-V2-V3-V4, our model groups V1 and V2 together and at some distance from V3. A major contrast with the hierarchy of FVE is the high position of area V3A in the dorsal pathway in our model. Human monkey comparison in FMRI experiments point to an analogy between human and monkey V3A (**Orban et al., 2004**). In humans V3A is a part of the motion processing system and expresses 3D motion related activity. While some of these properties have not been revealed in monkey V3A, its location high in the hierarchy is in accordance with it being part of or interacting with the MT, MST and FST complex. A number of studies have suggested that MT and V4 have lateral connections as indicated in the FVE model **(Ungerleider et al., 2008)**. In our study MT has feedback relations with V4 and lateral connections with TEO. Compared to FVE's model the other areas which are shifted to a higher hierarchical position in the dorsal pathway in our model is FST, LIP, STP and 7A. Globally the ventral stream shows less differencies than does the dorsal stream with respect to the FVE model. One difference what is worth remarking on is the slight drop of TH/TF in our hierarchy compared to FVE's. This could reflect the tighter interaction of area 36 with prefrontal areas and TH/TF with occipital cortices **(Suzuki and Amaral, 1994, Lavenex**

et al., 2002). The major finding of our model is that area 45B has a lateral position with V4 in contrast to its high location in FVE's model (**Barone et al., 2000**). The present study goes considerably further than our earlier findings in this respect in a number of ways. Firstly, we show previously unknown projections of both V1 and V2 to area 45B reinforcing its position at an early stage of the visual system. This is reinforced by the relatively high coherance of the SLN values of 45B with the other visual areas (**Fig 3.2C**) Secondly the cumulative FLN of its connections with ventral stream areas and its connections with TH/TF prompt placing this prefrontal area at the early stages of the ventral stream hierarchy. This relatively low location in the visual hierarchy is compatible the possibility that area 45B drives attentional processes in area V4 (**refs**).

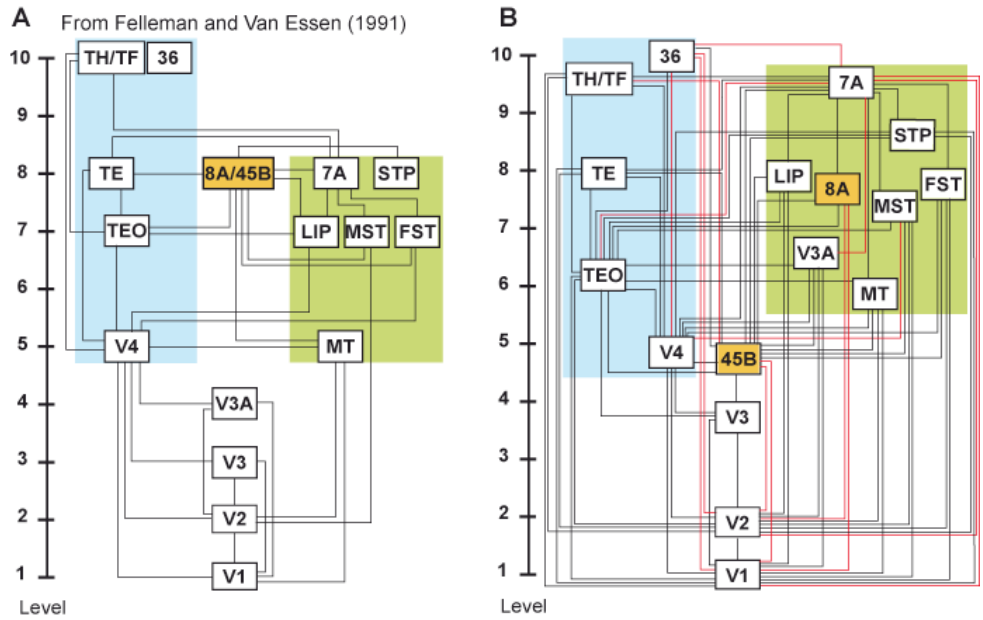

Figure 3.4 Hierarchies A: model of hierarchy of visual areas derived from Felleman and Van Essen (1991); **B**: Model of hierarchy of visual areas built form SLN and FLN values

Combinatory distance rules determine the SLN

The SLN as an indicator of hierarchy comes down to the fact that feedforward projections invariably exhibit more supragranular parent neurons, while feedback projections originate predominantly from infragranular projections. The fact that SLN indicates hierarchical distance means that with increasing distance there is a steady decline in the proportion infragranular layer projections neurons in the feedforward direction, and conversely a similar decline with distance in the proportion of supragranular neurons in the feedback direction. Here we address whether these decreases reflect distance rules governing the projection distances of these two sets of neurons in feedforward and feedback pathways.

The parent neurons of a cortical pathway are rarely strictly infra- or supragranular (**Fig 3.5A)**. Hence for a feedforward pathway the supragranular layer constitutes the *major* and the infragranular layer the *minor* layer, conversely for feedback pathways. Identifying the major layer in the source area in retrograde labeling studies and/or complementing it by identifying the type of axonal termination in the target area by anteriograde studies constituted the criteria that Felleman and Van Essen (1991) used to construct their hierarchy by pairwise comparisons. Note that the model of Felleman and Van Essen can be matched to the physical layout of the cortex, where roughly feedforward are rostral directed and feedback caudal directed. The SLN

parameter is able to capture these feedforward-feedback relations and in addition points to a hierarchical distance and **(this study and (Barone et al., 2000))**. Hence, the projection from V1 to V2, corresponds to a short hierarchical distance, is largely bi-laminar SLN (=74%), and the physical distance is short. This contrasts with the projection from V1 to V4 corresponding to a large hierarchical distance, has a SLN of 99% and the physical distance is high.

The above considerations suggest that there is a relationship between the projection distances of neurons in the different layers and whether they are projecting up or down the hierarchy. So as to explore this possibility we expressed in all 93 pathways the normalized number of parent neurons in either the major or minor layers as a function of the physical distance traversed by their axons. In all cases we observe a decrease of the number of labelled neurons with increasing distance. Although data points are relatively few and quite noisy, in both feedforward or feedback pathways the rate of decrease is significantly steeper for the minor compared to the major layer **(Fig 3.5B, C)**. This implies higher sensitivity to distance for projection from the minor layers and explains how SLN reveals hierarchy. Figure **3.5D** shows the ratio major/minor layer, which sharpens with increasing distance meaning that the major layer is projecting at longer distances with higher numbers**.**

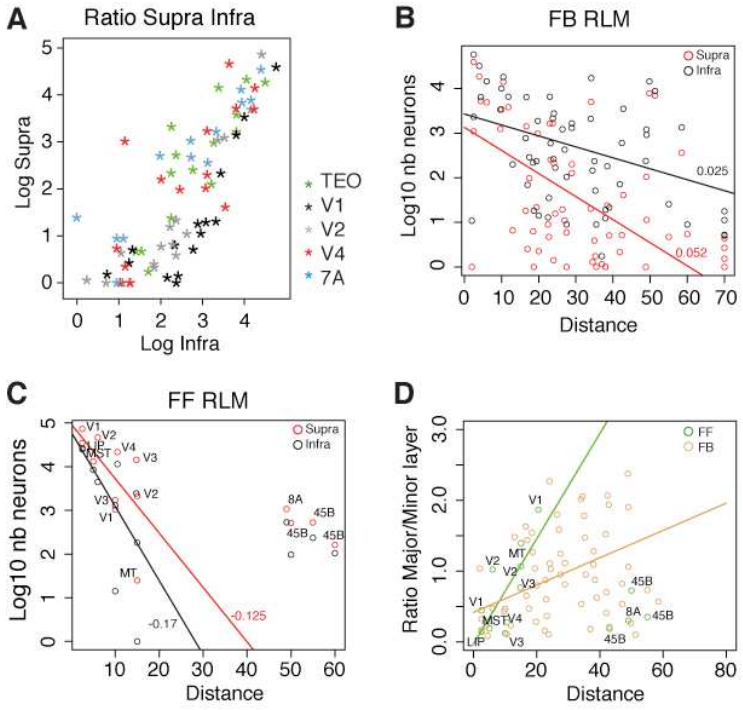

Figure 3.5 Physical distance of projection is related to the ratio between major and minor layer. A: Majority of pathways show participation from both the supragranular and infragranular layers, visualized here in a log log plot of number of neurons. **B:** Feedback projections , fit with a resistant linear model to the major and minor layer numbers of neurons expressed as function of projection distance. **C:** Same analysis as in B for the feedforward projections (ignoring projections from FEF and V3A). **D:** Projection pathways were identified by SLN and then the ratio of the normalized number of neurons in the major vs minor layer were plotted against the physical distance of projection. Green line fits to the ratios of FF pathways (ignoring projections from the FEF and V3A) slope= 0.074 (* P= 0,01) . The brown line is the fit for FB projections slope = 0.019 (* P = 0,02).

Incidence and magnitude of feedforward and feedback pathways.

A number of anatomical studies have described feedback pathways as being more frequent than feedforward pathways **(Perkel et al., 1986, Salin and Bullier, 1995)**. Here we have quantified the frequency and the magnitude of feedback and feedforward projections in the 61 pathways of the early visual cortex projecting to areas V2, V4, TEO and 7a. This shows that there are twice as many feedback pathways as there are feedforward pathways **(Fig 3.6A, B).** This predominance of feedback pathways is tempered when one considers the relative magnitude of cortical pathways. The total number of neurons involved in feedforward and feedback pathways is approximately equal (**Fig 3.6D**). However, distance is found to have a larger influence on the cumulative strength of pathways. Feedforward projecting neurons dominate over short distances and feedback over long distances, hence around 80% of feedforward neurons project no further than 11mm; while 50% of feedback neurons have projections extending between 20 and 80mm. (**Fig 3.6C**).

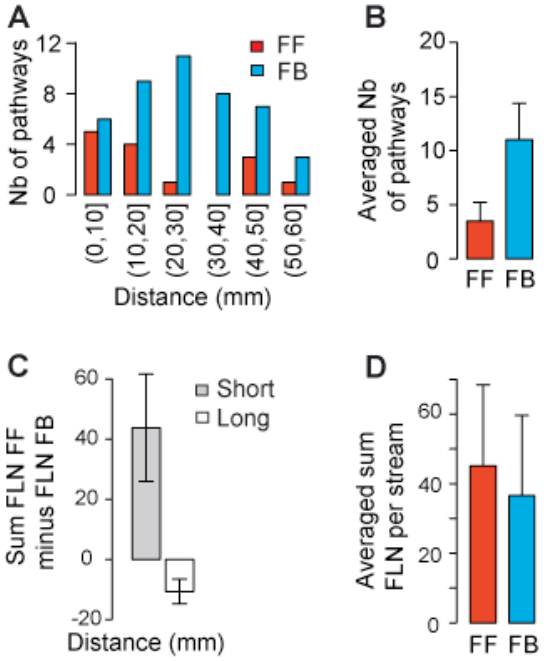

Figure 3.6 Distribution of FLN across the brain A: Incidence of feedforward (100% >= SLN% >= 55%) and feedback (0% <= SLN% <= 45%) pathways with distance following injections in V2, V4, TEO, 7A; **B**: Comparison of the numbers of feedforward and feedback pathways for injections in A; **C:** Influence of distance on the median FLN of feedforward neurons minus the median FLN of feedback neurons; **D**: Average sum of FLN in feedforward and feedback pathways

Topography of feedforward and feedback projections.

There have been numerous claims that compared to feedforward projections, feedback projections exhibit higher bifurcation frequencies and are more diffuse **(Salin and Bullier, 1995, Friston, 2003)**. If supra- and infragranular layer neurons showed the marked differences in topographical precision, then the reported differences in feedforward and feedback pathways could stem from the differences in the relative contributions of upper and lower layers (i.e.supragranular being preponderant in feedforward and infragranular in feedback projections). To examine if this is the case we have measured the topographical precision both sets of layers participating in feedforward and feedback pathways.

Previous studies have shown that topographical precision can be investigated by making side-by-side injections with tracers such as those used here (Fast Blue and diamidino yellow)

that are readily distinguishable in the retrogradely labeled neurons and which have been shown to have restricted and clearly defined pick-up zones **(Perkel et al., 1986, Salin et al., 1989, Salin et al., 1992, Kennedy et al., 1994)**. Dual injections in the target area lead to two populations of retrogradely labeled neurons in the source areas, where the degree of overlap of the two populations reflects the inter-injection separation as well as the topographical precision of the connections between the source and target areas. Within the region of overlap is a small population of double-labeled neurons, which we have shown are neurons with collaterals targeting both injection sites (**Bullier and Kennedy, 1987**). The dimensions of the overlap-zone and the number of double-labeled neurons are used to gauge the topographical precision of the projection neurons in the source area.

Side-by-side injections of FsB and DY were made in areas V1 or V4. We measured (i) the spatial extent of the projection zones to each injection; (ii) the spatial extent of the overlap of the projection zones and (iii) the percentage of double-labeled neurons in the overlap zones (**Fig 3.7, 3.8, 3.9**) **(Perkel et al., 1986, Barone et al., 2000)**.

This made it possible to compare the topographical precision of projection neurons in both sets of pathways. This shows that supragranular layer projection neurons in feedforward and feedback pathways have similar topgraphical properties, and likewise for infragranular projection neurons. Irrespective of whether a feedback or feedforward pathway, the spatial extent of the projection zone and the degree of overlap of these zones as well as the frequency in double-labelled neurons is significantly higher in infra- compared to supragranular layers (**Fig 3.9**).

These results show that the convergence and divergence as well as the rates of bifurcation of cortical projections coming out of the infragranular layers is higher than those coming out of the supragranular layers independently of being feedforward or feedback. These results show that it is the differential contributions of these layers to the two sets of pathways that largely define their topographical precision.

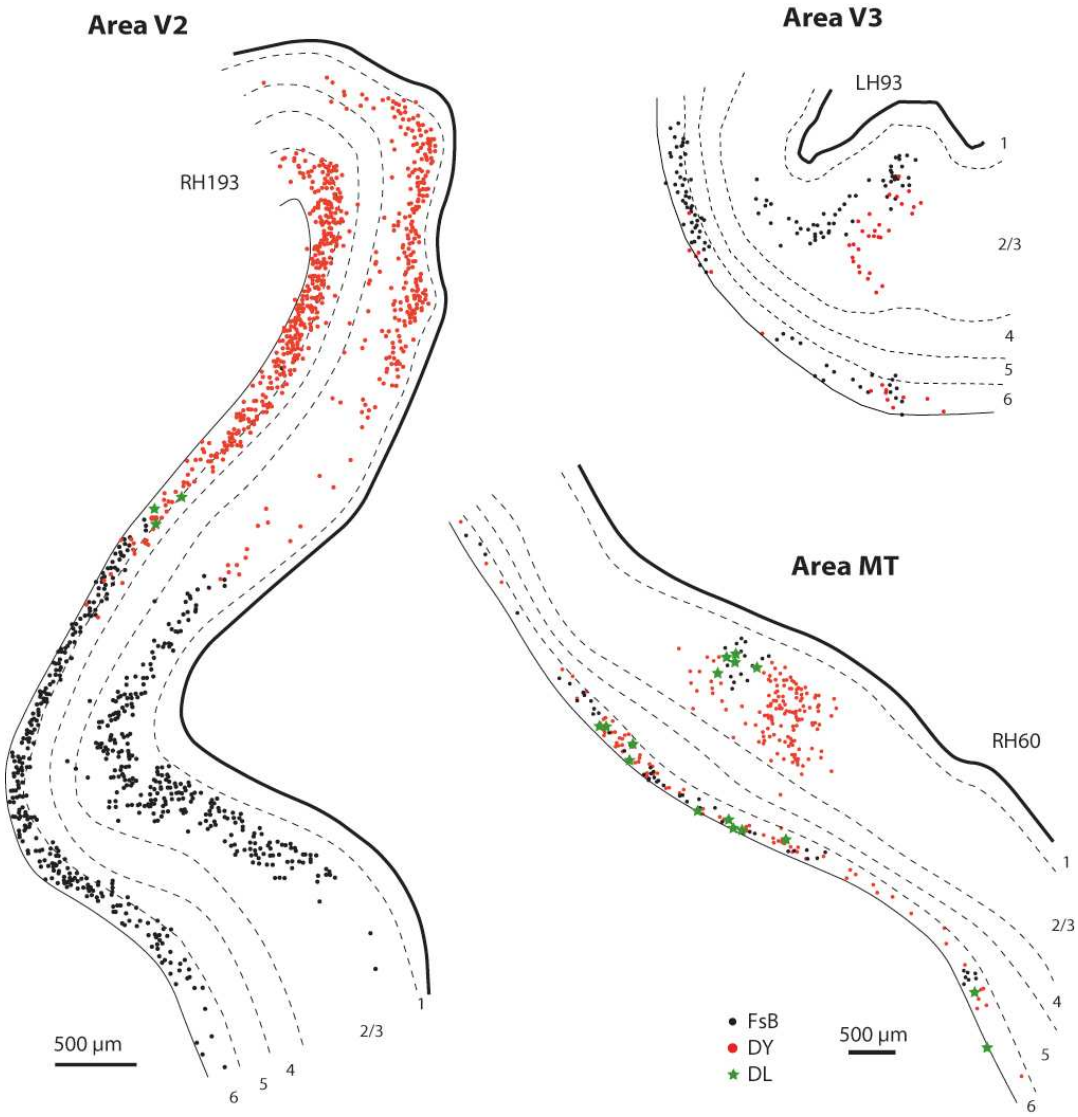

Figure 3.7 Plotmap - charts of labelled neurons in extrastriate areas following dual injections in area V1. Abbreviations: FsB fast blue, DY dyamidino yellow, DL double labeled

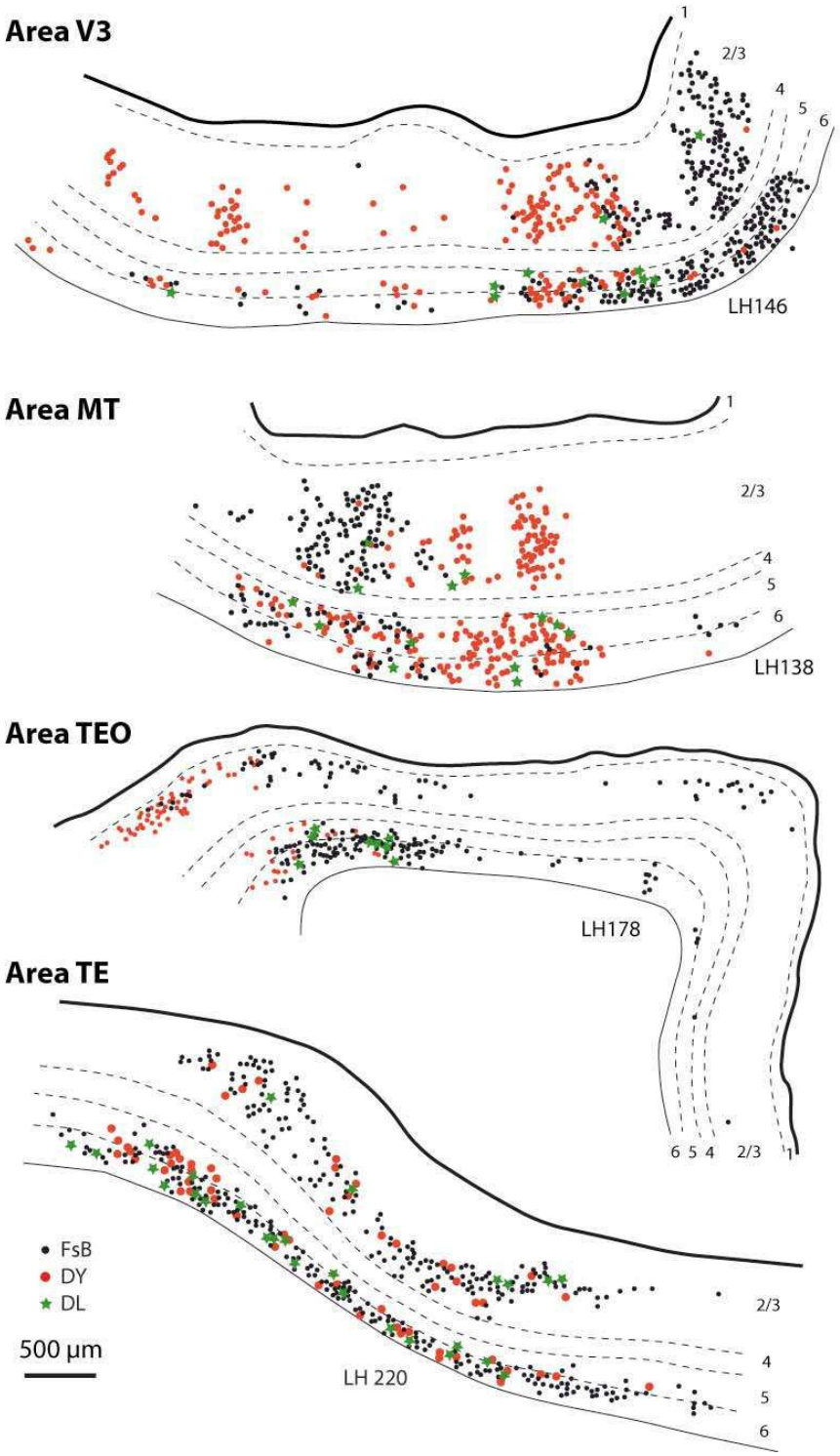

Figure 3.8 Plotmap - charts of labelled neurons in areas in extrastriate areas following dual injections in area V4. Abbreviations: FsB fast blue, DY dyamidino yellow, DL double labeled

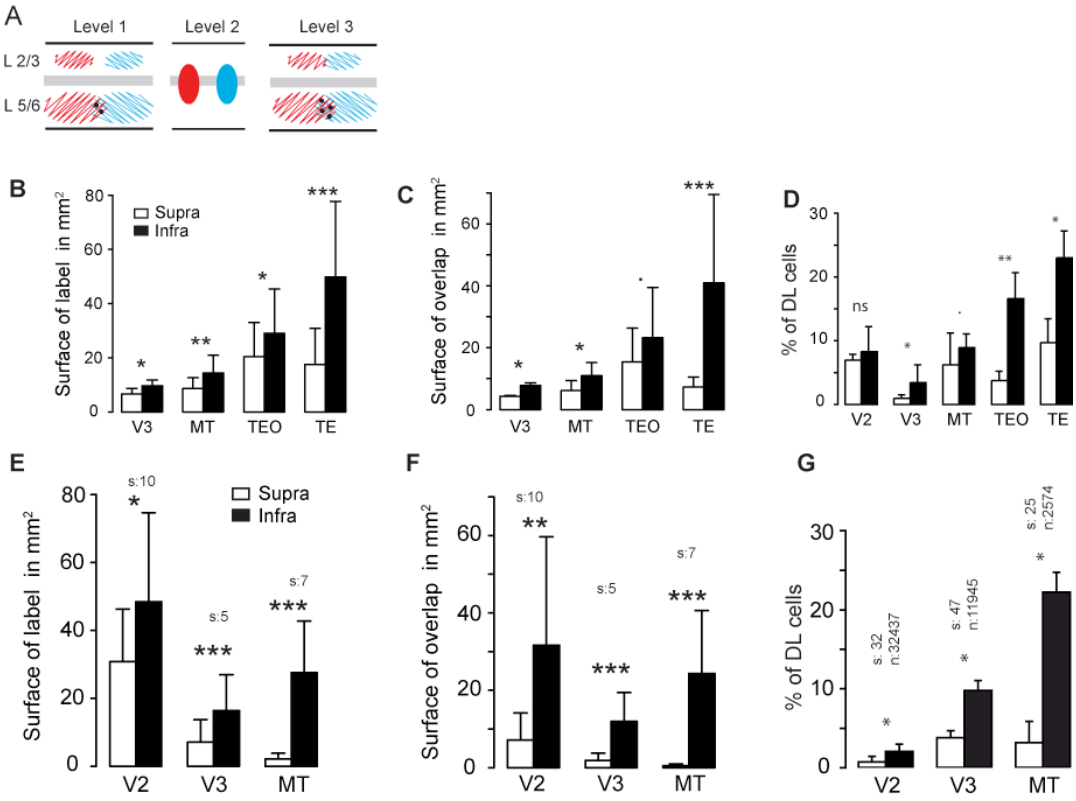

Figure 3.9 Spatial extent, overlap and proportions of double-labeled neurons in extrastriate areas following dual injections of area V4 (**B, C, D**) or V1 (**E, F, G**); **A** Schematic representation; **B, E**: Surface area in mm2 (B: number of sections for reconstructions: V3 =6, MT=9, TEO=4, TE=6); **C, F**: Surface area in mm2 of the overlap zone of FB and DY labeled neurons (C: number of sections as in B); **D, G:** Percentage of double-labeled neurons (D: V2 number of sections =58, neurons =13,231; V3 sections =12, neurons=6773; MT sections =13, neurons =3352; TEO sections=3, neurons 1971; TE sections=5, neurons =2291). Abbreviations FsB fast blue, DY dyamidino yellow, DL double labeled; empty bars supragranular layers, filled bars infragranular layers. p value *** 0.001, ** 0.01, * 0.05.

Specificity of supragranular versus difuseness of infragranular layers statistical procedure

For the analysis of areas of infra- and supragranular projections, with respect to double injections in V1 or V4, we have reconstructed the surface of label from serial sections through the projection zones. The plots of the mean vs. SD of these surface areas, indicated that SD increased monotonically with the mean. Separate analyses were performed for each target area (V1 and V4), and area of projection origin was treated as a main effect. A Box-Cox analysis (Box and Cox, 1964, Venables and Ripley, 2002) was performed to evaluate if a transformation of the form (y^lambda - 1)/lambda, for lambda not = 0, log(y) for lambda = 0 would render the variance more homoscedastic. The results suggested that a log transformation would be adequate. Finally for the measures of surface of projection zone a linear mixed-effects model (**Pinheiro and Bates, 2000**) was used to estimate whether the differences in log area between the infra and supragranular projection zones were significant. Animal was treated as a random effect. The analysis of V1 injections was done in 3 animals over 3 source areas (V2, V3, MT); there were 18 observations of the response variable, which is the difference between the logs of the reconstructed projection zone surfaces (supra vs infra). The analysis showed the infragranular projection zones to be significantly larger (on average by a factor of 4) than the supragranular projection zones ($F(3, 13) = 74.7$, $p < 0.0001$). The effect was significant for each

of the three source areas (all $p < 0.03$). The analysis of the V4 injections was done in 3 animals over 4 source areas (V3, MT, TE, TEO); there were 24 observations of the response variable, computed in the same way as in the V1 injections. The analysis showed that the infragranular projection zones were significantly larger (on average by a factor of2) than the supragranular ($F(4, 18) = 18.34$, $p < 0.0001$). The effect was significant for each of the four source areas (all $p < 0.03$).

Diffuseness of supragranular vs infragranular layers

These paired injections of fast-blue and and diamidino yellow also provided information on the extent of local connectivity of supra- and infragranular layers. Injections spaced 3mm apart showed less than 1.5% double labelled neurons, in either supra or infra. Reducing separation to 2 mm, led to a sharp increase in double-labelling that was largely restricted to the infragranular layers where bifurcating neurons were up to 8% while supra remained at around 1.5%.

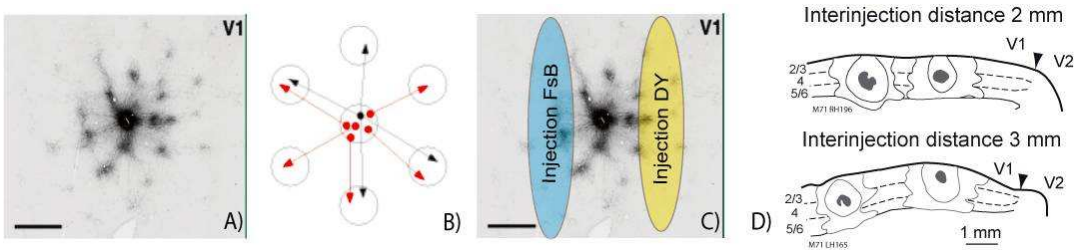

Figure 3.10 Specificity vs diffuseness of supra and infragranular layers in V1 A) The "daisy" architecture revealed by small local biocytin injection in area V1. B) The two possible organisations of the local projections originating in the center of the "daisy" (black = diffuse connections, red = selective projections. C) Shematic of the experimental principle. D) Drawings of the injection sites at 2mm vs 3mm interinjection distance.

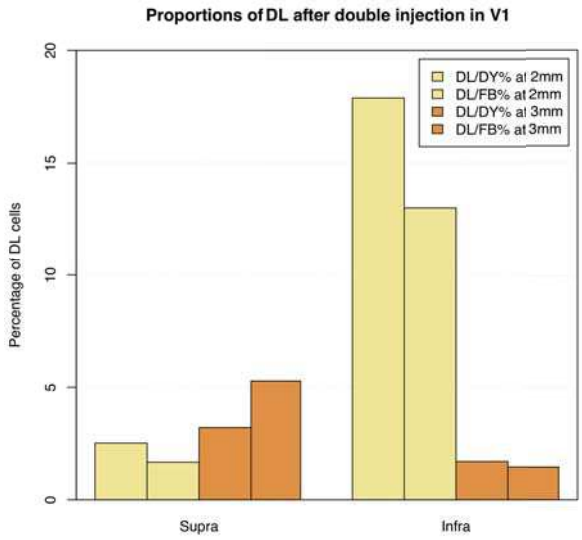

Figure 3.11 Ultralaminar specificity vs diffuseness of intrinsic projections. Histogram correspond to intrinsic DL counts after the injections shown in figure **3.10D**

Integration between long short distance projections

Simultaneous injections of fast-blue and diamidino yellow retinotopically corresponding location in V1 and V4, makes it possible to explore the degree of integration of feedback and feedforward projecting neurons into the local circuits of their source areas. In the supragranular layers of area V1, 2.6% of the feedforward projecting neurons targeting area V4 possessed a local collateral, this contrasted with the much higher percentage in V4, where 13.6% of the supragranular feedback neurons targeting V1 possessed locally projecting collaterals **(Fig. 3.12)**.

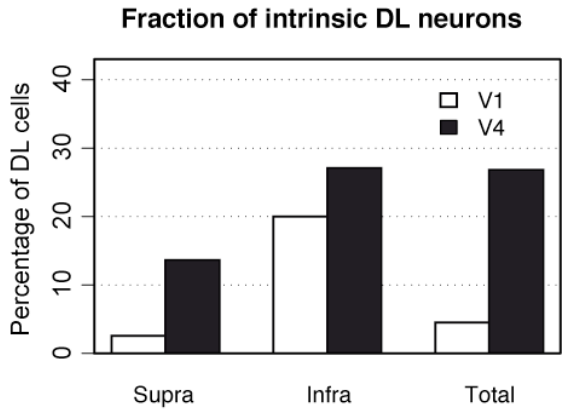

Figure 3.12 Amount of intrinsic colabelling of feedforward or feedback projecting neurons. Injections are in V1 and V4 and histogram correspond to the percentage of DL within each of the injected areas.

Segregation of feedforward and feedback projecting neurons.

Early reports on the connectivity of macaque extrastriate cortex hint at the possibility of a vertical separation of rostral and caudal directed projections emitted from the supragranular layers **(Rockland and Pandya, 1979).** We explored this by making simultaneous injections of two distinguishable retrograde tracers, diamidino yellow in area V1 and fast blue in area V4.

The distribution of labelled neurons in V2 shown in **Figure 3.13A** shows that there is a clear segregation of the two populations of projection neurons. In the supragranular layers, the population of feedback projecting neurons targeting V1 are concentrated in layer 3A and appear largely separated from the population of feedforward projecting neurons targeting V4 concentrated in layer 3B. In the infragranular layers, the two populations were largely intermingled, feedback neurons targeting V1 were located in layer 6 and the bottom of layer 5, while the population of feedforward neurons targeting V4 were found throughout layers 5 and 6 **(Fig 3.13A)** identical pattern of segregation was observed in V3**.** However, because of the heterogeneity in the laminar distribution of cortico-cortical neurons in the projection zone of a given pathway, demonstration of segregation of pathways requires high-frequency sampling throughout the projection zone **(Batardiere et al., 1998).** In order to quantitatively explore the patterns of cells of origins we analysed, a number of injections of low and high hierarchical levels (areas V1, V2, V4, LIP, TEO and STP). We have examined the pattern of the cells of origin in 17 of the feedforward and feedback pathways in select source areas : V2, V3, LIP, and MST. This analysis demonstrates that the segregation of feedforward and feedback projecting neurons is a consistent feature across the cortex (**Fig 3.13A and 3.13D**). While not obvious for the infragranular layers the supragranular layers show a clear segregation in to a feedforward and feedback compartment **(Fig 3.13 C,D,E).**

Following the paired injections V1/V4 not only were the two populations of neurons within V2 much more intermingled in the infragranular layers compared to the supragranular layers but the proportion of neurons possessing both feedforward and feedback collaterals were extremely rare in the supragranular layers (0.33%) compared to the infragranular layers (4%). Note that in areas higher than area V4, the two populations of neurons projecting to both V1 and V4 constitute feedback projecting neurons. In these higher areas and contrary to early areas, both sets of neurons are largely co-localised in the same cortical layers (**Fig 3.13B**). Here neurons with collaterals projecting to both cortical areas are very frequent (15-30%) as commonly found elsewhere in the cortex **(Kennedy and Bullier, 1985, Sincich and Horton, 2005)**. These findings show that area V1 and V4 projecting neurons are highly segregated in areas where they constitute respectively feedback and feedforward connections, but not when both sets of neurons constitute feedback connections.

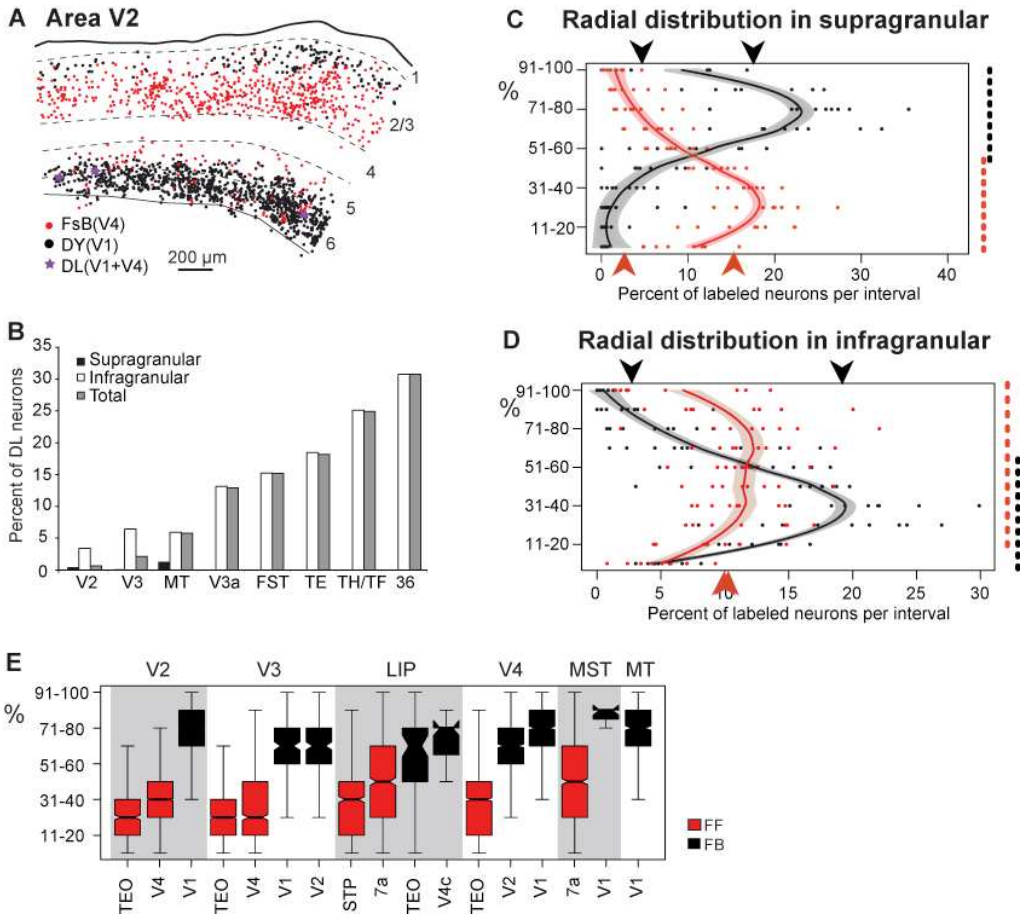

Figure 3.13 Segregation of feedforward and feedback pathways. A: Charts of retrograde labeled neurons in a parassagital section of area V2 following injections of DY in area V1 and FsB in area V4; **B**: Laminar distribution of double labeled neurons in visual areas V2, V3, V3a, MT, FST, MST, TF/TH, area 36; **C**: Percentage of labeled feedforward and feedback neurons per interval in supragranular layers of extrastriate cortex (areas V2, V3, V4, LIP, MST, MT see Fig. 3.9E)., Black and red vertical segments indicate the intervals associated respectivelly with feedback and feedforward directed projections. Envelope corresponds to a loess predicted distribution. 0 top of layer 4, 100 bottom of layer 1. Abbreviations: FsB fast blue, DY dyamidino yellow, DL double labeled. **D:** Same analysis as C applyed to infragranular layers. E: Boxplot of the distribution of feedforward and feedback projecting neurons within individual source target pairs.

Morphology of feedforward and feedback neurons

The integration of the feedforward and feedback connections into the laminar structure of the cortex depends not only on the laminar location of the parent pyramidal soma but also on its dendritic arborisation. It is thought that whereas cortico-cortical neurons in the supragranular layers have apical dendrites extending to and forming tufts in layer 1, infragranular cortico-cortical neurons have slender apical dendrites that do not reach layer 1 **(Katz, 1987, Hubener et al., 1990).** Because long-range cortical projections are formed by only a minute fraction of cortical neurons **(Lee and Winer, 2008)**, what is known about differences in cell morphology in upper and lower layers does not allow us to come to a very precise conclusion concerning the possible differences in the cell morphology of the parent neurons of the two sets of pathways.

To explore this issue we used retrograde tracers to identify both sets of neurons in area V2 and then carried out in vitro cell filling (see methods). All 46 filled neurons recovered had clear pyramidal cell type morphologies with a well-defined apical dendrite **(Fig 3.14).** Our results show that all supragranular layer neurons irrespective of whether they are feedforward or feedback possess a tufted apical dendrite. In the infragranular layers, feedforward and feedback layer 6 pyramidal neurons as well as feedback layer 5 neurons had slender apical dendrites and therefore conform to the morphology of cortico-cortical neurons described in these layers **(Klein et al., 1986, Katz, 1987, Hallman et al., 1988, Hubener et al., Kasper et al., 1994)**. Unexpectedly we found that of the 9 feedforward neurons in layer 5, 4 had apical dendrites that reached layer 1, 3 of which formed multiple branches in layer 1 and therefore correspond to the tall-simple pyramidal neuron type that has been shown to participate in controlateral cortico-cortical projections in mouse **(Larsen et al., 2007)**.

These results are unexpected because it is currently believed that cortico-cortical neurons in layer 5 are slender, while the tufted layer 5 neurons target the superior colliculus (Katz, 1987, Kasper et al., 1994). They results show that monkey layer 5 neurons have apical dendrites reaching layer 1, and this could be a characteristic feature of feedforward neurons in this layer. In the feedback population apical tufts were only located in the small contingent of short distance projecting feedback neurons located in layer 3A corroborated by previous studies (Rockland et al., 1994). Layer 1 has been hypothesised to provide a unique structure to allow integration of top down signals and sensory inputs **(Cauller, 1995, Larkum et al., 1999)**. These results suggest that modulation of pyramidal neuron activity via feedback projections to layer 1 **(Cauller, 1995)** will preferentially influence feedforward and short distance feedback projections (see discussion).

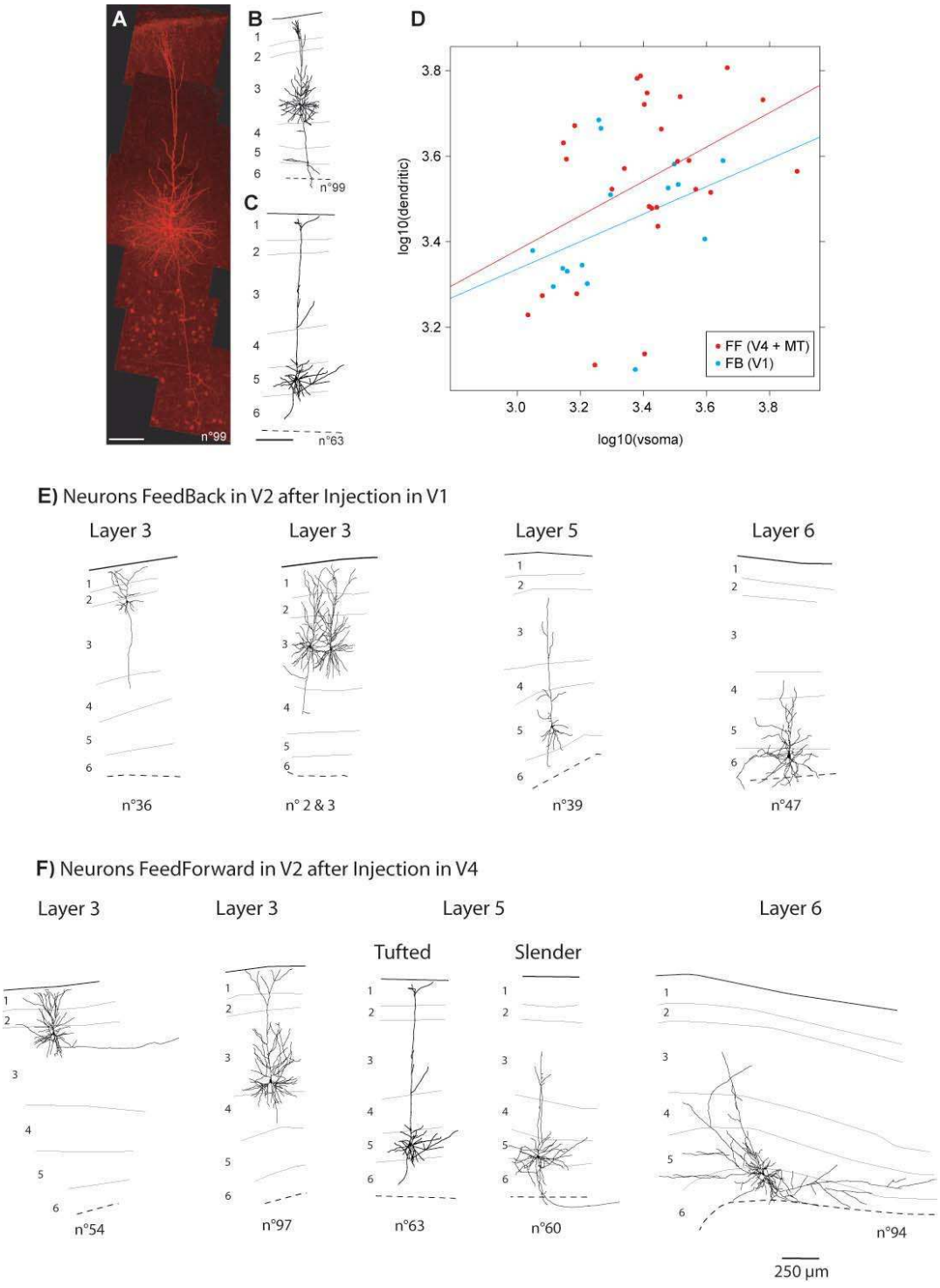

Figure 3.14 Morphology of projection neurons in V2. **A**: Photomontage reconstruction of a layer 3B feedforward neuron; **B**: Drawing of the feedforward tufted layer 3B neuron shown in A; **C**: Simple-tall feedforward layer 5 neuron. **D**: Scattergram of cell soma size and dendritic arbors with linear fit. **E-F:** Morphology types of reconstructed neurons from each path.

Layer 2, is analog to layer 4?

Determining the extent of cortical layers is not always an easy task and the majority of the electrophysiological experiments do not differentiate between layer 2 and layer 3 of the cortex. To my knowledge only one paper reports to date a rigorous study of the differences between physiological properties of layer 2 vs layer 3 (Gur and Snodderly, 2008). Another study with more general approach also makes some suggestions of difference in the selectivity of feedback recipient layers and a possible role in the feature binding (Shipp et al., 2009). Our results here suggest that ignoring the differences between layers 2 and 3A, 3B may cause to neglect an important structural element of the cortical hierarchy.

In the laminar nomenclature layer 4 is referred to as the "internal granular layer" and layer 2 as the "external granular layer" **(cf. fig 3.15)**. Layer 4 is characterised by granule cells having local connections and being the recipient of the thalamo-cortical inputs or the feed-forward interareal connections. Layer 4c projects to layer 3 but not to layer 2 (Lachica et al., 1992, Levitt et al., 1996, Yabuta and Callaway, 1998, Sawatari and Callaway, 2000). Interestingly the work of Rockland shows that there is a specific micromodularity of the positions of neurons in layer 2 that are offset from the dendrites of thalamorecipient cells(Ichinohe and Rockland, 2004). This can be interpreted in terms of segregation between the FF and FB streams. A recent paper also identifies a gene that is expressend in many layers of associative areas but very specifically in layer 2 of the primary areas (Takaji et al., 2009). Under the light of the continuous indications of segregation between FF and FB streams that we find in this work these elements can (Watakabe, 2009)rise the question of the place of layer 2 in the anatomy of the hierarchical interrelations.

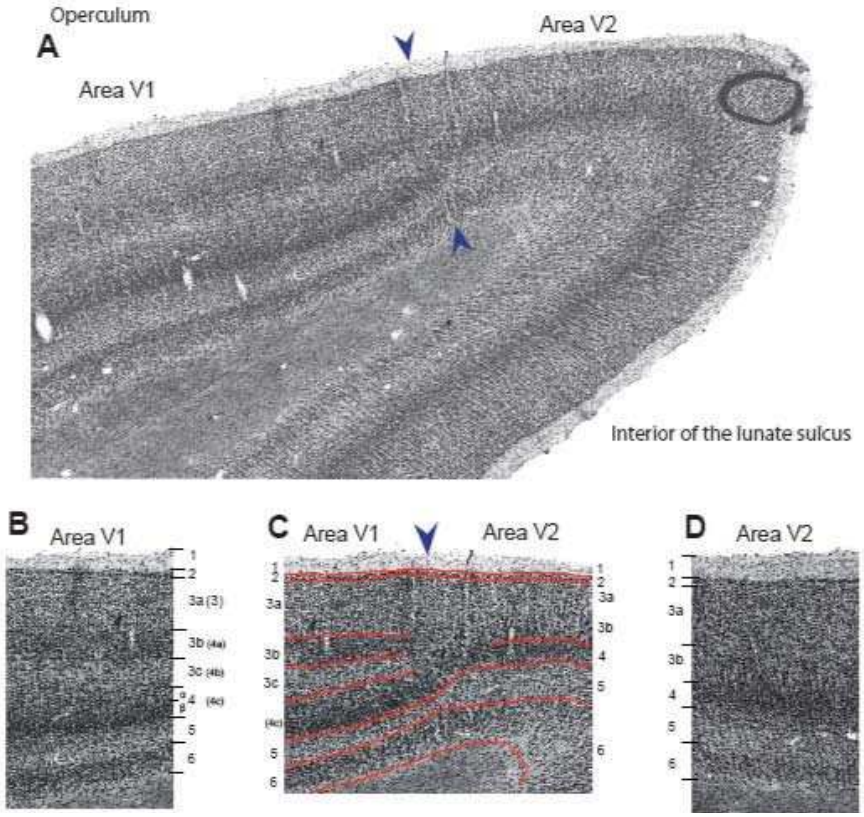

Figure 3.15 Lamination of striate and extrastriate cortex. A: Low power photomicrograph of horrizontal section showing area V1 on the operculum and area V2 within the lunate sulcus. The areal border is indicated by two arrowheads. B: Laminar structure of Area V1. The sequence 1,2,3,4a,4b,4c corresponds to Brodman's nomenclature (Brodmann, 1909). The alternative sequence 1,2,3a,3b,3c,4,5,6

is derived from the nomenclature of Hassler **(Hassler 1967)** used in Tigges (Tigges et al., 1977)**,** Fitzpatrick (Fitzpatrick et al., 1983). C: The transition between areas V1 and V2 in the macaque monkey. Brodman has interpreted this transition as the convergence of the two lamina of layer 4 (4a and 4c) in to one single layer in extrastriate cortex where layer 4b remained without analog. Further explorations , reviewed in Casagrande and Kaas , based on the cytoarchitectonic, chemoarchitectonic and interspecies comparison showed that this interpretation is not consistent and plead that brodmans 4b merges within layer 3 of area V2 while 4a has no analogue in extrastriate cortex. The laminar nomenclature in extrastriate areas is less controversal and a general subdivision in to 6 layers is quite conventional (**Polyak, 1957**) **(Casagrande and Kaas 1983)**. D: Laminar organisation of V2 . 1- Plexiform layer : characterised by a paucicellular structure and rich in neuronal terminations; 2- Outer granular layer : formed of occasional granular cells and of very small cells of pyramidal shape with an apical dendrite directed toward layer 1 their connectivity is principally intrinsic (find the ref about layer 2 intra); 3 – Pyramidal cell layer that can be subdivided into two compartments (3a and 3b) based on the cell size and density , also layer 3A does not receive intrinsic projections from layer 4 while 3B is the major target of layer 4 neurons (Boyd et al., 2000).; 4- Inner granular layer : layer of denselly packed true granule cells with some occasional pyramidal cells. 5 - Ganglion cell layer : characterised by large pyramidal cells with lesser density than the bordering layers 4 and 6; 6 – Multiform cell layer : cells are of large size with various forms and higher density than in layer 5.

After an injection in area V1 on the operculum we have carefully plotted the labelled cells in area V2. As already reported the projecting neurons are found in the uppermost parts of the supragranular layer but interestingly there is a very thin layer of cells at the interface with layer 1 where the cells do not send projections to the injected site(fig. 3.16). We identified this layer as layer 2 and conclude that it is likely that layer 2 will have majorly intrinsic projections in a manner analogous to layer 4. This observation rises in our minds very strongly the question of the role of layer 2 in the processing of the FB inputs and the possible role of this layer.

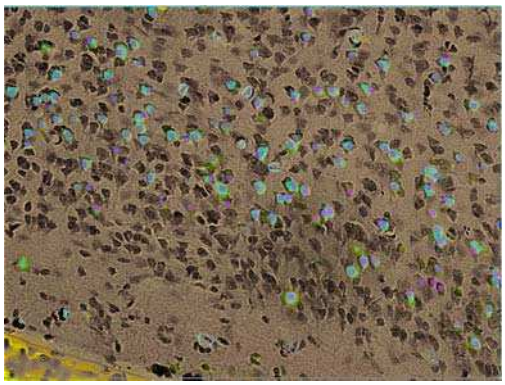

Figure 3.16 Layer 2 does not participate in to interareal connectivty. Photomontage of Nissl stain , plot map and Fluorescence photomicrograph from area V2 after injection in V1.

DISCUSSION

The cortical hierarchy

The use of SLN weighted by FLN has enabled us to constrain the cortical hierarchy of the early visual areas based on a continuous scale. Compared to models with discrete scales, it has the advantage to determining hierarchical relations but in addition of providing a hierarchical distance measure that may reflect underlying functional processes. While our hierarchy shares many of the features of that of Felleman and Van Essen (1991), it shows some interesting differences that need to be addressed.

The relation between physical, hierarchical distance and SLN

Since the first hints on the notion of feedforward and feedback projection streams there was drawn a relation between the geometry of the distribution of projection cells and terminals and the projection type (**Rockland and Pandya, 1979**). In a simplistic view the feedforward was associated with supragranular cells of origin and terminations in layer 4 while feedback was meant to originate from infragranular layers and terminate outside of layer 4. The geometry of feedforward and feedback efferents is actually more complex. As shown in **Figure 3.5A** there are only very rare pathways that do not have projections from both supra and infragranular layers.

So obviously emerges the question how these complex relations may generate a simple dichotomy between feedforward where the supragranular layers are the most populated ones and the feedback where the infragranular dominate. In order to be able to compare the label generated by our injections we have computed the average total of labelled neurons from the injections (V1, V2, V4, TEO, 7a) and we normalized the number of labelled neurons in each source area, so as to fit to this mean. This minimizes the effect of the size of injection on the number of labelled neurons per area and preserves the FLN and SLN of the area. A plot of these data is presented in **figure 3.5B, C**, it represents the evolution of the number of neurons in each compartment as function of the distance of projection.

In all situations there is a decrease of the number of labelled neurons with distance. The linear models fit to the data points show a bit steeper decrease in the infragranular compartment in feedforward projections and the supragranular compartment in feedback projections. These fits suggest that it may be that for a given projection pathway the decrease of labelled neurons with distance is more pronounced in the layer that is less associated with the type of the pathway. Stemming from this we can call the compartments that are less sensitive to distance increase the major compartments (supragranular in feedforward; infragranular in feedback) as opposed to this the other compartment should take the adjective of minor compartment (infragranular in feedforward; supragranular in feedback). To strengthen this we can represent the ratio of the major against the minor compartment **(Figure 3.5D).** The observed increase with distance fits to our bibliographic survey that suggested gradients in cell origins and terminals expressed in the hierarchical relations of ascending and descending pathways. As discussed in the main text the interaction between physical and hierarchical distance may be at the basis of the serial processing in the brain and the match between physical and hierarchical distance highlights the embedded nature of the brain network.

Segregation of pathways.

This study has characterized a feedback pathway located in layer 3A of the supragranular feedback compartment. The feedback neurons in layer 3A are integrated with the over-lying with what Polyac and others have identified as the external granular layer, layer 2 and the feedback plexiform layer, layer 1 by particularly robust tufted apical dendrites (**Polyak, 1957**). These feedback neurons receive feedback input from upper areas and their output is sent to the upper layers of downstream areas **(Lund et al., 1981, Henry et al., 1991, Angelucci and Bressloff, 2006)**, thus participating in a feedback cascade.

Consideration of the present retrograde labelling studies in conjunction with earlier anterograde studies reveals to set of pathways in the supra- and infragranular layers. The layer 3B feedforward neurons are integrated with the underlying input layer, the internal granular layer, layer 4 via their basal dendrites and receive feedforward input directly from layer 3B of lower-stream areas and target layer 4 of high order areas **(Lund et al., 1981).** The infragranular layers, layer 6 neurons constitute the major feedback pathway relaying input from neurons in the lower layers of upstream areas over short to medium distances, and in addition provides

input to layer 1 over long-range distances **(Lund et al., 1981, Henry et al., 1991, Angelucci and Bressloff, 2006).**

The present results show that the location of feedback in layer 3A and feedforward stream in 3B is a feature of extrastriate cortex and allows us to propose a general schema of feedforward and feedback connections in visual cortex, where a topologically organized counterstream is located in supragranular layers and a diffuse set of feedforward and feedback connections in infragranular layers (**Fig 3.17**). The present results show that all the supragranular feedforward neurons and 50% of the feedforward neurons in layer 5 have apical dendrites reaching layer 1. Amongst the feedback pathways, the major contingent of feedback neurons, which is located in layer 6, has no contact with layer 1 in contrast to the feedback layer 3A neurons which do have apical tufts in layer 1 **(Fig 3.17B**). Feedback neurons along with the spiny stellate neurons of layer 4 might be more tuned to respond to thalamocortical and corticocortical feedforward input, whereas layers 2/3 and 5 have been shown to be the only layers that respond to layer 1 **(Cauller et al., 1998)** and show monosynaptic response to feedback activation **(Rockland et al., 1994, Johnson and Burkhalter, 1997)**.

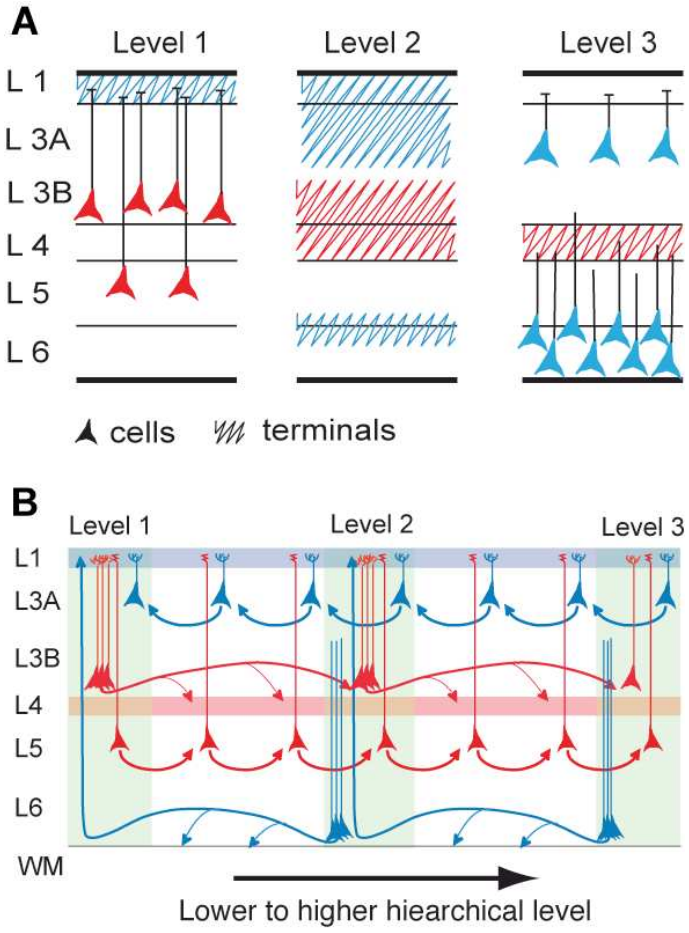

Figure 3.17 Summary of the anatomy of hierarchy. **A: i**nfluence of distance on distribution of terminals. Feedforward level 1 neurons project to layer 4 and layer 3B in level 2 and layer 4 of level 3. Level 3 layer 3A feedback neurons project to layers 1, 2 and 3A of level 2 and layer 1 of level 1. Level 3 layer 6 feedback neurons project to layer 6 in level 2 and layer 1 of level 1; **B**: long-distance feedforward pathway in layer 3B, tightly integrated with layer 4 via basal dendrites and the targeting of layer 4 of upstream areas. Long-distance feedback pathway in layer 6 targeting layer 6 of adjacent areas and layer 1 of far-distant downstream areas (Rockland and Van Hoesen, 1994). In the layer 3A there is a short-distance feedback pathway tightly integrated with layer 1 via apical dendritic tufts. In infragranular layers there are two short distance feedforward pathways in layer 5 and 6, the layer 5 pathway being in contact

with layer 1 via its apical dendrites. The parent populations of feedforward and feedback are highly distinct, and neurons very rarely have feedforward and feedback collaterals.

Distance rules in the cortex

SLN has been proposed as a hierarchical distance measure between areas **(Barone et al., 2000)**. The present results show that the 93 or so pathways interconnecting the early visual areas show a high degree of correlation of their SLN values as predicted by the operation of a hierarchical distance rule (**Tables 3.1, 3.2 and Fig 3.1, 3.2C**). The high correlation of SLN values of areas that are widely distributed both across the cortex and the hierarchy confirms that the laminar distribution of projection neurons constitutes a powerful regularity of the cortex that needs to be interpreted with the connectivity diagram shown in **Figure 3.17B**. The fact that SLN increases with increasing distance reflects that layer 3B is a long-distance feedforward stream in contrast to layer 5/6, which is a short distance feedforward stream. Likewise, the fact that SLN decreases with feedback distance reflects that layer 3A is a short distance feedback stream whereas layer 5/6 is a long distance feedback stream. Hence, the hierarchical organization is the expression of combinatorial distance rules acting in parallel in the feedforward and feedback streams of the supra- and infragranular layers**.**

Physical distance is an important factor to be kept in mind when comparing interareal pathways in the cortical hierarchy. 75% of interareal connections are short to medium ranges where supragranular and infragranular layers are all participating in both feedforward and feedback pathways, and where each layer contributes its characteristic features to both sets of pathways. It is only the long-distance pathways that will show the sharp dichotomy, where feedforward connections stem uniquely from the supragranular layers, exhibit point to point connectivity and target layer 4 and where feedback connections stem uniquely from the infragranular layers, exhibit diffuse connectivity and target layer 1.

The supragranular layers undergo expansion in primates **(Pollard et al., 2006)** and this has importance for the highly segregated point to point long-distance feedforward and short distance feedback pathways that are housed in these layers. Feedback neurons in layer 3A target upper layers of an area downstream in the hierarchy and so they will participate in a FB chain of topologically precise excitatory projections (**Rockland et al., 1994**). Whereas feedforward neurons in layer 3B receive their major input via their basal dendrites in layer 4 and participate in a feedforward chain. Both these pathways differ markedly from the infragranular feedback pathway which fail to contact layer and is therefore not influenced by input to this layer. These pathways are fully compatible with the counter stream theory of information flow in the cortex **(Ullman, 1995)**. The distance rule that we show set up the cortical hierarchy, has implications for hierarchical generative models of perceptual inference. The topographically organized counterstreams in the supragranular layers between adjacent levels could provide the substrate for linear prediction coding **(Rao and Ballard, 1999)**, whereas the long-distance feedback pathways in the infragranular layers have the appropriate configuration to be involved in the non-linear, modulatory processes **(Friston, 2005, Ekstrom et al., 2008, Chen et al., 2009)**. Because these pathways stem from the infragranular layers they are expected to be tightly integrated with subcortical input to the cortex and the feedback control over the sub-cortical structures associated with these layers.

Chapter IV

PERSPECTIVES

In modern approaches of brain exploration, retrograde tracing techniques and the anatomical exploration as a whole have largely lost ground, to be replaced by such methods as molecular characterization and functional and imaging studies of brain operation. In this context a recent review from Raichle **(raichle trends in cognitive sciences 2010)** depicts two opposing views that have driven research on the brain. The first goes back to the work of Sir Charles Sherrington, who viewed the brain as a reflective system, favouring the importance of extrinsic stimuli in the generation of the behavioural responses of the brain. The second point of view is to be found in Raichle's own work and has it's roots in that of William James **(James 1890)** who argued that a significant part of conscious experience resides in the intrinsic workings of the brain. It could be envisaged that the modern investigation of brain function is more squarely anchored in James' view of the brain. Alternatively, no self-standing, purely bottom-up or top-down view of the brain can be entirely satisfactory. In fact as we have shown, careful anatomical experiments using retrograde tract tracing are able to shed light on both viewpoints. In line with the view put forward by Raichle, our results emphasize on the one hand the paucity of the thalamo-cortical pathways as well as the very few neurons participating in the interactions between hierarchical levels of the cortex and on the other, the sheer importance of intrinsic connectivity in terms of numbers of neurons. However our results also address the Sherrington concept of the brain as an integrator and coordinator of function. We show that the cortical network is built upon the interaction of two highly segregated counter-streams arranged in a circuit-like structure of high bandwidth transmission where there are direct moderate to weak links between the majority of brain areas. Hence here I shall argue for the need to combine modern neuroscience technology with long established approaches to the determination of structure in order to firmly establish the structural constraints on brain function. As is to be expected in a scientific endeavour, the results and analyses presented in this thesis raise more questions than they provide answers. The following paragraphs summarize some further steps that can be taken. Some of them could remain on a wish list others are already being undertaken.

Large-scale exploration of connectivity profiles in macaque

To date we have described the full connectivity of 26 areas out of the 83 areas of the cortical sheet. The approximately even distribution of target areas across the cortex, the fact that the average degree (number of input areas) to each of them is fairly clustered around a mean value combined together with the results of the minimum dominating set analysis make it very likely that the high cortico-cortical network density that we report here will remain true -even if we were to inject every single area in the brain.

While the work done so far shows us many of the structural principals of the cortex, important details are still missing. The high density network of the 26 areas explored here reveals *a* functional backbone, but it does not tell us about *the* functional backbone. These results raise the possibility that modulation of threshold (silencing of weak projections as activity rises) could indeed play an important role in the functional connectivity of the cortex. Future exploration of the 83-26=57 remaining areas is needed to provide an understanding of the actual structure of the backbone.

Recent MR DTI studies have identified the precuneus region as a central functional and structural hub of human cortex(Nelissen et al., 2006, Hagmann et al., 2008). So one of the first candidate areas for future injection will be areas 7m and 31. There are numerous other areas that remain to be explored and that will have an important impact on our future understanding of the

cortex. The retrosplenial cortex, has strong reciprocal connections with dorsal prefrontal and ventro-temporal areas and may play a relay role in prefronto-temporal interactions. Areas V3 and V3A, the later being involved in 3D movement processing are also of major interest. Areas LIP and MIP region are candidates because of their role in parieto-prefrontal interactions. The visual motion processing areas in the Superior temporal sulcus MT, FST and the yet to be understood LST (Nelissen et al., 2006) need in depth exploration of their connectivity patterns. In the temporal lobe the various subdivisions of area TE are particularly interesting. All these tracing experiments represent individual interest for the functional importance of the injected area and when done will enrich our understanding of anatomical interactions in the brain. This will lead us to increase further the size of our database of inter-areal connections and to obtain an ever-growing, weighted subgraph. At every step of the way we will get a richer understanding of the backbone structure and we will be able to have a higher fidelity model of the brain network.

Because the retrograde tracing is a relatively slow and time consuming method the accomplishment of the full connectivity of the monkey will require the development of automated techniques for tract tracing using fast blue and diamidino yellow. There are a number of promising complementary methods, which will need to be technically improved to rival the precision of the wet tract tracing. For example, magnetic resonance, either using diffusion tensor or using the use of contrast molecules both need improvements in order to be able to reveal projection weights. Published papers have sought to trace and reconstruct projection pathways using these methods (Hagmann et al., 2003, Hagmann et al., 2007). This approach will be very interesting as it tells not only which two areas are interconnected but it is also makes it possible to reconstruct the path of the projection through the white matter and measure it's length. At the current stage one of the methodological problems is the inability of this method to reliably capture the FLN of a projection. In this manuscript we have shown that projection magnitude is constrained by the distance rule and so it should be possible to use distance information in order to calibrate the DTI tracing so to be able to approximate the FLN value of a projection. Another problem standing in front of magnetic resonance pathway tracing is the lack of information on the direction of a projection and low sensitivity for weak pathways. A combination between conventional retrograde tract tracing and MR-tracing techniques could make it possible to calibrate the latter by means of the former and eventually lead to a full scale connectivity matrix of the brain.

Relevance to the human connectome project

There is a vast amount of information concerning the connectivity of the macaque brain but the human brain connectivity remains largely a "terra incognita". Inspired from a philosophy similar to the one that led to the human genome is the new project on complete human connectome (Sporns et al., 2005). Human studies cannot use invasive methods and so the only available method is the MR approach. In regard of the previous paragraph and the conclusions about the importance of FLN values for understanding the cortical network it will be greatly profitable that an effort be made in the calibration of the MR in macaque so as to then export it in humans and use the same techniques to generate a weighted human connectome. A byproduct of this approach will be the improvement of the knowledge about the homologies between the human and macaque brain. The CARET software provides the possibility to wrap Macaque cortical maps onto human (Van Essen, 2002a, 2004, 2005). This standardized tool that is already available should play a central role in setting the homologies between the macaque and human cortices and connectomes. If this can be accomplished, it will provide the long needed interfacing gate for interpolation of the known physiology of the macaque to the human.

Dynamics of the network

We have sought to determine the structure of the macaque cortico-cortical network and this led us to question some of the fundamental principles believed to govern the structure-function interaction. It is generally accepted that dynamic synchrony reveals functional networks in the brain (Sejnowski and Paulsen, 2006). Currently this mechanism is explained as the result of few long distance connections generating the small world architecture of the cortex. This explanation implies that synchrony will be built in the network by means of propagation through the few "shortcut" lines. Such a synchrony generation mechanism would be very inefficient and difficult to control. Our data suggests that this is not the solution retained by the brain. Synchrony in the brain can be efficiently coordinated by direct links that can be extremely weak (Slotine and Lohmiller, 2001, Hahnloser et al., 2003, Wang and Slotine, 2005, Pham and Slotine, 2007, Girard et al., 2008, Tabareau et al., 2010). The dense cortical network with distance constrained lognormal distribution of FLN is optimized to minimize total wiring length while providing direct input between the majority of brain areas. These weak direct links may well be on the basis of the inter-areal network synchrony operating the brain. Armed with the data about the backbone, the FLN distribution, inter-areal distances and paths it will be possible to model this network and explore the types of synchronization that it provides. As a first approach the model can assume that a given area will integrate it's inputs, activity will be generated and transmitted to all targets the same way and with a given time pattern. But the full understanding of the inter-areal interactions will need to integrate the fact that all the projections are not equivalent as suggested by the segregated counterstreams that we explored in chapter 3.

Another perspective that can be explored is related to the fact that we found the strongest subcortical input to every area to be from the Claustrum. Very little is known about the function of the claustrum but some publications point to a capacity of this structure to inhibit cortical areas by targeting inhibitory neurons. If this is put in parallel with the default network theory (the logic of it will not be developed here) one can imagine a role in the Claustrum in the control of shifting of state from default to task related. Some publications on Claustrum (Irvine and Brugge, 1980, Tsumoto and Suda, 1982, Vakolyuk et al., 1983, Crescimanno et al., 1984, Salerno et al., 1984, LeVay, 1986, Crescimanno et al., 1989, 1990, Wojcik et al., 2004, Douglas and Martin, 2007). The default network has been discovered in humans but it is also present in monkeys (Vincent et al., 2007b). The experiment that can be done to test whether the claustrum is instrumental in the shifting from activity within the default network in to task related activity in the cortex is to combine fMRI with electrophysiological recordings in the claustrum. The paradigm can include as well recordings as stimulations that will lead to reversible inactivation(desorganisation) of the claustral activity. It is also interesting to remember that the unilateral removal of the Claustrum has been claimed to be fully compensated in humans (Duffau et al., 2007).

Feedforward and feedback counterstreams

In chapter 3 we have shown that the inter-areal connections come in two flavours, projections originating from the bottom of layer 3 i.e. in the center of the cortical sheet corresponding to a feedforward projection reciprocated by projections originating and terminating in the margins of the cortical sheet corresponding to feedback. Our results showed that these two streams are highly segregated and contrary to common belief, in the supragranular layers the arrangement of the cell-machinery in terms of projection topology is actually quite similar for the feedforward and the feed back streams. This opens two important directions of exploration of these counter streams. Firstly, to characterize, their level of segregation, their integration in the local microcircuit and their capacity to implement inference (Friston, 2003, O'Connor et al., 2009). Secondly, to explore the differences in protein expression that will be resonant to functional (operational) differences between either the layers associated to given pahtway or the individual projection neurons (Watakabe, 2009).

We have used laser micro-dissection (LMD) to isolate cells from each layer projecting either in the feedforward or the feedback direction. After injection in V1 (DY) and V4 (FsB) and appropriate survival time we have dissected and snap frozen the cortex of area V2. We used LMD on 20µm semi thin unstained sections to identify and dissect the numerous feedback projecting cells from layer 3a and also the few feedback projecting cells found in layer 3b. Using the difference of colour we dissected from the same area the numerous feedforward projecting cells from layer 3b and the few feedforward projecting cells that we could find in layer 3a. We isolated RNA from these preparations and ran it on the Affymetrix Macaque array. This gave us the possibility to compare the gene expression in cell populations defined by their layer 3a/3b or the projection in the feedforward or feedback pathway. Our aim here is to identify if there is a clear-cut feedforward vs feedback identity and/or respectively if there is a layer dependant identity that is common to all cells (FF and FB) from the same layer. The results are complex to interpret, as there are genes specific to every contrast made. There are 23 genes present in layer 3b and absent in layer 3a, and 14 genes expressed in layer 3a but not 3b. In the other contrast there were 10 genes uniquely present in FF cells and 30 present only in FB. A simple array experiment is adapted for prospective exploration but contains false positives. As a first step we selected a group of expressed genes in the array and we ran qRT-PCR on our samples. This revealed 4 genes expressed in the FF projecting cells of layer 3b but absent in both FB projecting cells of both layers 3a and 3b i.e. these genes seem to be markers for FF projecting cells. The 4 marker candidates are:

16. KIF5B – the heavy chain of kinesin molecules, associated with microtubules and involved in membrane organelles (i.e. vesicle) transport.

17. RAB3A – member of the G protein superfamily involved in Ca2+ dependent vesicular exocytosis.

18. EFNB1 – member of the ephrin family with roles in cell adhesion, development and maintenance of the CNS.

19. EMX1 – transcription factor with roles in the regionalization of cortex, neuronal differentiation absent in GABA-ergic cortical cells.

What remains to be done is to use this procedure to shorten the list of candidate markers and then use in situ hybridization in order to confirm that they are ubiquitously expressed in association of the appropriate cell population i.e. either given sub-layer or a projection type.

Chapter V

MATERIALS AND METHODS

Retrograde tracing

The choice of DY and FsB

There is a large spectrum of available retrograde tracers and the characteristics of the tracers differ in several aspects: the uptake mechanism, interaction with other tracers, method of visualization, cell toxicity and fading. For optimizing results it is critical to choose the tracers best suited for the intended application. In our 3 aims to characterise *i) the magnitude of input to given cortical area, ii) the amount of collateralisation to two areas, iii) to isolate and genetically characterise FF and FB cells*, we needed tracers that have high tracing sensitivity, are distinguishable in the same observation conditions, efficiently co-label cells having collaterals to the two target sites and do not show toxicity in the labelled cells.

Physical and chemical characteristics

Fast Blue (FsB) and Diamidino Yellow (DY) were introduced in the early eighties (Bentivoglio et al., 1980, Keizer et al., 1983). The chemical formula of FsB is *trans-1-(5-Amidino-2-benzofuranyl(-2-(6-amidino-2-indolyl)ethtylene dihydroclorid.* At pH=5.0 in Cacodylate buffer the peak of excitation is 376nm; in octanol the excitation peak is at 385nm.

The formula of DY is still protected, it exist in two forms: i) –dihydrochloride (DY•2HCL) and ii) –diaceturate (DY•2aa). The diaceturate isoform substitute of DY is easily soluble in water and at 2% dilution it produces clear but viscous solution that is difficult to inject and spills out trough the needle track. It also has high propensity to leak out of the labelled cells (**Keizer et al., 1983**). For that reason we concentrate on DY•2HCL that we shortly call DY in this manuscript. Some of the characteristics of DY may vary according to the provider. With the traditional provider: Dr Illing, cited in (**Payne, 1987**), the excitation/emission wavelengths were 390/520nm (in distilled water and in vivo). The contemporary quality control

at *Sigma*™ is for λmax =400nm in methanol. The DY provided by Dr Illing had also higher capacity to generate double labelling with FsB. We find the sigma provided DY to generate colour perception that is shifted to the blue and makes it less easily distinguishable from FsB for that reason we choose the EMS-Polyloy[1] provided tracers.

Efficiency for tracing experiments

Numerous studies have compared the reliability of other tracers with FB and DY, either for neuronal tracing or double labelling experiments (Bentivoglio et al., 1980, Kuypers et al., 1980, Keizer et al., 1983, Conde, 1987, Payne, 1987, Craig et al., 1989, Novikova et al., 1997, Vince et al., 1997, Puigdellivol-Sanchez et al., 2000, Panto et al., 2001, Puigdellivol-Sanchez et al., 2002). The advantages of the combination of FsB and DY are numerous. The survival times needed for efficient transport at long distance are similar: 7-12 days. The tracer efficiency is comparable: applied to sectioned nerves the success of labell is 70-80% of source cells. The two tracers accumulate in two different cell compartments: DY into the cell nucleus and FsB in the cytoplasm. The tracers can be observed with the same filter cube and distinguished even if both show in the same cell (**Table 4.1**). Either an A or D cube are convenient. With the A filer the DY labelled cells are less excited, which is compensated by the better covering of FsB emission spectra. The dry mounted sections can be stored ad -20°C for more than 8 years.

Table 4.1: *Filter cubes for simultaneous observation of FsB and DY*

Cube	Exciter filter	Dichroic mirror	Emission filter
A	UV band pass 340 – 380 nm	400nm	Long pass 425nm
D	UV- Violet band pass 355-425nm	455nm	Long pass 470nm

Another important question is the possible uptake by fibers of passage. Both tracers have been shown to efficiently label transsected nerves. The central nervous system has different myelination characteristics but still, experiments with injection of DY in to the optic tract lead to labelling of ganglionic cells in the retina. Overview of the literature in **(Payne, 1987)** leads to the conclusion that uptake is only from damaged axons and that the intact axons should not generate serious label. In the monkey interareal projections are trough the white matter so the uptake by fibers of passage is to be taken in to account specificly when intrinsic connections are explored. It has been shown that FB and DY generate focalised necrosis close to the injection site although this necrosis occurs some time after the injection itself and may not lead to uptake at this level (**Keizer et al., 1983**). Several papers explored the characteristics of the uptake zone (Perkel et al., 1986, Conde, 1987). In this ’86 paper (**Perkel et al., 1986**) Kennedy and collegues take advantage from the topological precision of thalamocortical projections to asses the extent of the uptake zone. Side by side injections in area V1 generate well defined columns of labelled cells spreading trough all the layers of LGN (Lateral Geniculate Nucleus). The more central the injection is in area V1 the more caudo-medial the position of labelled cells. When the interinjection distance is of 2-3mm the two columns are adjacent at the level of the magnocellular layers and more distant in the parvocellular layers. The DL cells are present but very rare. Increasing the interinjection distance to 3mm leads to completely separated populations and total absence of DL cells. If the interinjection distance is of 1.9 mm the two columns are abutting on each other and few labelled cells are present. For

[1] Synthesized by Dr. Florian Blumenthal; Gruppenleiter; Chromatographie; F&E/Analytik; EMS-GRIVORY; Reichenauerstrasse; CH-7013 Domat/Ems; Tel.: +41 81 632 7726; Fax.: +41 81 632 7434; florian.blumenthal@emsgrivory.com.

closer injections there is partial merging of the tracer labelled cells and DL are frequent in the zone of overlap. Both overlap and DL are higher at the level of magnocellular layers than in parvocellular. Reducing the distance to 1.1 mm leads to complete merge of the two populations in the magnocellular layers while there is still some separation in the parvocellular layers and less DL. This illustrates the larger axonal arborisation of magnocellular layers. If one considers 1.9mm as maximal interinjection distance without crosinvolvement and 0.4mm as spread of axon terminals it remains that the diameter of the uptake zone will be of 1.5mm. This diameter grossly corresponds to the area of dense fluorescent tissue surrounding the injection site. This result is consistent with the later paper of Condé (**Conde, 1987**) that subdivides the different zones of the injection site and explores the effective uptake area. She subdivides it in to 3 concentric zones around the needle track. The region at the tip of the needle track, which contains the injected tracer is defined as zone 0. Zone 0 corresponds to the tissue disruption by the needle where either FB or DY form a crystal of yellow orange colour.This crystal is visible even under transmitted light on Nissl stained sections. Immediately surrounding this space is an area of tissue in which the cytoarchitecture is disrupted, it is called zone 1. The intensity of fluorescence decreases from center to periphery of zone 1. The most central parts of it contain cells densely staining with Thionin. These cells are filled with tracer granules but it is likely that they be either glial or macrophagial cells or even lymphocytes. Condé could not identify any cell with Nissl bodies in this zone. Adjacent to zone 1 there is the zone 2 that contains still lot of glial cells. This area already presents labelled neurons. The amount of glial cells gradually decreases to the periphery of the injection site this zone is called zone 3. There the labelled neurons show labelled neurites and in Nissl sections the cytoarchitecture appears normal. Condé gives the following measurements of these zones: Zone 1 is 500-700µm with DY and less than 100µm in FB injections; Zone 2 is in all cases narrower than 100µm; Zone 3 extends in the milimeter range. If survival time is of only 15-30 minutes the necrotic outer region of zone 1 and the glial zone 2 are not observed. (Put here the figures of Kennedy about the LGN projection on V1 and then a figure of an injection site in fluo and nissl in order to get the zones o;1;2;3. It may also serve to identify the local projections in layer 2 and layer 4 the story about the external granular layer) The needle track shows fluorescent tracer and is immediately surrounded by tissue similar to the zone 3 of longer survival periods. The paper concludes that only zone 0 is source for effective uptake and thus the efficient label of neurons is produced only if the axons are damaged. This supposes uptake zones of diameter lesser than 200µm. This observation is an advantage for exploring the connectivity to a given cortical area because it makes more easy the restriction of the injection site to the point of interest. The obvious limitation to double labelling procedures is easily overcome by enlargening the injection site by repeated penetrations and large injection volumes.

Injection and histology of fluorescent tracers

Anaesthesia and surgery

Cynomolgus monkeys (Macaca fasicularis) (**Table 4.2**) were premedicated for surgery with atropine (1.25mg, i.m.), dexamethasone (4 mg, i.m.), animals were then anaesthetized with ketamine hydrochloride (20mg/kg, i.m.) and chloropromazine (2mg/kg, i.m.). Heart rate was monitored and artificial respiration was adjusted to maintain the end-tidal CO2 at 4.5-6%. The rectal temperature was maintained at 37°C. A surgical plane of anesthesia was maintained with 1-2% halothane in N2O and O2 (70:30).

Injections of retrograde tracers

Brainsight system :

Accurate injection sites are obtained by using an image-guided stereotaxic system (Brainsight Frameless, Rogue Research Inc.). The target area is identified on the monkey's MRI based on clear visualisation of the sulcal landmarks both on a 3D reconstruction of the

monkey brain or in any plane (coronal, parasagital or horizontal) of transversal section (**Frey et al., 2004**) The advent of the system Brainsight improves both the accuracy of injection placement and animal wellbeing. The injection procedure is split to 3 steps. Before an MRI scan the monkey is fitted with bone implanted fiducial markers, afterwards during the injection of the tracer the system is able to match online the positions of the fiducial markers with the MRI image and to monitor the positions of the surgical tools with respect to the target site.

Implantation of the fiducial markers :

Implantation of fiducial pegs is performed under deep anaesthesia and asceptical conditions. The anesthetised animal is placed in the surgical headclamp and rested on the upright surgical chair. Incision is operated in the scalp and the bone is exposed. A scalp punch is placed to the animal head to imprint the drilling positions. The drilling depth of 2 mm ensures stable hold for the screws without involving perforation of the bone. The fiducial post is then affixed to the scull with 9 screws and secured with dental ciment. At the top of the post there is a position for the placement of a platform composed of 3 – 5 arms sticked with radio opaque fiducial markers (IZI Medical Products Baltimore, USA), this platform is attached to the peg only during the MRI scan. Each of the fiducial markers has a small hole at it's center in which the tip of a pointing device can be placed to locate the center of the fiducial marker.

MRI scan :

One week after implant of fiducial pegs, the monkey is anesthetised with Zoletil at 15 mg/kg. MRI scans are performed in a 1,5T Siemens Sonata scanner and T1 acquisition routine. The monkey is placed in the scanner in a classical MRI compatible stereotaxic apparatus.

Injection :

During the surgery the Brainsight system monitors online the position of the tools and assures injections precision within the millimeter range (For details see supplementary methods). Injections of the fluorescent tracer FsB and DY were made into V1, V2, V4 TEO,TE STPa, STPm, STPp, AudPba, AudPbp, 5, 7A, 7B, F1, F2, F7, 2, 8A, 45B, 9/46d, 9/46v, 46d, F5, ProM, 24c. The paired injections in V1 and V4 of case M73 were made under manual guidance at a shallow angle to the cortical surface and the tracer injected while the Hamilton microsyringe was withdrawn from the cortex so as to form longitudinal injection sites (2-3mm) largely restricted to the cortical gray matter. Within V1 the penetration sites were at the dorsal half of the operculum and covered a surface, spanning from the tip of the lunate sulcus to the median line and were 2 mm offset from the V1/V2 border, caudally the penetration sites were extending to the ectocalcarine sulcus. The V4 injection was also made with multiple penetrations starting at the junction of the tips of lunate sulcus and the inferior occipital sulculs and extended dorsally until the limit with area DP. In andimals with side-by-side FsB and DY injections either in V1 or V4, the injections were separated by 3mm and were done in a single penetration. The dyes (small injections 0.2 - 0.3 micro liters; large multiple injections 3-5µl), were injected at a concentration of 3% FsB and 2.0 DY%. Injections were made so as to span the full depth of the cortex.

Table 2.2: of repeat injections for the FLN profile

Case	Animal	Hemisphere	Tracers	Injection site	Plane of section
1	M81	LH	DY	V1 central	H
2	M85	LH	FB	V1 central	H
3	M85	RH	FB+DY	V1 central	H
4	M88	RH	FB	V1 central	H
5	M121	RH	DY	V1 central	C
6	M101	LH	DY	V2 central	C
7	M101	RH	FB	V2 central	C
8	M103	LH	DY	V2 central	C
9	BB187	LH	FB	V4 central	H
10	M121	RH	FB	V4 central	C
11	M123	LH	DY	V4 central	C
12	M119	LH	FB	TEO	C
13	M106	LH	FB	9/46d	C
14	M106	RH	DY	F5	C
15	BB272	LH	DY	8A	C
16	BB272	RH	FB	45B	C
17	BB135	LH	DY	7A	H

Perfusion :

Following a 10-13 days survival period, the animals were deeply anaesthetized and perfused through the heart with 2,7% saline + procain 1‰ untill blood clearing, followed by 4-8% paraformaldehyd + 0.05% gluteraldehyd in 0.1 M phosphate buffer (pH = 7.4) for 40 minutes (≈ 3 liters), and 10-20-30% sucrose or 5-10-20% glycerol gradient in phosphate buffer (pH = 7.4). The brains were then blocked on the coronal plane, and cut on a freezing microtome. Section thickness was 40 microns. One in three sections were immediately mounted from 0.45% saline solution onto 3% gelatin-coated slides. Sections at regular intervals were reacted for cytochrome oxidase and acetylcholinesterase (AChE) activity (**Barone et al., 2000**) and SMI-32 (**Hof and Morrison, 1995**). Sections were observed with a Leitz or Leica DMRE fluorescent microsope equipped with a D-filter set (355-425nm). A computer-assisted program (Explora Nova®) was used with a motorized microscope stage so as to electronically trace out sections and record neuron positions with high precision (+/- 10µm).

Segmentation of cortical areas

Area V2

Area V2 shares borders with : V1, V3, V4, Prostriata, TF/TH.

Papers in relation with the segmentation of V2 : (Zeki, 1971, 1977, 1978b, a, Gattass et al., 1981, Van Essen et al., 1986, DeYoe et al., 1990, Hof and Morrison, 1995, Roe and Ts'o, 1995, Hof et al., 1996, Gattass et al., 1997, Lewis and Van Essen, 2000b, Brewer et al., 2002, Xu et al., 2003, Nakamura et al., 2004, Galletti et al., 2005, Gattass et al., 2005)

Gross landmarks

Area V2 is a strip located at the posterior bank of the lunate sulcus (LS). At the ventral limit of the LS it crosses on to the IOS. Dorsally V2 starts with occupying the whole of the

posterior bank of POS and then progressively steps away from the center of this sulcus to let the position open for area V3 (the step off the center of the sulcus can be identified in horizontal sections by the appearing of a protuberance which will later build up the anectant gyrus). In horizontal sections, once the operculum and the parietal lobe are joined and the LS apparent V2 is constrained posterior to the fundus of LS .

The limit between V1 and V2 is defined by it's classical position : +-2mm posterior to the LS on the surface of the operculum(a trace of a large blood vessel on the surface indicates the border at this position). As one goes ventrally the LS becomes progressively shallower and IOS appears. At the point where the LS and IOS sulci are of equal depth, V3 disappears from the anterior bank of the LS and V2 crosses the fundus of the LS to extend on to the anterior bank of the LS around 2,5mm behind the anterior lip of the LS. This border is maintained till the complete receding of the LS. At this point, area V2 is present in the IOS and occupies its posterior bank. At all the positions where we are able to identify the prelunate gyrus, it is devoted to V4. Where the gyrus is still apparent between the LS and IOS, LS is greatly reduced and IOS is halfsize opened; in these cases V2 is present inside LS and at the posterior bank of IOS. The limit with V4 is more or less close to the posterior lip of IOS. At more ventral positions V2 crosses the fundus of the IOS to invade a small portion of it's anterior bank.

Cytoarchitecture

The cytoarchitectonic criteria of SMI-32 immunolabel, that we observe, comply with those described by Hof and Morrison (Hof and Morrison, 1995, Hof et al., 1996) a difference that should be noted was that we observe some modules in the pattern of V2 label, while they do not mention them (modules which may correspond to thin thick stripes).

In SMI-32 the limit V1/V2 is apparent as layer 5 of V1 has a number of stellate densely stained cells while in V2 this layer has only occasional pyramids sending their apical dendrite to the pial surface. The area V2 itself shows a non homogenous pattern of labeling. There are stripes with a V2 typical profile (strongly labeled neurites and cell bodies in LIIIb while the label in other layers is poor) then other stripes looking like V3d (with labeled pyramids in layer II and LIIIa; and dominat LIIIb with radial dendrites)(This is coherent with the thick thin interstripe cytox structure of area V2). In V2, layer 5 has big densely stained pyramids with large dendrites ascending trough superficial layers and which are regularly spaced (and quite rare). The limit V2/ V3d can be identified as while in V2 the LII presents bands of pyramidal cells followed by bands devoid of this type of label in V3 the LII had a regularly distributed and denser population of the same cells.

Our Nissl staining criteria are in correspondence with literature (**Nakamura et al., 2004**). Layer 1 is finer in V3v compared to V2v. In V2v layer 2 and layer 3 seem much more continuous and layer 3 is more homogenous. The contrast between layer 2 and layer 3 limit is sharper in V3v than V2v. In V3v it is easier to differentiate between the deep and superficial layer 3 (the superficial layer 3a is populated with smaller and more granular and less densely stained cells) while 3b has bigger compacted densely stained pyramids. Area V3v presents more compacted layer 4 than V2v. In V2v layer 6 is hardly distinguishable from layer 5, the cells of layer 5 are less condensed in V3v than in V2v. Layer 6 clearly forms a row of large densely labeled pyramids in V3v. The fact that it is better separated from the profound layer 5 makes it appear (to Nakamura) more condensed in V3v.

Area V3

Area V3 shares borders with : V2, V3a, V4, DP (at dorsolateral positions in LS), PIP, V6;

Gross landmarks

We consider area V3d and V3v (the latter is sometimes referred to as VP) as one and the same area with a complete representation of the visual field. The dorsal segment of area V3 occupies the fundus of the LS and extends on to the caudal and medial part of the anectant gyrus. The anectant gyrus is burred in the fundus of POS where it forms the parieto-occipital junction. In horizontal sections V3 is absent dorsally, and it appears first caudally when the operculum is near to joining the parietal cortex and a convex structure (protuberance) forms on the anterior part of the operculum between the LS and the POS. At the level of the parieto-occipital junction (annectant gyrus) the fundus of the LS still has a certain width and is devoted to area V3, more laterally at the anterior bank of the LS there is a convex structure that we assign to area V3A on it's medial halve and toV3 on the lateral halve. At more ventral positions the LS is completely formed and the anterior border of area V3 invades the anterior bank of the LS as one goes ventrally and at levels where the IOS appears and the LS is very shallow, the 2/3 of the anterior bank of LS are devoted to area V3 (here V3 borders V4 and V3A is absent. Once the LS is about the same depth as the IOS and is about to dissapear, area V3d is replaced by V2. At more ventral positions IOS broadens and starts to be S shaped, so area V3v appears on the anterior bank of the IOS (at this level V3v expands). More ventrally V3v keeps a very constant position and width (3mm); meanwhile going ventrally the IOS becomes deeper the newly appearing medial parts of it's anterior bank are devoid to V2. V3 never goes onto the posterior banks of the LS or IOS.

Cytoarchitecture

The means of differentiating the border between V2 and V3 in SMI-32 immunostaining is described in the section about area V2. The border between V3d and V4 is characterised by the denser cells in layer 2 of V4 which appear in clusters (pack of 2/3 cells).

Layer 3b shows at least 3 floors of large pyramids and layers 5 and 6 appear as two lightly stained bands (labelled neurites). In V3 layers 5 and 6 does not appear as two separated laminae. Layer 3b cells and also layer 2 labelled cells are less dense in V3. The most remarkable feature to distinguish between V3 and V3a is that V3A does not have pyramids in layer 2. Layer 3b is less dense in V3A than in V3. Layers 5 and 6 appear more stained in V3A (bit like in V4). The identification in Nissl stained sections of the V2/V3 limit is described in the V2 section.

Area V3A

Area V3a shares borders with: V3, DP, PIP, V4.

Gross landmarks

Area V3A lies on the anterior bank of the LS. In horizontal sections, dorsomedially it is limited by the caudal lip of the IPS. V3A never enters in the IPS. The medial limit of V3a is on the caudo-lateral lip of IOS. Area V3a appears medial when DP starts to retract from the POS. As one goes ventrally area V3A maintains the same position medially but extends its lateral border closer to the lip of the LS (never more than 2-2,5mm from it's lip). At dorsal levels it shares borders with DP and more ventrally with V4 (this is not necessarily the only opinion in the literature but seems the most coherent it means that at levels where V4 is present on the prelunate gyrus there are still some parts of DP on the anterior lip of LS). More ventrally, where, in horizontal sections, the operculum joins the parietal cortex, V3A takes position medial

to the anectant gyrus and is not observed on the banks of LS. At these levels V3a is extending from the convexity that will form the dorsal most part of the anectant gyrus to the lip of IPS. As V3a is situated on the anectant gyrus it also appears in the caudal bank of the POS. This position is to be identified in latter explorations.

Cytoarchitecture

In SMI-32 immunostaining the border V3d/V3A is easy to recognise as V3A has no stained pyramidal cells in layer 2.The staining in layer 3b is less dense in V3A than in V3d. Layer 5 and 6 appear more stained in V3A (bit like in V4). The limit between PIP and V3A is distinguishable by the increased density of labelled cells in layer 3 of PIP and the presence of a regular label large pyramids in of layer 5. Using Nissl staining method the limit V3A/V3 is identified by the les clear cut between layer 2 and layer 3 in V3 than in V3A also in V3A the segmentation of layer 3 in to 3a and 3b is easier to see than in V3. In V3a the layer 3b has a narrow band of medium sized darkly stained cells. To distinguish V3A from DP in Nissl stain we use the layer 4 which is more developed in DP than in V3A and so it appears more separated from the pyramids of layer 3b. At the limit between V3A and DP the layers 5 and 6 are less easily distinguishable and have a columnar distribution of large pyramids.

The V4 Complex

What we refer to as V4 complex is actually V4 proper, V4t and DP. Each of these, being considered as a distinct cortical area. DP shares borders with: V3A, V4, MST, 7A, LIP. V4 shares borders with V2, V3A, V4, MST, V4t. V4t shares borders with: V4, TEO, MT, MST.

Gross landmarks

Areas V4 and DP

DP is on the dorsal part of the lunate gyrus. In horizontal sections at the positions where STS is just beginning and the lunate gyrus haven't got a plane appearance area DP starts at the fundus of STS and ends at the lip of IPS. More ventrally the anterior wall of the POS starts to curve, at these levels DP steps more lateral and V3A appears between the lip of the IPS (medially) and the protuberance forming (laterally). At these levels DP also retracts from the posterior bank of STS to let the place free for area MST. Several millimetres ventral, and in most cases before the lateral fissure opens, the gyrus gets a mushroom like shape with flanks narrower than the surface exposed part. At these levels DP disappears to let the gyrus to V4. Something unproven in the literature that comes out from my observations of the cytoarchitecture in the horizontal and parasaggittal plane is that even at these levels and bit more ventral DP is present between the lip of the LS and ¼ of it's anterior bank.

Area V4 spreads on the lunate gyrus dorsally and more ventrally runs on the anterior bank of IOS. When IOS appears, the whole of IOS is in V4. With IOS appears TEO, located rostral to the anterior lip of IOS. ((**Boussaoud et al., 1991**) describe that in half of monkey cases: the lip and the beginning of the anterior bank of IOS were devoted to TEO while in other cases TEO ends before the lip and do not enter IOS. We generally put the limit on the lip.). Till the last point where we can identify the prelunate gyrus, IOS and also the exposed cortex of the prelunate gyrus are assigned to V4. The exception comes sometimes on the posterior bank of the IOS where V2 appears to take 2/3 of its medial length. Where the LS disappear, there is no prelunate gyrus, V4v now borders V2v and the V4v/V2 border moves from the LS (which is now absent) to the fundus of IOS. When V3v appears V4v is reduced to a width of 3-4mm. Tough someone goes ventrally the absolute position of the lip of IOS becomes more and more caudal, this means that the area devoted to V4v is more and more narrow. V4v runs ventrally inside IOS but reaches medially to the fundus of OTS.

V4t

Area V4t lies between MT and cortices more lateral to it (V4, TEO. It is an elongated area forming an arc around MT. The lateral limit is always on the lip of the STS and the medial limit is 0,5 to 1mm more medial at the posterior bank of the STS. This limit is fixed by particular landmarks, dips or changes in the orientation of the cortical surface. This area runs ventrally and anteriorly over almost the whole extent of area MT. MRI analysis using the same principle as Zeki (the vertical meridian) Shows that there is an area buried between MT and TEO in the STS authors let a question mark on the flatmap but cite V4t (**Brewer et al., 2002**).

Cytoarchitecture

In Nissl sections layers 2 and 3 of area V4 appear columnar and are hardly distinguishable one from one another, while in V3 it is easier to separate them. In low magnification the main fature of V4 we have only one band of highly dense cells while in V3 we have 2. In area V4 layer 6 is columnar and enters diffusedly the WM. In V3 the cells of layer 6 can be followed tangentially (rows), the limit with the WM is sharper. In Nissl sections area V4t forms a mix between the cytoarchitectonic characteristics of V4 and MT. In many cases it looks like MT. The major difference is that layer 6 of V4t enters the white matter in more diffuse manner (bit like V4) while in MT this limit is very sharp (due to a tangential plexus of richly myelinated fibers entering MT). The limit between V4/ V3d is detectable in SMI-32 as in V4 the layer 2 cells are denser and may appear in clusters (two-three in a pack). In SMI-32 stained sections, DP is a stripe of cortex that has a pattern midway between V3A, V4 and 7a. There are almost no cells in layer 2 (like V3A). There are moderately big darkly stained cells in layer 5 that send dendrites trough layer 3. The intensity of stain in layer 3 is lighter than in V4. In layer 6 there are much lower numbers of horizontal basal dendrites than V3 (layer 6 is much cleaner). The border between V4/V4t is characterized by cell bodies of layer 3 which become smaller in V4t and the dendrites are less apparent in their radial orientation. In V4t there are less cells in layer 2. The border V4t/MST or MT is apparent in SMI-32 as layer 3a is more densely populated with bigger cells in MST and MT than in V4t. In the areas MT and MST the label of layer 5and layer 6 is very proeminent and appears in 2 parallel bands.

Area TEO

Area TEO shares borders with: areas PIT, TE, TF, V4

Gross landmarks

In horizontal sections TEO appears with the IOS, its anterior border is on the posterior lip of the STS and its posterior border is on the anterior lip of IOS. More ventrally the distance between STS and the IOS becomes large and a virtual vertical is projected at 1,5mm anterior to the PMTS, this forms the anterior border of TEO with area TE. PMTS is a marker of TEO and the central visual field is represented there. At the most ventral positions TEO stretches out to OTS where it shares a common border with TH/TF at the medial bank of OTS 1mm away from it's fundus. In practice once TEO has attained it's maximal extent at around the PMTS sulcus it is sufficient to project two virtual vertical lines ventrally to identify it's anterior and posterior border.

PIT

It is poorly defined area. It has firs been described by Van Essen but papers from Zeki **(cite zeki)** detect a special color sensitive, motion and light intensity insensitive zone on the caudal bank of STS lateral to MT and stopping at around the lip of STS. In our studies area PIT is part divided between V4t and TE. The most caudal extend of PIT should be at around the levels of the middle of MT. The most lateral extent of PIT never overcomes the ventral lip of STS. In practice the anterior and posterior limit of PIT are corresponding to the projection of area TEO inside the STS.

Parahippocampal cortex

The parahippocampal cortex is composed by areas TH and TF, it surrounds the hippocampal formation. Caudally area TF abuts on V2v, V3v and V4v. The border corresponds to the caudal most level of the hippocampus. The lateral limit that it shares with area TE is around 1mm offset from the medial lip of the OT sulcus. The medial limit of area TF is with it's sibling area TH which occupies the medial most ¼ of the hippocampal gyrus. At more anterior levels the OTS receeds and the rhinal fissure (rf) is open, there TF shares a medial border with the entorhinal cortex (ER) and anteriorly with the caudal part of area 36. Area TH is an antero-posterior extending narrow strip medial to TF. Its medial limit is with the parasubiculum of the hippocampus and it has a thickness that correspond approximately to ¼ of the parahippocampal gyrus.

Cytoarchitecture

Area TF is subdivided to a medial TFm and lateral TFl halves. TFm is a narrow strip of disgranular cortex between TH and TFl. In Nissl stains layer 2 shows small, round and lightly stained neurons. The overal thickness of the layer is larger than TH. The cells of layer 3 show the same round shape but are of bigger size. At more rostral positions the whole tickness of the layer presents homogenous cell populations while at more caudal positions the layer has darker, larger cells at it's deep portion. Globally the layer 3 of TF is thicker than the one of TH and the cells are slightly smaller and less densely packed. While at rostral levels TFm is clearly disgranular at more caudolateral positions layer 4 is better formed. At rostral positions the distinction between TF and TH can be made by identification of lamina dissecans that characterises the agranular area TH, more caudally both TF and TH have a layer 4 but the one of TH is poorly formed. Layers 5 and 6 have both large darkly stained pyramids that makes them hardly distinguishable but in TF the cells of layer 5 are smaller and more pyramidal-shaped than in TH. Layer 6 often presents thin rounded lightly stained cells situated deep in to the white matter. The SMI-32 label is slightly stronger in TFm than in TH but SMI-32 is a bad marker for this boundary as the differences occur in a gradient manner. Layers 1-2 contain only light label of neuropil and no cell bodies or processe. Layer 3 contains also light neuropil and only occasional cells and processes can be seen mostly at the lateral portions of TFm. Layer 5 contains light to moderate label of both cells and processes. Layer 6 contains only weakly labelled cell bodies and processes. The limit between TFm/V4v presents a distinctive change in layer 5 where the larger moderately stained cells of TFm are replaced by smaller cells in V4.

TFl is the largest the thickest and most laminated of the parahippocampal cortices. In Nissl stain layer 2 is prominent made up of small rounded cells, it may be distinguished from the one of TFm by it's increased thickness and neuronal packing density. Layer 2 has clearly bilaminate appearance and is thicker than the one of TFm. Compared to it's superficial portion the deeper portion has larger and darker cells. Layer 4 is better defined than in TFm.

Layer 5 is distinctive and characterised of population of large pyramidal cells that tend to congregate in the middle of the layer, while the superficial and deeper parts of the layer are populated by smaller neurons. This is in contrast with the homogenous layer 5 of TFm. Layer 6 has a heterogenous population of cells bigger at it's superficial parts and smaller more lightly stained at it's deep parts. The limit TFl/V4v can be seen as V4v is thicker and more densely packed. The density of LV increases from TFl to V4 where large pyramidal cells are homogenously distributed throughout the layer so it looses its banding pattern characteristic for TFl. At the border between TFl/TE when compared to TFl the neurons in TE are more radially oriented, tend to be more lightly stained and more distinctly pyramidal in shape. The obvious separation between layers 5 and 6 in TE is absent in TFl. Layer 2 contains smaller more densely packed cells and tends to be slightly thicker than in TFl. In layer 3 the cells are smaller more fusiform rather than round in area TFl. Layer 4 of TE is completelly formed and thicker than in TFl. Layer 5 lacks the large pyramidal cells in TE. Layer 6 is wider in TE and more denselly packed populated and made up of a more homogenous population of smaller cells than layer 6 of TFl.

The pattern of SMI-32 presents the strongest label for the parahippocampal cortex. Yet in layer 1-2 there is no SMI-32 label. Layer 3 is relatively thick band of densely labelled pyramidal cells deep in the layer. Layer 4 has little or no SMI-32. Layer 5 is densely stained.

Layer 6 also has SMI-32 label but the density is weaker than in the layer 5.

SMI-32 is useless for defining the limit between TFl and TE.

In Nissl sections area TH is a thin rather primitive looking predominantly agranular cortex. Recognisable even in low magnification by it's layer V made up of large darkly stained cells that generates a contrast to the smaller lighter stained cells in LII and LIII. It appears as a cortex with two equally large layers : lightly stained superficial layer and darkly stained deep layer. Rostraly layers 2 and 3 are not distinguishable from each other if not for the smaller and denser cells in layer 2 and larger rounder and sparser cells inlayer 3. At extreme caudal positions the two layers may become distinguishable. Layer 4 is absent in most of the area however at most caudal and lateral positions a weak layer appears. Layer 5 is by far the most distinctive feature of area TH it is made of large darkly stained cells. There is no separation between LV and LVI and both layers are approximately the same thickness. However LVI is easily distinguished from layer V because it is made up of a population of smaller more lightly stained and densely packed cells. The limit TH/V4 may be identified by the changes in layer 5 and the more clearly laminated structure of V4. In layer 5 the cells of V4 are generally smaller than the cells of TH. Another feature is the thicker and better-organised layer 4 of V4. Area TH has the lightest SMI-32 staining of the parahippocampal cortex, there is no SMI-32 labelling visible in the superficial layers. Layer 5 presents weak label of cells and processes. Layer 6 contains weak or no SMI-32 stain. It is easy to distinguish TH from the densely stained parasubiculum in SMI-32 stained sections.

Perirhinal cortex

The perirhinal cortex is a band of cortex lateral to the fundus of the rhinal fissure (rf), it extends down the rostral face of the temporal lobe, forming the medial portion of what is typically referred to as the temporal pole. It continues caudally on to the ventral surface of the temporal lobe. It's caudal border is typically found 2-3mm beyond the caudal limit of the rf, approximately at the level of the genu of the hippocampus and the caudal end of LGN. Areas 35 and 36 form the perirhinal cortex. The medial border of the perirhinal cortex is coincident with the fundus of the rhinal sulcus. The structures that form the medial border of the perirhinal cortex vary at different rostrocaudal levels. Rostrally, it is bordered by the piriform and periamygaloid cortices. Medially it is bordered with the entorhinal cortex and laterally with TE. The parahippocampal cortex forms the caudal boundary of the caudal perirhinal cortex.

Gross landmarks

Area 36 has 5 subdivisions : A36rm (Rostromedial part of area 36) ; A36rl (Rostrolateral part of area 36) ; A36cm (Caudomedial part of area 36) ; A36cl (Caudolateral subdivision of area 36) ; A36d (dorsomedial part of the temporal pole). Area 36d (the dorsal subdivision of area 36) is located at the most rostral and dorsal extent of the perirhinal cortex and makes up approximately the dorsal one third of what is typically referred to as the temporal pole (area 38 of Brodman 1909; area TG of Von Bonin and Bailey'47) (Brodmann, 1909, Von Bonin and Bailey, 1947). Caudally adjacent to area 36d is area 36r (rostral subdivision of area 36). The limit between 36rm and 36cm is approximately at the junction between the Hippocampus and the Amygdala. Relative to the entorhinal cortex the transition takes place approximately at the rostral limit of the Ec (caudal division of the entorhinal). Area 35 is a long, narrow, agranular strip of cortex situated in the fundus of the rhinal sulcus.

Cytoarchitecture

Area 36 is a 6 layered disgranular cortex. Layer 2 has prominent aggregates of cells in the superficial portions. Layer 4 is very thin medially and rostrally but fairly thick laterally and

caudally. Infragranullar layers have large darkly stained cells. Layer 6 is thick and bilaminate, the superficial part being made of more densely packed darkly staining pyramidal and multipolar cells. The deep portion of layer 6 is thicker but more sparsely populated. In Nissl preparations the border 36rl/TE can be identified as in layer 2 of TE we do not have the same aggregates of cells as in 36rl. The layer 2 of area TE is thicker and unlamented, the cells are smaller and more lightly stained. Layer 3 is more radially patterned in TE (similarity to V4 and TEO) here the gradient from bigger to smaller cells is more obvious than in 36. Layer 4 is thicker in TE than in 36 and more densely populated. The infragranular cells are smaller in TE than in 36 and also there is a distinctive paucicellular band between layers 5 and 6 which is absent in 36. In contrast to 36 in area TE layer 6 has a sharp border with the white matter.

The AMTS possesses a cortical sheet that is substantially thinner than in the surrounding regions. The overal cytoarchitecture of the sulcus resssembles more to TE than to 36. The transition TE/36 is more medial for layer 2 and more lateral for the deep layers 5 and 6. SMI-32 may be a useful marker of the border between 36rl and TE. Layer 3 is the best indicator it is lightly stained in area 36rl and more densely stained in TE (in its deep portions more densely labelled cells and processes).

Nissl sections of 36cm globally resemble 36rm but the cortex is much thinner, less densely populated, cells are smaller and more radially oriented. Layer 2 of 36rm is thicker than in 36cm and the cell aggregates are smaller and more irregularly spaced. The limit with LI is much sharper. The deep portion of LII is thicker more densely populated but lacks the satelite glia at the limit between layers 2 and 3. Layer 3 appears unlamented with rounded lightly staining cells. Layer 4 is more prominent than in 36rm with a high density of smaller granule cells. Often there is an acellular gap in the deep part of layer (at the medial portion of 36cm). The bilaminate stricture of layer 5 in 36cm is different of 36rm because the superficial part is wider while the deep is thinner and made up of smaller cells. Layer 6 is thinner than in area 36rm and contains smaller rounder cells. The deep diffuse portion of the layer is also thinner.In SMI-32 stained sections 36rm and 36cm look quite similar. Layer 5 is moderate to heavy stained while layer 6 is less densely stained. A subtle mediolateral gradient is present in LIII's deep portion where in the more lateral portion the cells are more densely stained. The caudolateral field of area 36 (36cl) is the most laminated and columnar field of the perirhinal cortex. The limit between this part of perirhinal cortex and area TE is even easier to identify in Nissl preparations as while layers 5 and 6 are more easy to separate in TE in 36 they are continuous. Layer 4 of TE is better developped in TE than in 36cl. SMI-32 provides excellent marker for the 36cl/TE border, there is much more label at the deep portion of layer 3 in TE than in 36cl. Area 36d is the least organised and laminated subdivision of area 36. It's appearence depends of the plane of section but in general layer 2 presents aggregates of neurons and appears irregular (bilaminate) at the extreme pole only occasional aggregates are observed. This layer is thinner than the more caudal parts of area 36. Layer 3 has mediolateral gradient of differentiation with large rounded cells in medial positions and more elongated radially oriented smaller cells at lateral and dorsal positions. Layer 4 is either very weak or absent. The deep layers 5 and 6 appear as an unique layer (one of it's most distinctive features). In SMI-32 staining the label is fairly ressembling to the other parts of area 36. Layers 1 and 2 have no label and layer 3 has only some occasional cells. Layers 5 and 6 have moderate to densely labelled band of cells and processes. The lack of cells in layer 3 is sufficient to distinguish this area from the surrounding cortices.

In Nissl stained sections the organization of layers II and III of area 35 varies substantially from brain to brain. In most cases, the large and small cells of layers II and III are so completely intermixed that they appear to form a single layer. The layer II cells of area 35 can be distinguished from those of the entorhinal cortex because they are more uniformly pyramidal in shape, while the entorhinal cells tend to be multipolar. The layer II cells of area 35 sometimes have numerous satellite glial cells associated with them. Even when layers II and III cannot be distinguished from each other, the satellite glia are only seen in the superficial portion of the intermixed layer. Area 35 is agranular and one can detect the " lamina dissecans" (this

distinguishes it from area 36 which is disgranular). Layer 5 has a large band of dense pyramidal and multipolar darkly stained cells (it's most prominent characteristic). The packing density of these cells is higher from either area 36 or enthorhinal layer 5. Layer 6 is separated from layer 5 by a sparsely populated zone of lightly stained cells and is continuous with the LVI of the entorhinal cortex, although less densely populated.

The region just deep to LVI contains diffuse population of polymorphic cells. This gives to the limit with the white matter a diffuse appearance.

In SMI-32 stained material layer 2 has neurons and neural processes that are labelled while all the surrounding areas do not have label in layer2. At the most anterior portions this clearly delimits area 35 from the surrounding Entorhinal cortex. At more caudal levels the label is stronger but the entorhinal cortex also gets label and the border can't be identified.

The strongly labelled cells inlayer 2 of area 35 extend beneath the largelly unlabelled cells of layer 3 of area 36 and ultimately merge with the strongly labelled cells of layer 5 of area 36. It is possible to detect a clear band between the cells of these two layers (layer 2 of area 35 and layer 5 of area 36). This observation confirms the one of the oblique border between areas 35/36 in Nissl stained tissue.

Area MT

MT shares borders with : MST,V4t (PIT),FST;

Gross landmarks

MT is on the posterior bank of the STS. Situated between MST and V4t it shares its anterior border with FST. Generally in atlases of Rhesus monkeys MT starts at the very opening of the STS. The latter is untrue for the cynomolgus monkey. On horizontal sections at levels where the STS starts its posterior bank is first occupied by DP. After several millimetres DP starts to retract and the lateral half of the bank is occupied by V4t, while on the medial part we have area MST. To identify these changes we can use as an indicator the apparent depth and curvature of the sulcus. DP is on the posterior bank only at levels where the sulcus is straight and half size in depth. Once the sulcus starts to curve area DP disappears and V4 takes the lip, while V4t is on the lateral halve of the bank and MST on its medial halve. The general orientation of STS is that it starts with running quite vertical at its dorsal parts and more ventrally just before or at the moment when the lateral fissure appears it changes its slope to less abrupt. On horizontal sections this change is visible on the anterior bank of the sulcus where the cortex is not cut normally anymore and so it appears thicker. This transformation is just the level where MT appears first. At parasagittal sections this change in orientation is more obvious and seems to be a good indicator of the most dorsal extent of MT. Once MT appears, it will be laterally bordered by V4t. If the plan of horizontal section is relatively correct the ventral limit of MT will be found at around the level where the LS is already closed and IOS and/or PMT are open. Another indication of the ventral limit of MT is the appraisal of FST on the fundus of STS. In horizontal sections FST appears at levels where the fundus of STS starts. This seems bit surprising regarding the fact that in coronal sections and flatmaps MT and even MST seem to step sometimes on what could be qualified as the fundus (unsolved problem).

Cytoarchitecture

V4t/MT Nissl

The border between V4t and MT is difficult to distinguish in Nissl stained sections, V4t forms a mix between the cytoarchitectonic characteristics of V4 and MT. In many cases it looks like MT. The major difference is that layer 6 in V4t enters the white matter in more diffuse manner (bit like V4) while in MT this limit is very sharp (due to a tangential plexus of richly myelinated fibers entering MT). A cue for the MT/V4t border in SMI-32 ist that layer 3a is more densely populated with bigger cells in MT than in V4t. In area MT the label of layers 5 and 6 is very prominent. By the same staining technique the border MT/MST is detectable as

layer 6 is darker in area MST than in MT. In MT layer 3a has more cells and it appears thicker than in MST. Area MT has some cells in Layer 2 and 3a while they are absent in MST.

Area MST

Area MST shares borders with: DP, V4t, STP, MT, FST

Gross landmarks

MST is situated in the STS. In horizontal sections dorsally, area MST extends on the anterior and very briefly on the posterior banks of the sulcus. As one goes ventrally the flat shape of STS becomes curved and the ventrolateral border of MST is retracted to stay at the fundus of STS. The majority of authors consider the existence of a dorsal and ventral halves of MST i.e. MSTd and MSTv this explains the two patches of label after V1 injection. The dorsolateral border of MST with STP is situated about 1/3 mediolateral on the anterior bank of STS at ventral positions but at more dorsal levels before the formation of MT, more than 2/3 of the anterior bank of STS is devoted to MST. When MT appears, MST retracts from the posterior bank of STS to make the area +-4mm wide. When the fundus of the STS opens wide (large and flat) area MST quickly disappears to be replaced by FST. When the plane of section is correct at these levels correspond dorso-ventraly to the level where the LS gives place to the IOS.

Cytoarchitecture

In SMI-32 layer 3a of MST can be recognised from the surrounding MT or V4t as it is more densely populated with bigger cells in MST than in V4t. In the areas MT and MST the label of layers 5 and 6 very prominent. The SMI-32 pattern that serves to recognise MST from MT is the darker label in layer 2 of MST. In MT layer 3a is more denselly populated and appears thicker than in MST, also MT posses labelled cells in layers 2 and 3a while MST does not. Nissl stain of MST is characterised by medium and large pyramids. The limit between layers 5 and 6 is distinguishable thanks to a change in the density of stain. Layer 6 is more densely packed and has more rowish orientation while layer 5 will look organized in radial columns. In layer 5 there are occasional equidistant megacells that are darkly stained in Nissl as well as in SMI-32. The location of these cells corresponds to a zone projecting on V1. In this area the big pyramids are more frequently met than in 7a and there is no gradient between layers 3b and 3a. The limits between layers 2, 3b and 3a appear more clear-cut in MST.

In Nissl stain the profile of 7a is more parietal like (except for the columnar appearance that is absent in 7a) and this differentiates it from MST. Layers 3 and 5a have more numerous big pyramids than in MST. These cells are evenly distributed in these layers but not very frequent. Layer 6 seems denser in MST than in 7a.

Areas FST and LST

Gross landmarks

FST is an area inside the STS that appears anterior to MST and MT on the fundus of the STS (When it becomes large and flat) and then takes hold on all of the STS fundus. On horizontal sections it never extends on the anterior nor the posterior bank of the STS. Ventrally it continues till the T shape of STS disappears. At these levels or a bit more dorsal it is replaced by LST. LST is in majority of segmentations incorporated in to FST but authors have shown that this anterior part has different connectivity and integration in to the cortical network.

Cytoarchitecture

It is difficult to distinguish the border between STP and FST on the basis of cytoarchitectonic criteria. In SMI-32 stained sections STP should have more prominent layer 5 than the neighboring areas. On sections in the horizontal plane FST may be identified thanks to a change of the orientation of cells and so the sections do not represent simultaneously the cell

body and the apical dendrite. FST is characterized by the presence of small SMI-32 immunoresponsive neurons in LIII and LV. The numbers of labeled neurons in area FST is lower than in MT or MST. In SMI-32 PGa has more labelled neurons in layer 5 than FST. They are big and darkly stained with extensive basal and apical dendrites.TE has a higher density of labeled cells and a characteristic laminar distribution that distinguishes it from FST/LST.

Area PIP

Area PIP shares borders with: V6,V6a,VIP,LIP,

Gross landmarks

On horizontal sections area PIP is a small dorso-ventrally elongated area on the anterior and posterior lips of IPS at the level of the orbitoparietal junction. Ventrally it ends up at the base of the IPS. On the ventral most positions when we cannot see anymore the IPS invagination we consider PIP is to have disappeared. Under MRI investigation the region situated at the caudal end of the ventral part of lateral IPS is characterized by a strong myelination and selectively activated by 3D static or moving shapes. In the Logothetis paper this region is more specifically activated than the adjacent IPS (area LIP) and anectant gyrus (areaV3a). The anatomically defined region has been identified as the zone LOP by Van Essen. He stated that the cytoarchitecture of this region is transient between the part of PIP on the medial bank of IPS and the classical LIP. He did not definitively associates it to one or other area. The paper of Nakamura seems to be a good source for cytoarchitectonic criteria but one should be careful about LOP. They seem to ignore it and describe this position as the “curved part of LIP (That has 3D related activity)”. Part of it corresponds to our LIP but a small part is PIP in our segmentations. They say PIP is lateral to V3a and so it could not appear at this position. We say it is lateral to V3a but also extends anterior to become contingent to VIP. In this decision we have followed Lewis (Lewis and Van Essen, 2000a), his position seems to be that part of LOP may be associated with LIP and another to PIP.

Cytoarchitecture

We can distinguish the limit between V3A and PIP as at this level a regular label of pyramids appears in layer 5. The density of cells in layer 3 increases. The limit between VIP and PIP is very clear cut under SMI-32 with increasing density of label in LIIIb, more stain in LV and LVI.

Area LIP

Gross landmarks

Occupies the full extent of the lateral bank of IPS and has it’s ventral limit with VIP at 1,5mm from the fundus of the IPS. On horizontal sections the caudal border is with area DP dorsally on the lateral lip of IPS. At more ventral positions where area PIP appears the limit is retracted to more anterior positions at around 5mm from the lip (just before the curving of the sulcus). The anterior limit of LIP is with area AIP it has not been defined in this exploration.

Cytoarchitecture

Area VIP

Occupyes the fundus of the IPS and extends at about 1,5mm on the lateral lip of IPS (section 80 and ventrally to it). The medial limit is two lengths more dorsal.

Cytoarchitecture

The limit PIP/VIP is a very clear cut limit with increasing density of label in layer 3b and also layers 5 and 6.

Area 7a

Area 7a shares borders with areas : LIP, DP,MST,TPO,STP,7b.

Gross landmarks

Area 7a is situated on the inferior parietal lobule. In many studies the zone is separated in areas Opt, PG, PGop, PFG. The medial border of area 7a follows the lateral lip of IPS. The caudal limit of area 7a is with area DP on the dorsal most part of the prelunate gyrus. In horizontal sections the extreme dorsal positions on the anterior bank of STS are devoted to 7a while the posterior bank is devoted to DP; the limit is on the fundus. On coronal sections this border is also identical at caudal levels where the future STS appears more as a dip than a complete sulcus. Once the STS starts to open the area MST takes the position on the bank pushing 7a on to the anterior lip. More lateral and anterior the lateral fissure (lf) appears and then the border of 7a is on the dorsal lip of the lf; the neighbouring area being TPO and later on it is STP. The anterior border of 7a is with 7b; it occurs roughly on the half of the inferior parietal lobule.

Cytoarchitecture

The granules of layer 4 are present in a larger stripe (mixing with cells from layers 3b and 5). In the more superficial part of layer 2 the cells are small and round. There is a clear cut between layers 1 and 2. In the profound part of layer 2 and the upper part of layer 3 there is a continuous gradient of increasing cell size making the limit of layers 2b/3a not obvious. Layer 3b is composed of medium sized (a bit bigger even) darkly stained cells. Layer 5a presents a mixed population of medium and large darkly stained pyramids and also small granular cells. The transition between layers 5 and 6 is gradual and so the two layers are hardly distinguishable one from another. Layer 6 has medium sized to small darkly stained pyramids and a relatively clear limit with the white matter.

BIBLIOGRAPHY

Akaike H (1993) Information theory and an extension of the maximum likelihood principle. In: Second International Symposium on information theory(Petrov, B. N. and Csaki, F., eds), pp 267-281 Budapest: Akademiai Kiado.

Angelucci A, Bressloff PC (Contribution of feedforward, lateral and feedback connections to the classical receptive field center and extra-classical receptive field surround of primate V1 neurons. Prog Brain Res 154:93-120.2006).

Azouz R, Gray CM (Adaptive coincidence detection and dynamic gain control in visual cortical neurons in vivo. Neuron 37:513-523.2003).

Baizer JS, Ungerleider LG, Desimone R (Organization of visual inputs to the inferior temporal and posterior parietal cortex in macaques. J Neurosci 11:168-190.1991).

Barabasi AL, Albert R (Emergence of scaling in random networks. Science 286:509-512.1999).

Barone P, Batardiere A, Knoblauch K, Kennedy H (Laminar distribution of neurons in extrastriate areas projecting to visual areas V1 and V4 correlates with the hierarchical rank and indicates the operation of a distance rule. J Neurosci 20:3263-3281.2000).

Barthélemy M, Barrat A, Pastor-Satorras, Verspignani A (Characterization and modeling of weighted networks. Physica A 34-43.2005).

Batardiere A, Barone P, Dehay C, Kennedy H (Area-specific laminar distribution of cortical feedback neurons projecting to cat area 17: quantitative analysis in the adult and during ontogeny. J Comp Neurol 396:493-510.1998).

Bentivoglio M, Kuypers HG, Catsman-Berrevoets CE, Loewe H, Dann O (Two new fluorescent retrograde neuronal tracers which are transported over long distances. Neurosci Lett 18:25-30.1980).

Binzegger T, Douglas RJ, Martin KA (A quantitative map of the circuit of cat primary visual cortex. J Neurosci 24:8441-8453.2004).

Binzegger T, Douglas RJ, Martin KA (Topology and dynamics of the canonical circuit of cat V1. Neural Netw 22:1071-1078.2009).

Boccaletti S, Latora V, Moreno Y, Chavez M, Hwang DU (Complex networks: structure and dynamics. Physics reports 424:175-308.2006).

Boussaoud D, Desimone R, Ungerleider LG (Visual topography of area TEO in the macaque. J Comp Neurol 306:554-575.1991).
Boussaoud D, Ungerleider LG, Desimone R (Pathways for motion analysis: cortical connections of the medial superior temporal and fundus of the superior temporal visual areas in the macaque. J Comp Neurol 296:462-495.1990).
Box GEP, Cox DR (An analysis of transformations (with discussion). J Roy Stat Soc B 26:211-252.1964).
Boyd JD, Mavity-Hudson JA, Casagrande VA (The connections of layer 4 subdivisions in the primary visual cortex (V1) of the owl monkey. Cereb Cortex 10:644-662.2000).
Braitenberg V, Schüz A (1998) Cortex: statistics and geometry of neuronal connectivity. Berlin: Springer-Verlag.
Brewer AA, Press WA, Logothetis NK, Wandell BA (Visual areas in macaque cortex measured using functional magnetic resonance imaging. J Neurosci 22:10416-10426.2002).
Brodmann K (1909) Vergleichende Lokalisationslehre des Grosshirninde in Ihren Prinzipien dargestellt auf Grund des Zellenbauen. Liepzig: Barth.
Bullier J, Kennedy H (Projection of the lateral geniculate nucleus onto cortical area V2 in the macaque monkey. Exp Brain Res 53:168-172.1983).
Bullier J, Kennedy H (Axonal bifurcation in the visual system. Trends Neurosci 10:205-210.1987).
Bullier J, Kennedy H, Salinger W (Branching and laminar origin of projections between visual cortical areas in the cat. J Comp Neurol 228:329-341.1984b).
Bullmore E, Sporns O (Complex brain networks: graph theoretical analysis of structural and functional systems. Nat Rev Neurosci 10:186-198.2009).
Buzsaki G (The structure of consciousness. Nature 446:267.2007).
Buzsaki G, Draguhn A (Neuronal oscillations in cortical networks. Science 304:1926-1929.2004).
Cauller L (Layer I of primary sensory neocortex: where top-down converges upon bottom-up. Behav Brain Res 71:163-170.1995).
Cauller LJ, Clancy B, Connors BW (Backward cortical projections to primary somatosensory cortex in rats extend long horizontal axons in layer I. J Comp Neurol 390:297-310.1998).
Chen CC, Henson RN, Stephan KE, Kilner JM, Friston KJ (Forward and backward connections in the brain: a DCM study of functional asymmetries. Neuroimage 45:453-462.2009).
Cherniak C, Mokhtarzada Z, Rodriguez-Esteban R, Changizi K (Global optimization of cerebral cortex layout. Proc Natl Acad Sci U S A.2004).
Chklovskii DB, Schikorski T, Stevens CF (Wiring optimization in cortical circuits. Neuron 34:341-347.2002).

Clavagnier S, Falchier A, Kennedy H (Long-distance feedback projections to area V1: implications for multimodal integration, spatial awarness and visual consciousness. Cogn Affect Behav Neurosci 4:117-126.2004).

Cleveland WS, Grosse E, Shyu WM (1992) Local regression models. In: Statistical Models in S(Chambers, J. M. and Hastie, T. J., eds), p Chapter 8.

Conde F (Further studies on the use of the fluorescent tracers fast blue and diamidino yellow: effective uptake area and cellular storage sites. J Neurosci Methods 21:31-43.1987).

Cornette L, Dupont P, Spileers W, Sunaert S, Michiels J, Van Hecke P, Mortelmans L, Orban GA (Human cerebral activity evoked by motion reversal and motion onset. A PET study. Brain 121:143-157.1998).

Cragg BG (The topography of the afferent projections in the circumstriate visual cortex of the monkey studied by the Nauta method. Vision Res 9:733-747.1969).

Craig AD, Jr., Linington AJ, Kniffki KD (Significant differences in the retrograde labeling of spinothalamic tract cells by horseradish peroxidase and the fluorescent tracers fast blue and diamidino yellow. Exp Brain Res 74:431-436.1989).

Crescimanno G, Salerno MT, Cortimiglia R, Amato G (Claustral influence on ipsi- and contralateral motor cortical areas, in the cat. Brain Res Bull 22:839-843.1989).

Crescimanno G, Salerno MT, Cortimiglia R, Amato G (Effect of claustrum stimulation on neurons of the contralateral medial oculomotor area, in the cat. Neurosci Lett 114:289-294.1990).

Crescimanno G, Salerno MT, Cortimiglia R, Amato G, Infantellina F (Functional relationship between claustrum and pyramidal tract neurons, in the cat. Neurosci Lett 44:125-129.1984).

Crick FC, Koch C (What is the function of the claustrum? Philos Trans R Soc Lond B Biol Sci 360:1271-1279.2005).

da Costa NM, Martin KA (The proportion of synapses formed by the axons of the lateral geniculate nucleus in layer 4 of area 17 of the cat. J Comp Neurol 516:264-276.2009).

Dehay C, Kennedy H, Bullier J, Berland M (Absence of interhemispheric connections of area 17 during development in the monkey. Nature 331:348-350.1988).

Destexhe A, Pare D (Impact of network activity on the integrative properties of neocortical pyramidal neurons in vivo. J Neurophysiol 81:1531-1547.1999).

DeYoe EA, Hockfield S, Garren H, Van Essen DC (Antibody labeling of functional subdivisions in visual cortex: Cat-301 immunoreactivity in striate and extrastriate cortex of the macaque monkey. Vis Neurosci 5:67-81.1990).

Douglas RJ, Koch C, Mahowald M, Martin KA, Suarez HH (Recurrent excitation in neocortical circuits. Science 269:981-985.1995).

Douglas RJ, Martin KA (The butterfly and the loom. Brain Res Rev 55:314-328.2007).

Duffau H, Mandonnet E, Gatignol P, Capelle L (Functional compensation of the claustrum: lessons from low-grade glioma surgery. J Neurooncol 81:327-329.2007).

Ekstrom LB, Roelfsema PR, Arsenault JT, Bonmassar G, Vanduffel W (Bottom-up dependent gating of frontal signals in early visual cortex. Science 321:414-417.2008).

Falchier A, Clavagnier S, Barone P, Kennedy H (Anatomical evidence of multimodal integration in primate striate cortex. J Neurosci 22:5749-5759.2002).

Feinerman O, Rotem A, Moses E (Reliable neuronal logic devices from patterned hippocampal cultures. Nat Phys 4:967-973.2008).

Felleman DJ, Burkhalter A, Van Essen DC (Cortical connections of areas V3 and VP of macaque monkey extrastriate visual cortex. J Comp Neurol 379:21-47.1997).

Felleman DJ, Van Essen DC (Distributed hierarchical processing in the primate cerebral cortex. Cereb Cortex 1:1-47.1991).

Fitzpatrick D, Itoh K, Diamond IT (The laminar organization of the lateral geniculate body and the striate cortex in the squirrel monkey (Saimiri sciureus). J Neurosci 3:673-702.1983).

Fox MD, Raichle ME (Spontaneous fluctuations in brain activity observed with functional magnetic resonance imaging. Nat Rev Neurosci 8:700-711.2007).

Fox MD, Snyder AZ, Vincent JL, Corbetta M, Van Essen DC, Raichle ME (The human brain is intrinsically organized into dynamic, anticorrelated functional networks. Proc Natl Acad Sci U S A 102:9673-9678.2005).

Frey S, Comeau R, Hynes B, Mackey S, Petrides M (Frameless stereotaxy in the nonhuman primate. Neuroimage 23:1226-1234.2004).

Friston K (Learning and inference in the brain. Neural Netw 16:1325-1352.2003).

Friston K (A theory of cortical responses. Philos Trans R Soc Lond B Biol Sci 360:815-836.2005).

Galletti C, Gamberini M, Kutz DF, Baldinotti I, Fattori P (The relationship between V6 and PO in macaque extrastriate cortex. Eur J Neurosci 21:959-970.2005).

Gattass R, Gross CG, Sandell JH (Visual topography of V2 in the macaque. J Comp Neurol 201:519-539.1981).

Gattass R, Nascimento-Silva S, Soares JG, Lima B, Jansen AK, Diogo AC, Farias MF, Botelho MM, Mariani OS, Azzi J, Fiorani M (Cortical visual areas in monkeys: location, topography, connections, columns, plasticity and cortical dynamics. Philos Trans R Soc Lond B Biol Sci 360:709-731.2005).

Gattass R, Sousa AP, Mishkin M, Ungerleider LG (Cortical projections of area V2 in the macaque. Cereb Cortex 7:110-129.1997).

Girard B, Tabareau N, Pham QC, Berthoz A, Slotine JJ (Where neuroscience and dynamic system theory meet autonomous robotics: a contracting basal ganglia model for action selection. Neural Netw 21:628-641.2008).

Goodhill GJ, Simmen MW, Willshaw DJ (An evaluation of the use of multidimensional scaling for understanding brain connectivity. Philos Trans R Soc Lond B Biol Sci 348:265-280.1995).

Gur M, Snodderly DM (Physiological differences between neurons in layer 2 and layer 3 of primary visual cortex (V1) of alert macaque monkeys. J Physiol 586:2293-2306.2008).

Hagmann P, Cammoun L, Gigandet X, Meuli R, Honey CJ, Wedeen VJ, Sporns O (Mapping the Structural Core of Human Cerebral Cortex. PLoS biology 6:e159.2008).

Hagmann P, Kurant M, Gigandet X, Thiran P, Wedeen VJ, Meuli R, Thiran JP (Mapping human whole-brain structural networks with diffusion MRI. PLoS ONE 2:e597.2007).

Hagmann P, Thiran JP, Jonasson L, Vandergheynst P, Clarke S, Maeder P, Meuli R (DTI mapping of human brain connectivity: statistical fibre tracking and virtual dissection. Neuroimage 19:545-554.2003).

Hahnloser RH, Seung HS, Slotine JJ (Permitted and forbidden sets in symmetric threshold-linear networks. Neural Comput 15:621-638.2003).

Haider B, Krause MR, Duque A, Yu Y, Touryan J, Mazer JA, McCormick DA (Synaptic and network mechanisms of sparse and reliable visual cortical activity during nonclassical receptive field stimulation. Neuron 65:107-121.2010).

Hallman LE, Schofield BR, Lin CS (Dendritic morphology and axon collaterals of corticotectal, corticopontine, and callosal neurons in layer V of primary visual cortex of the hooded rat. J Comp Neurol 272:149-160.1988).

Hastie TJ, Tibshirani RJ (1990) Generalized Additive Models: CRC Press.

Hawkins J, George D, Niemasik J (Sequence memory for prediction, inference and behaviour. Philos Trans R Soc Lond B Biol Sci 364:1203-1209.2009).

Henry GH, Salin PA, Bullier J (Projections from Area-18 and Area-19 to Cat Striate Cortex - Divergence and Laminar Specificity. Eur J Neurosci 3:186-200.1991).

Hilbe JM (2007) Negative Binomial Regression. Cambridge: Cambridge University Press.

Hilgetag CC, Burns GA, O'Neill MA, Scannell JW, Young MP (Anatomical connectivity defines the organization of clusters of cortical areas in the macaque monkey and the cat. Philos Trans R Soc Lond B Biol Sci 355:91-110.2000a).

Hilgetag CC, O'Neill MA, Young MP (Indeterminate organization of the visual system. Science 271:776-777.1996).

Hilgetag CC, O'Neill MA, Young MP (Hierarchical organization of macaque and cat cortical sensory systems explored with a novel network processor. Philos Trans R Soc Lond B Biol Sci 355:71-89.2000b).

Hochstein S, Ahissar M (View from the top: hierarchies and reverse hierarchies in the visual system. Neuron 36:791-804.2002).

Hof PR, Morrison JH (Neurofilament protein defines regional patterns of cortical organization in the macaque monkey visual system: a quantitative immunohistochemical analysis. J Comp Neurol 352:161-186.1995).

Hof PR, Ungerleider LG, Webster MJ, Gattass R, Adams MM, Sailstad CA, Morrison JH (Neurofilament protein is differentially distributed in subpopulations of corticocortical projection neurons in the macaque monkey visual pathways. J Comp Neurol 376:112-127.1996).

Honey CJ, Kotter R, Breakspear M, Sporns O (Network structure of cerebral cortex shapes functional connectivity on multiple time scales. Proc Natl Acad Sci U S A 104:10240-10245.2007).

Honey CJ, Sporns O, Cammoun L, Gigandet X, Thiran JP, Meuli R, Hagmann P (Predicting human resting-state functional connectivity from structural connectivity. Proc Natl Acad Sci U S A 106:2035-2040.2009).

Hubener M, Schwarz C, Bolz J (Morphological types of projection neurons in layer 5 of cat visual cortex. J Comp Neurol 301:655-674.1990).

Hupé JM, James AC, Payne BR, Lomber SG, Girard P, Bullier J (Cortical feedback improves discrimination between figure and background by V1, V2 and V3 neurons. Nature 394:784-787.1998).

Ichinohe N, Rockland KS (Region Specific Micromodularity in the Uppermost Layers in Primate Cerebral Cortex. Cereb Cortex.2004).

Irvine DR, Brugge JF (Afferent and efferent connections between the claustrum and parietal association cortex in cat: a horseradish peroxidase and autoradiographic study. Neurosci Lett 20:5-10.1980).

Ishai A, Sagi D (Common mechanisms of visual imagery and perception. Science 268:1772-1774.1995).

Iwai E, Yukie M (A direct projection from hippocampal field CA1 to ventral area TE of inferotemporal cortex in the monkey. Brain Res 444:397-401.1988).

Jaynes ET (Information theory and statistical mechanics. Phys Rev 106:620-630.1957).

Jehee JF, Roelfsema PR, Deco G, Murre JM, Lamme VA (Interactions between higher and lower visual areas improve shape selectivity of higher level neurons-explaining crowding phenomena. Brain Res 1157:167-176.2007).

Johansen-Berg H, Behrens TEJ (2009) Diffusion MRI: From quantitative measurement to in-vivo neuroanatomy: Academic Press.

Johnson RR, Burkhalter A (A polysynaptic feedback circuit in rat visual cortex. J Neurosci 17:7129-7140.1997).

Jouve B, Rosenstiehl P, Imbert M (A mathematical approach to the connectivity between the cortical visual areas of the macaque monkey. Cereb Cortex 8:28-39.1998).

Juan CH, Walsh V (Feedback to V1: a reverse hierarchy in vision. Exp Brain Res 150:259-263.2003).

Kaas JH, Collins CE (The organization of sensory cortex. Curr Opin Neurobiol 11:498-504.2001).

Kaas JH, Lin CS (Cortical projections of area 18 in owl monkeys. Vision Res 17:739-741.1977).

Kasper EM, Lubke J, Larkman AU, Blakemore C (Pyramidal Neurons in Layer-5 of the Rat Visual-Cortex .3. Differential Maturation of Axon Targeting, Dendritic Morphology, and Electrophysiological Properties. J Comp Neurol 339:495-518.1994).

Katz LC (Local circuitry of identified projection neurons in cat visual cortex brain slices. J Neurosci 7:1223-1249.1987).

Keizer K, Kuypers HGJM, Huisman AM, Dann O (Diamidino Yellow dihydrochloride (DY 2HCl): a new fluorescent retrograde neuronal tracer, which migrates only very slowly out of the cell. Exp Brain Res 51:179-191.1983).

Kenet T, Bibitchkov D, Tsodyks M, Grinvald A, Arieli A (Spontaneously emerging cortical representations of visual attributes. Nature 425:954-956.2003).

Kennedy H, Bullier J (A double-labeling investigation of the afferent connectivity to cortical areas V1 and V2 of the macaque monkey. J Neurosci 5:2815-2830.1985).

Kennedy H, Salin P, Bullier J, Horsburgh G (Topography of developing thalamic and cortical pathways in the visual system of the cat. J Comp Neurol 348:298-319.1994).

Klein BG, Mooney RD, Fish SE, Rhoades RW (The structural and functional characteristics of striate cortical neurons that innervate the superior colliculus and lateral posterior nucleus in hamster. Neuroscience 17:57-78.1986).

Kopell N, Ermentrout GB, Whittington MA, Traub RD (Gamma rhythms and beta rhythms have different synchronization properties. Proc Natl Acad Sci U S A 97:1867-1872.2000).

Krubitzer LA, Kaas JH (Cortical integration of parallel pathways in the visual system of primates. Brain Res 478:161-165.1989).

Krubitzer LA, Kaas JH (Cortical connections of MT in four species of primates: areal, modular, and retinotopic patterns. Vis Neurosci 5:165-204.1990).

Krubitzer LA, Kaas JH (The dorsomedial visual area of owl monkeys: connections, myeloarchitecture, and homologies in other primates. J Comp Neurol 334:497-528.1993).

Kuypers HGJM, Bentivoglio M, Catsman-Berrevoets CE, Bahros AT (Double retrograde neuronal labelling through divergent axon collaterals using two fluorescent tracers with the same ecitation wave length which label different features of the cell. Exp Brain Res 40:383-392.1980).

Kuypers HGJM, Szwarcbart MK, Mishkin M, Rosvold HE (Occipitotemporal corticortical connections in the rhesus monkey. Exp Neurol 11:245-262.1965).

Lachica EA, Beck PD, Casagrande VA (Parallel pathways in macaque monkey striate cortex : anatomically defined columns in layer III. Proc Natl Acad Sci USA 89:3566-3570.1992).

Lakatos P, Karmos G, Mehta AD, Ulbert I, Schroeder CE (Entrainment of neuronal oscillations as a mechanism of attentional selection. Science 320:110-113.2008).

Lamme VA (Recurrent corticocortical interactions in neural disease. Arch Neurol 60:178-184.2003).

Lamme VA, Zipser K, Spekreijse H (Figure-ground activity in primary visual cortex is suppressed by anesthesia. Proc Natl Acad Sci U S A 95:3263-3268.1998).

Larkum ME, Zhu JJ, Sakmann B (A new cellular mechanism for coupling inputs arriving at different cortical layers. Nature 398:338-341.1999).

Larsen DD, Wickersham IR, Callaway EM (Retrograde tracing with recombinant rabies virus reveals correlations between projection targets and dendritic architecture in layer 5 of mouse barrel cortex. Frontiers in neural circuits 1:5.2007).

Latora V, Marchiori M (Economic small-world behavior in weighted networks. Eur Phys J B 32:249-263.2003).

Laughlin SB, Sejnowski TJ (Communication in neuronal networks. Science 301:1870-1874.2003).

Lavenex P, Suzuki WA, Amaral DG (Perirhinal and parahippocampal cortices of the macaque monkey: projections to the neocortex. J Comp Neurol 447:394-420.2002).

Lee CC, Winer JA (Connections of cat auditory cortex: III. Corticocortical system. J Comp Neurol 507:1920-1943.2008).

Lee TS, Yang CF, Romero RD, Mumford D (Neural activity in early visual cortex reflects behavioral experience and higher-order perceptual saliency. Nat Neurosci 5:589-597.2002).

LeVay S (Synaptic organization of claustral and geniculate afferents to the visual cortex of the cat. J Neurosci 6:3564-3575.1986).

Levitt JB, Lund JS, Yoshioka T (Anatomical Substrates for Early Stages in Cortical Processing of Visual Information in the Macaque Monkey. Behav Brain Res 76:5-19.1996).

Lewis JW, Van Essen DC (Corticocortical connections of visual, sensorimotor, and multimodal processing areas in the parietal lobe of the macaque monkey. J Comp Neurol 428:112-137.2000a).

Lewis JW, Van Essen DC (Mapping of architectonic subdivisions in the macaque monkey, with emphasis on parieto-occipital cortex. J Comp Neurol 428:79-111.2000b).
Lindsey JK (1999) Models Repeated Measurements. Oxford Oxford University Press.
Llinas R, Ribary U, Contreras D, Pedroarena C (The neuronal basis for consciousness. Philos Trans R Soc Lond B Biol Sci 353:1841-1849.1998).
Lund JS, Hendrickson AE, Ogren MP, Tobin EA (Anatomical organization of primate visual cortex area V1. J Comp Neurol 202:19-45.1981).
Lund JS, Lund RD, Hendrickson AE, Bunt AH, Fuchs AF (The origin of efferent pathways from the primary visual cortex of the macaque monkey as shown by retrograde transport of horseradish peroxydase. J Comp Neurol 164:287-304.1975).
MacNeil MA, Lomber SG, Payne BR (Thalamic and cortical projections to middle suprasylvian cortex of cats: constancy and variation. Exp Brain Res 114:24-32.1997).
Markov NT, Ercsey-Ravasz MM, Gariel MA, Dehay C, Knoblauch A, Toroczkai Z, Kennedy H (2011) The tribal networks of the cerebral cortex. In: Cerebral Plasticity(Chalupa, L. M. et al., eds), p in press Cambridge MA: MIT Press.
Markov NT, Misery P, Vezoli J, Quilodran R, Lamy C, Falchier A, Giroud P, Gariel MA, Ercsey-Ravasz MM, Huissoud C, Barone P, Dehay C, Toroczkai Z, Kennedy H, Knoblauch K (Regularity of the profiles of cortical connectivity. J Neurosci.submitted).
Martinez-Millan L, Hollander H (Cortico-cortical projections from striate cortex of the squirrel monkey (saimiri sciureus). A radioautographic study. Brain Res 83:405-417.1975).
Maunsell JH, van Essen DC (The connections of the middle temporal visual area (MT) and their relationship to a cortical hierarchy in the macaque monkey. J Neurosci 3:2563-2586.1983).
McCullagh P, Nelder JA (1989) Generalized linear models. Boca Raton: Chapman & Hall/CRC.
Milgram S (The small world problem. Psychology Today 1:60-67.1967).
Milo R, Shen-Orr S, Itzkovitz S, Kashtan N, Chklovskii D, Alon U (Network motifs: simple building blocks of complex networks. Science 298:824-827.2002).
Miyashita Y (How the brain creates imagery: projection to primary visual cortex. Science 268:1719-1720.1995).
Moran J, Desimone R (Selective attention gates visual processing in the extrastriate cortex. Science 229:782-784.1985).
Motter BC (Focal attention produces spatially selective processing in visual cortical areas V1, V2, and V4 in the presence of competing stimuli. J Neurophysiol 70:909-919.1993).

Musil SY, Olson CR (Organization of cortical and subcortical projections to anterior cingulate cortex in the cat. J Comp Neurol 272:203-218.1988a).

Musil SY, Olson CR (Organization of cortical and subcortical projections to medial prefrontal cortex in the cat. J Comp Neurol 272:219-241.1988b).

Nakamura H, Gattass R, Desimone R, Ungerleider LG (The modular organization of projections from areas V1 and V2 to areas V4 and TEO in macaques. J Neurosci 13:3681-3691.1993).

Nakamura H, Le WR, Wakita M, Mikami A, Itoh K (Projections from the cytochrome oxidase modules of visual area V2 to the ventral posterior area in the macaque. Exp Brain Res 155:102-110.2004).

Neal JW, Pearson RC, Powell TP (The connections of area PG, 7a, with cortex in the parietal, occipital and temporal lobes of the monkey. Brain Res 532:249-264.1990).

Nelissen K, Vanduffel W, Orban GA (Charting the lower superior temporal region, a new motion-sensitive region in monkey superior temporal sulcus. J Neurosci 26:5929-5947.2006).

Newman MEJ (The Structure and Function of Complex Networks. SIAM Review 45:167-256.2003).

Novikova L, Novikov L, Kellerth JO (Persistent neuronal labeling by retrograde fluorescent tracers: a comparison between Fast Blue, Fluoro-Gold and various dextran conjugates. J Neurosci Methods 74:9-15.1997).

O'Connor DH, Huber D, Svoboda K (Reverse engineering the mouse brain. Nature 461:923-929.2009).

Olson CR, Musil SY (Topographic organization of cortical and subcortical projections to posterior cingulate cortex in the cat: evidence for somatic, ocular, and complex subregions. J Comp Neurol 324:237-260.1992).

Orban GA, Van Essen D, Vanduffel W (Comparative mapping of higher visual areas in monkeys and humans. Trends Cogn Sci 8:315-324.2004).

Panto MR, Zappala A, Parenti R, Serapide MF, Cicirata F (Corticonuclear projections of the cerebellum preserve both anteroposterior and mediolateral pairing patterns. Eur J Neurosci 13:694-708.2001).

Pascual-Leone A, Walsh V (Fast backprojections from the motion to the primary visual area necessary for visual awareness. Science 292:510-512.2001).

Payne JN (Comparisons between the use of true blue and diamidino yellow as retrograde fluorescent tracers. Exp Brain Res 68:631-642.1987).

Perkel DJ, Bullier J, Kennedy H (Topography of the afferent connectivity of area 17 in the macaque monkey: a double-labelling study. J Comp Neurol 253:374-402.1986).

Pham QC, Slotine JJ (Stable concurrent synchronization in dynamic system networks. Neural Netw 20:62-77.2007).

Pinheiro JC, Bates DM (2000) Mixed Effects Models in S and S-Plus. New York: Springer Verlag.

Pollard KS, Salama SR, Lambert N, Lambot MA, Coppens S, Pedersen JS, Katzman S, King B, Onodera C, Siepel A, Kern AD, Dehay C, Igel H, Ares M, Jr., Vanderhaeghen P, Haussler D (An RNA gene expressed during cortical development evolved rapidly in humans. Nature 443:167-172.2006).

Polyak S (1957) Cortical visual centers. In: The vertebrate visual system(Kluver, H., ed), pp 446-539 Chicago: University of Chicago Press.

Puigdellivol-Sanchez A, Prats-Galino A, Ruano-Gil D, Molander C (Fast blue and diamidino yellow as retrograde tracers in peripheral nerves: efficacy of combined nerve injection and capsule application to transected nerves in the adult rat. J Neurosci Methods 95:103-110.2000).

Puigdellivol-Sanchez A, Valero-Cabre A, Prats-Galino A, Navarro X, Molander C (On the use of fast blue, fluoro-gold and diamidino yellow for retrograde tracing after peripheral nerve injury: uptake, fading, dye interactions, and toxicity. J Neurosci Methods 115:115-127.2002).

Raichle ME, Mintun MA (Brain work and brain imaging. Annu Rev Neurosci 29:449-476.2006).

Rao RP, Ballard DH (Predictive coding in the visual cortex: a functional interpretation of some extra-classical receptive-field effects. Nat Neurosci 2:79-87.1999).

Rockland KS, Pandya DN (Laminar origins and terminations of cortical connections of the occipital lobe in the rhesus monkey. Brain Res 179:3-20.1979).

Rockland KS, Pandya DN (Cortical connections of the occipital lobe in the rhesus monkey: interconnections between areas 17, 18, 19 and the superior temporal sulcus. Brain Res 212:249-270.1981).

Rockland KS, Saleem KS, Tanaka K (Divergent feedback connections from areasV4 and TEO in the macaque. Visual Neurosci 11:579-600.1994).

Rockland KS, Van Hoesen GW (Direct temporal-occipital feedback connections to striate cortex (V1) in the macaque monkey. Cereb Cortex 4:300-313.1994).

Rockland KS, Virga A (Terminal arbors of individual "feedback" axons projecting from area V2 to V1 in the macaque monkey: a study using immunohistochemistry of anterogradely transported Phaseolus vulgaris-leucoagglutinin. J Comp Neurol 285:54-72.1989).

Roe AW, Ts'o DY (Visual topography in primate V2: multiple representation across functional stripes. J Neurosci 15:3689-3715.1995).

Roelfsema PR, Lamme VA, Spekreijse H (Synchrony and covariation of firing rates in the primary visual cortex during contour grouping. Nat Neurosci 7:982-991.2004).

Salerno MT, Cortimiglia R, Crescimanno G, Amato G, Infantellina F (Effects of claustrum stimulation on spontaneous bioelectrical activity of motor cortex neurons in the cat. Exp Neurol 86:227-239.1984).

Salin PA, Bullier J (Corticocortical connections in the visual system: structure and function. Physiol Rev 75:107-154.1995).

Salin PA, Bullier J, Kennedy H (Convergence and divergence in the afferent projections to cat area 17. J Comp Neurol 283:486-512.1989).

Salin PA, Girard P, Kennedy H, Bullier J (Visuotopic organization of corticocortical connections in the visual system of the cat. J Comp Neurol 320:415-434.1992).

Sawatari A, Callaway EM (Diversity and cell type specificity of local excitatory connections to neurons in layer 3B of monkey primary visual cortex. Neuron 25:459-471.2000).

Scannell JW, Grant S, Payne BR, Baddeley R (On variability in the density of corticocortical and thalamocortical connections. Philos Trans R Soc Lond B Biol Sci 355:21-35.2000).

Sejnowski TJ, Paulsen O (Network oscillations: emerging computational principles. J Neurosci 26:1673-1676.2006).

Seltzer B, Pandya DN (Post-rolandic cortical projections of the superior temporal sulcus in the rhesus monkey. J Comp Neurol 312:625-640.1991).

Shipp S, Adams DL, Moutoussis K, Zeki S (Feature Binding in the Feedback Layers of Area V2. Cereb Cortex.2009).

Shipp S, Grant S (Organization of reciprocal connections between area 17 and the lateral suprasylvian area of cat visual cortex. Vis Neurosci 6:339-355.1991).

Shipp S, Zeki S (The organisation of connections between areas V5 and V2 in macaque monkey visual cortex. Eur J Neurosci 308-331.1989a).

Shipp S, Zeki S (The organization of connections between areas V5 and V2 in macaque monkey visual cortex. Eur J Neurosci 1:308-331.1989b).

Shipp S, Zeki S (Segregation and convergence of specialised pathways in macaque monkey visual cortex. J Anat 187:547-562.1995).

Sincich LC, Horton JC (The circuitry of V1 and V2: integration of color, form, and motion. Annu Rev Neurosci 28:303-326.2005).

Slotine JJ, Lohmiller W (Modularity, evolution, and the binding problem: a view from stability theory. Neural Netw 14:137-145.2001).

Somers DC, Dale AM, Seiffert AE, Tootell RB (Functional MRI reveals spatially specific attentional modulation in human primary visual cortex. Proc Natl Acad Sci U S A 96:1663-1668.1999).

Song S, Sjostrom PJ, Reigl M, Nelson S, Chklovskii DB (Highly nonrandom features of synaptic connectivity in local cortical circuits. PLoS biology 3:e68.2005).

Spatz WB, Tigges J, Tigges M (Subcortical projections, cortical associations, and some intrinsic interlaminar connections of the striate cortex in the squirrel monkey (saimiri). J Comp Neurol 140:155-174.1970).

Sporns O, Honey CJ, Kotter R (Identification and classification of hubs in brain networks. PLoS ONE 2:e1049.2007).

Sporns O, Tononi G, Edelman GM (Theoretical neuroanatomy: relating anatomical and functional connectivity in graphs and cortical connection matrices. Cereb Cortex 10:127-141.2000).

Sporns O, Tononi G, Kotter R (The human connectome: A structural description of the human brain. PLoS computational biology 1:e42.2005).

Sporns O, Zwi JD (The small world of the cerebral cortex. Neuroinformatics 2:145-162.2004).

Stephan KE, Hilgetag CC, Burns GA, O'Neill MA, Young MP, Kotter R (Computational analysis of functional connectivity between areas of primate cerebral cortex. Philos Trans R Soc Lond B Biol Sci 355:111-126.2000).

Stepniewska I, Kaas JH (Topographic patterns of V2 cortical connections in macaque monkeys. J Comp Neurol 371:129-152.1996).

Super H, Spekreijse H, Lamme VA (Two distinct modes of sensory processing observed in monkey primary visual cortex (V1). Nat Neurosci 4:304-310.2001).

Suzuki WA, Amaral DG (Perirhinal and parahippocampal cortices of the macaque monkey: cortical afferents. J Comp Neurol 350:497-533.1994).

Tabareau N, Slotine JJ, Pham QC (How synchronization protects from noise. PLoS computational biology 6:e1000637.2010).

Takaji M, Komatsu Y, Watakabe A, Hashikawa T, Yamamori T (Paraneoplastic antigen-like 5 gene (PNMA5) is preferentially expressed in the association areas in a primate specific manner. Cereb Cortex 19:2865-2879.2009).

Tanaka M, Lindsley E, Lausmann S, Creutzfeldt OD (Afferent connections of the prelunate visual association cortex (areas V4 and DP). Anat Embryo 181:19-30.1990).

Tigges J, Spatz WB, Tigges M (Reciprocal point-to-point connections between parastriate and striate cortex in the squirrel monkey (saimiri). J Comp Neurol 148:481-490.1973).

Tigges J, Tigges M, Perachio AA (Complementary laminar terminations of afferents to area 17 originating in area 18 and in the lateral geniculate nucleus in squirrel monkey. J Comp Neurol 176:87-100.1977).

Tong F (Primary visual cortex and visual awareness. Nat Rev Neurosci 4:219-229.2003).

Tsodyks M, Kenet T, Grinvald A, Arieli A (Linking spontaneous activity of single cortical neurons and the underlying functional architecture. Science 286:1943-1946.1999).

Tsumoto T, Suda K (Effects of stimulation of the dorsocaudal claustrum on activities of striate cortex neurons in the cat. Brain Res 240:345-349.1982).

Uhlhaas PJ, Pipa G, Lima B, Melloni L, Neuenschwander S, Nikolic D, Singer W (Neural synchrony in cortical networks: history, concept and current status. Front Integr Neurosci 3:17.2009).

Ullman S (Sequence seeking and counter streams: a computational model for bidirectional information flow in the visual cortex. Cereb Cortex 5:1-11.1995).

Ungerleider LG, Desimone R (Cortical connections of visual area MT in the macaque. J Comp Neurol 248:190-222.1986).

Ungerleider LG, Galkin TW, Desimone R, Gattass R (Cortical connections of area V4 in the macaque. Cereb Cortex 18:477-499.2008).

Vakolyuk NI, Kosterina AV, Shlumukova AR (Electrical stimulation of the claustrum and conditioned-reflex activity. Neurosci Behav Physiol 13:158-163.1983).

Van Dijk KR, Hedden T, Venkataraman A, Evans KC, Lazar SW, Buckner RL (Intrinsic functional connectivity as a tool for human connectomics: theory, properties, and optimization. J Neurophysiol 103:297-321.2010).

Van Essen DC (Surface-based atlases of cerebellar cortex in the human, macaque, and mouse. Ann N Y Acad Sci 978:468-479.2002a).

Van Essen DC (Windows on the brain: the emerging role of atlases and databases in neuroscience. Curr Opin Neurobiol 12:574-579.2002b).

Van Essen DC (Surface-based approaches to spatial localization and registration in primate cerebral cortex. Neuroimage 23 Suppl 1:S97-107.2004).

Van Essen DC (A Population-Average, Landmark- and Surface-based (PALS) atlas of human cerebral cortex. Neuroimage 28:635-662.2005).

Van Essen DC, Newsome WT, Maunsell JH, Bixby JL (The projections from striate cortex (V1) to areas V2 and V3 in the macaque monkey: asymmetries, areal boundaries, and patchy connections. J Comp Neurol 244:451-480.1986).

Van Essen DC, Zeki S (The topographic organization of rhesus monkey prestriate cortex. J Physiol 277:193-226.1978).

Venables WN, Ripley BD (2002) Modern Applied Statistics with S. New York: Springer.

Vezoli J, Falchier A, Jouve B, Knoblauch K, Young M, Kennedy H (Quantitative analysis of connectivity in the visual cortex: extracting function from structure. Neuroscientist 10:476-482.2004).

Vince GH, Bouterfa H, Goldbrunner R, Roosen K, Tonn JC (Fast blue, a fluorescent tracer in glioma cell culture, affects cell proliferation and motility. Neurosci Lett 233:148-150.1997).

Vincent JL, Kahn I, Van Essen DC, Buckner RL (Functional Connectivity of the Macaque Posterior Parahippocampal Cortex. J Neurophysiol 103:793-800.2009).

Vincent JL, Larson-Prior LJ, Zempel JM, Snyder AZ (Moving GLM ballistocardiogram artifact reduction for EEG acquired simultaneously with fMRI. Clin Neurophysiol 118:981-998.2007a).

Vincent JL, Patel GH, Fox MD, Snyder AZ, Baker JT, Van Essen DC, Zempel JM, Snyder LH, Corbetta M, Raichle ME (Intrinsic functional architecture in the anaesthetized monkey brain. Nature 447:83-86.2007b).

Von Bonin G, Bailey P (The neocortex of *macaca mulata*. Urbana: University of Illinois Press.1947).

von Stein A, Chiang C, Konig P (Top-down processing mediated by interareal synchronization. Proc Natl Acad Sci U S A 97:14748-14753.2000).

Vragovic I, Louis E, Diaz-Guilera A (Efficiency of informational transfer in regular and complex networks. Phys Rev E Stat Nonlin Soft Matter Phys 71:036122.2005).

Wang W, Slotine JJ (On partial contraction analysis for coupled nonlinear oscillators. Biol Cybern 92:38-53.2005).

Watakabe A (Comparative molecular neuroanatomy of mammalian neocortex: what can gene expression tell us about areas and layers? Dev Growth Differ 51:343-354.2009).

Watanabe J, Iwai E (Neuronal activity in monkey visual areas V1, V2, V4 and TEO during fixation task. Brain Res Bull 40:143-150.1996).

Watts DJ (Networks, Dynamics, and the small-world phenomenon. Am J Sociology 105:493-527.1999).

Watts DJ, Strogatz SH (Collective dynamics of 'small-world' networks. Nature 393:440-442.1998).

Webster MJ, Ungerleider LG, Bachevalier J (Connections of inferior temporal areas TE and TEO with medial temporal-lobe Structures in infant and adult monkeys. J Neurosci 11:1095-1116.1991).

Wojcik S, Dziewiatkowski J, Spodnik E, Ludkiewicz B, Domaradzka-Pytel B, Kowianski P, Morys J (Analysis of calcium binding protein immunoreactivity in the claustrum and the endopiriform nucleus of the rabbit. Acta Neurobiol Exp (Wars) 64:449-460.2004).

Wong-Riley M (Reciprocal connections between striate and prestriate cortex in the squirrel monkey as demonstrated by combined peroxydase histochemistry and autoradiography. Brain Res 147:159-164.1978).

Wood SN (2006) Generalized Additive Models: An Introduction with R.: CRC Press.

Xu L, Tanigawa H, Fujita I (Distribution of alpha-amino-3-hydroxy-5-methyl-4-isoxazolepropionate-type glutamate receptor subunits (GluR2/3) along the ventral visual pathway in the monkey. J Comp Neurol 456:396-407.2003).

Yabuta NH, Callaway EM (Functional streams and local connections of layer 4C neurons in primary visual cortex of the macaque monkey. J Neurosci 18:9489-9499.1998).

Yoshioka T, Levitt JB, Lund JS (Intrinsic Lattice Connections of Macaque Monkey Visual Cortical Area-V4. J Neurosci 12:2785-2802.1992).

Young MP (Objective analysis of the topological organization of the primate cortical visual system. Nature 358:152-155.1992).

Young MP (The organization of neural systems in the primate cerebral cortex. Proc R Soc Lond B Biol Sci 252:13-18.1993).

Yukie M, Iwai E (Laminar origin of direct projection from cortex area V1 to V4 in the rhesus monkey. Brain Res 346:383-386.1985).

Zeki SM (Cortical projections from two prestriate areas in the monkey. Brain Res 34:19-35.1971).

Zeki SM (Simultaneous anatomical demonstration of the representation of the vertical and horizontal meridians in areas V2 and V3 of rhesus monkey visual cortex. Proc R Soc Lond B Biol Sci 195:517-523.1977).

Zeki SM (Functional specialisation in the visual cortex of the rhesus monkey. Nature 274:423-428.1978a).

Zeki SM (Uniformity and diversity of structure and function in rhesus monkey prestriate visual cortex. J Physiol (Lond) 277:273-290.1978b).

Zeki SM, Shipp S (The functional logic of cortical connections. Nature 335:311-317.1988).

Zeki SM, Shipp S (Modular organization between areas V2 and V4 of macaque monkey visual cortex. Eur J Neurosci 1:494-506.1989).

SUPPLEMENTARY FIGURES AND TABLES:

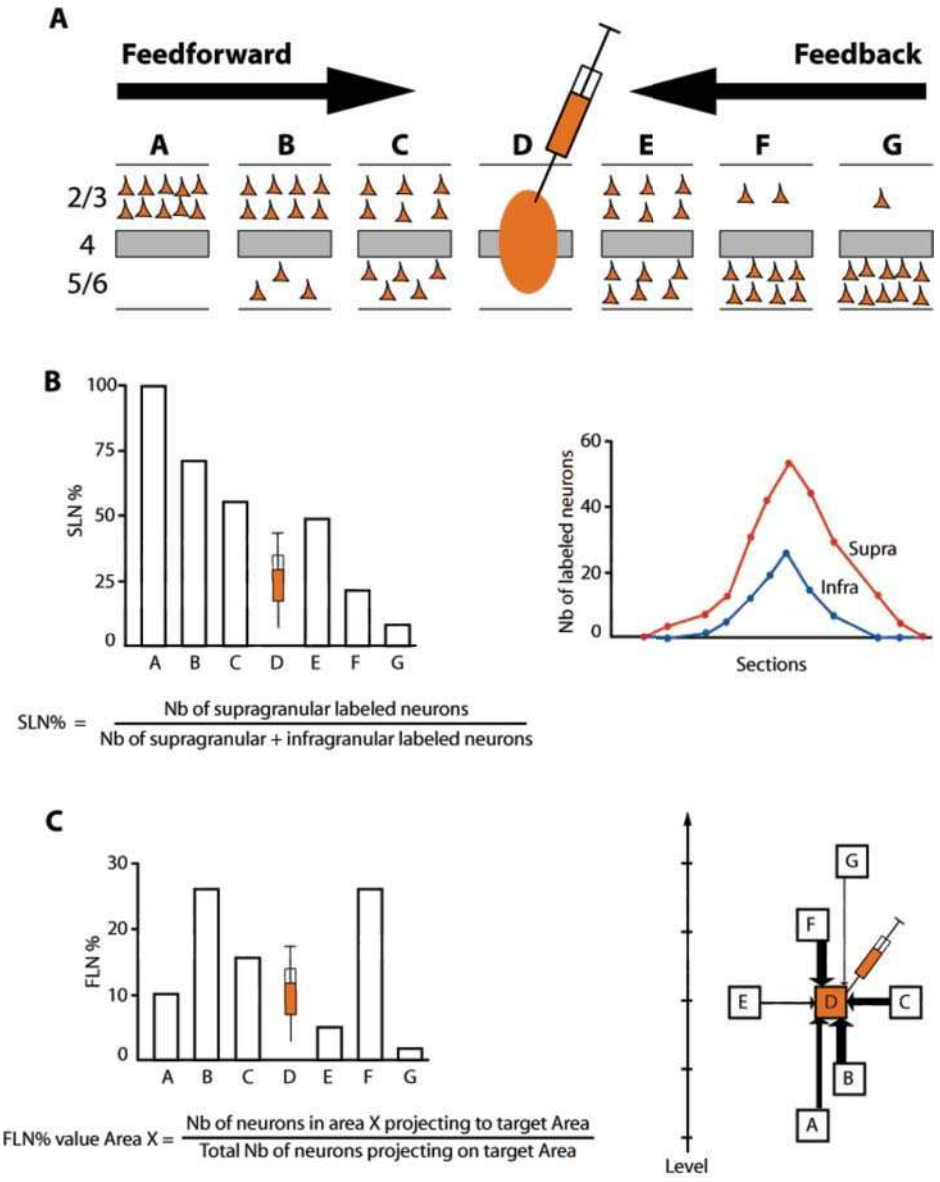

Figure S1. Quantitative parameters characterizing the hierarchy. A: The laminar distribution of parent neurons in each pathway, referred to as SLN (fraction of supragranular neurons) is determined by high frequency sampling and quantitative analysis of labelling. Supra- and infragranular layer neurons contribute to both feedback and feedforward pathways, but the two directions differ by their laminar pattern. For a given injection there is a gradient of SLN of the labelled areas, between purely FF (SLN = 100%, all the parent neurons are in the supragranular layers) to purely FB (SLN = 0%, all the parent neurons in the infragranular layers) and all the spectrum of intermediate connections; **B**: All labelled areas can then be ordered by decreasing SLN values and this order is consistent with hierarchical order according to Felleman and Van Essen. SLN is thus used as an indicator of hierarchical distance between areas from the same injection (Barone et al., 2000, Vezoli et al., 2004); **C**: FLN (fraction of labelled neurons) indicates the relative strength of each pathway (in number of labelled neurons) compared to the total number of neurons that are labelled in the brain after the injection. It requires counting labelled neurons on the sections spanning the whole brain, but gives insight into the weight of connections. Vezoli et al. (Vezoli et al., 2004) showed that short-distance connections have high FLN values, whereas the strength of connection decreases as physical distance between source and target areas increases